AD

USAAVLABS TECHNICAL REPORT 68-49A

AN INVESTIGATION OF THE DYNAMIC STABILITY CHARACTERISTICS OF A QUAD CONFIGURATION, DUCTED-PROPELLER V/STOL MODEL

VOLUME I

PHASE I - HOVERING

By

William F. Putman
Joseph J. Traybar
Howard C. Curtiss, Jr.
John P. Kukon

September 1968

U. S. ARMY AVIATION MATERIEL LABORATORIES
FORT EUSTIS, VIRGINIA

CONTRACT DAAJ02-67-C-0025
PRINCETON UNIVERSITY
PRINCETON, NEW JERSEY

Disclaimers

The findings in this report are not to be construed as an official Department of the Army position unless so designated by other authorized documents.

When Government drawings, specifications, or other data are used for any purpose other than in connection with a definitely related Government procurement operation, the United States Government thereby incurs no responsibility nor any obligation whatsoever; and the fact that the Government may have formulated, furnished, or in any way supplied the said drawings, specifications, or other data is not to be regarded by implication or otherwise as in any manner licensing the holder or any other person or corporation, or conveying any rights or permission, to manufacture, use, or sell any patented invention that may in any way be related thereto.

Disposition Instructions

Destroy this report when no longer needed. Do not return it to the originator.

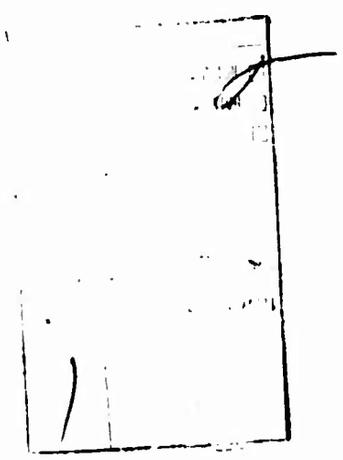

DEPARTMENT OF THE ARMY
U. S. ARMY AVIATION MATERIEL LABORATORIES
FORT EUSTIS, VIRGINIA 23604

This report has been reviewed by the U. S. Army Aviation Materiel Laboratories, the Naval Air Systems Command, and the Air Force Flight Dynamics Laboratories. It is considered to be technically sound.

This work, which was performed under Contract DAAJ02-67-C-0025, was undertaken to determine experimentally the dynamic stability characteristics of a quad configuration near the hover mode. The transient response characteristics of the configuration in various longitudinal and lateral degrees of freedom near hover were measured. Also, the static forces and moments acting on an isolated duct were measured. The Princeton Dynamic Model Track was utilized to perform the investigation.

This report is published for the exchange of information and the stimulation of ideas.

Task 1F125901A14233
Contract DAAJ02-67-C-0025
USAAVLABS Technical Report 68-49A
September 1968

AN INVESTIGATION OF THE DYNAMIC STABILITY CHARACTERISTICS OF A QUAD CONFIGURATION, DUCTED-PROPELLER V/STOL MODEL

Volume I

Final Data Report
Phase I - Hovering

Aerospace Sciences Report 835

By

William F. Putman
Joseph J. Traybar
Howard C. Curtiss, Jr.
John P. Kukon

Prepared by

Department of Aerospace and Mechanical Sciences
Princeton University
Princeton, New Jersey

for

U. S. ARMY AVIATION MATERIEL LABORATORIES
FORT EUSTIS, VIRGINIA

SUMMARY

Results are presented of experiments conducted to measure the dynamic stability characteristics of a quad configuration, ducted-propeller, dynamically similar model, V/STOL aircraft near hover. The data presented include longitudinal and lateral transient response characteristics of the dynamic model. Also included is a comparison with full-scale duct characteristics of the lift, drag, and pitching moment characteristics of an isolated duct from the model.

The model employed in the experiments is a generalized research model which was arranged to represent closely the Bell X-22A V/STOL aircraft.

The data presented in this report represent the first phase of a three-phase investigation of the dynamic stability of this type of V/STOL aircraft. The other two phases pertain to the longitudinal and lateral/directional characteristics at four low-speed and high-duct-incidence trim conditions.

FOREWORD

This research was performed by the Department of Aerospace and Mechanical Sciences, Princeton University, under the sponsorship of the United States Army Aviation Materiel Laboratories Contract DAAJ02-67-C-0025, with financial support from the United States Naval Air Systems Command and the Air Force Flight Dynamics Laboratory. The research was monitored by Mr. Robert P. Smith of the United States Army Aviation Materiel Laboratories.

The research was directed by Associate Professor H. C. Curtiss, Jr., and was conducted by Messrs. W. F. Putman, J. J. Traybar, and J. P. Kukon, all of Princeton University.

TABLE OF CONTENTS

	Page
SUMMARY	iii
FOREWORD	v
LIST OF ILLUSTRATIONS	viii
LIST OF SYMBOLS	xv
INTRODUCTION	1
DESCRIPTION OF APPARATUS	2
EXPERIMENTAL RESULTS AND DISCUSSION	5
REFERENCES	86
APPENDIX	
Equations of Motion	87
DISTRIBUTION	96

LIST OF ILLUSTRATIONS

Figure		Page
1	Photograph of Princeton Dynamic Model Track Showing Model Mounted on Longitudinal Dynamic Testing Apparatus.	15
2	Photograph of 0.145 Scale Quad Configuration Dynamic Model	16
3	General Arrangement Drawing of Quad Model in X-22A Configuration	17
4	Geometric Characteristics of Three-Bladed Model Propellers	18
5	Geometric Characteristics of Scaled Model Ducts.	19
6	Geometric Characteristics and Reference Locations for Model Duct System	20
7	Axis System for Isolated Duct Static Tests	21
8	Comparison of Isolated Ducted Propeller Model Data to Full-Scale Data of Reference 4. $\beta_{.75R} = 19.1^{\circ}$, $\delta = 0$.	22
9	Model Reference Stations, Location of Model cg and Axes Systems.	25
10	Axis System for Longitudinal Transient Response Data.	26
11	Axis System for Lateral/Directional Transient Response Data.	27
12	Longitudinal Transient Response. One Degree of Freedom, θ. $K_{\dot{\theta}} = 0.044$ sec. $\beta_{.75R} = 25.8^{\circ}$, rpm = 7000.	28
13	Longitudinal Transient Response. One Degree of Freedom, θ. $K_{\dot{\theta}} = 0.030$ sec. $\beta_{.75R} = 25.8^{\circ}$, rpm = 7000.	29

Figure		Page
14	Longitudinal Transient Response. One Degree of Freedom, θ. No Stability Augmentation. $\beta_{.75R} = 25.8^\circ$, rpm = 7000.	30
15	Longitudinal Transient Response. One Degree of Freedom, θ. $K_{\dot{\theta}} = 0.044$ sec. $\beta_{.75R} = 29.2^\circ$, rpm = 6400.	31
16	Longitudinal Transient Response. One Degree of Freedom, θ. $K_{\dot{\theta}} = 0.030$ sec. $\beta_{.75R} = 29.2^\circ$, rpm = 6400.	32
17	Longitudinal Transient Response. One Degree of Freedom, θ. No Stability Augmentation. $\beta_{.75R} = 29.2^\circ$, rpm = 6400.	33
18	Longitudinal Transient Response. One Degree of Freedom, θ. $K_{\dot{\theta}} = 0.044$ sec. $\beta_{.75R} = 25.8^\circ$, rpm = 6400.	34
19	Longitudinal Transient Response. One Degree of Freedom, θ. $K_{\dot{\theta}} = 0.030$ sec. $\beta_{.75R} = 25.8^\circ$, rpm = 6400.	35
20	Longitudinal Transient Response. One Degree of Freedom, θ. No Stability Augmentation. $\beta_{.75R} = 25.8^\circ$, rpm = 6400.	36
21	Longitudinal Transient Response. One Degree of Freedom, θ. $K_{\dot{\theta}} = 0.044$ sec. $\beta_{.75R} = 25.8^\circ$, rpm = zero.	37
22	Longitudinal Transient Response. One Degree of Freedom, θ. $K_{\dot{\theta}} = 0.030$ sec. $\beta_{.75R} = 25.8^\circ$, rpm = zero.	38
23	Longitudinal Transient Response. One Degree of Freedom, θ. No Stability Augmentation. $\beta_{.75R} = 25.8^\circ$, rpm = zero.	39
24	Longitudinal Transient Response. Two Degrees of Freedom, θ-U_f. No Stability Augmentation. $\beta_{.75R} = 25.8^\circ$, rpm = 7000.	40

Figure		Page
25	Longitudinal Transient Response. Two Degrees of Freedom, θ-U_f. No Stability Augmentation. $\beta_{.75R} = 25.8^\circ$, rpm = 7000.	41
26	Longitudinal Transient Response. Two Degrees of Freedom, θ-U_f. No Stability Augmentation. $\beta_{.75R} = 25.8^\circ$, rpm = 7000.	42
27	Longitudinal Transient Response. Two Degrees of Freedom, θ-U_f. No Stability Augmentation. $\beta_{.75R} = 25.8^\circ$, rpm = 7000.	43
28	Longitudinal Transient Response. Two Degrees of Freedom, θ-U_f. No Stability Augmentation. $\beta_{.75R} = 25.8^\circ$, rpm = 6400.	44
29	Longitudinal Transient Response. Two Degrees of Freedom, θ-U_f. No Stability Augmentation. $\beta_{.75R} = 25.8^\circ$, rpm = 6400.	45
30	Longitudinal Transient Response. Two Degrees of Freedom, θ-U_f. No Stability Augmentation. $\beta_{.75R} = 25.8^\circ$, rpm = 6400.	46
31	Longitudinal Transient Response. Two Degrees of Freedom, θ-U_f. No Stability Augmentation. $\beta_{.75R} = 25.8^\circ$, rpm = 6400.	47
32	Longitudinal Transient Response. Two Degrees of Freedom, θ-U_f. No Stability Augmentation. $\beta_{.75R} = 29.2^\circ$, rpm = 6400.	48
33	Longitudinal Transient Response. Two Degrees of Freedom, θ-U_f. No Stability Augmentation. $\beta_{.75R} = 29.2^\circ$, rpm = 6400.	49
34	Longitudinal Transient Response. Two Degrees of Freedom, θ-U_f. No Stability Augmentation. $\beta_{.75R} = 29.2^\circ$, rpm = 6400.	50
35	Longitudinal Transient Response. Two Degrees of Freedom, θ-U_f. No Stability Augmentation. $\beta_{.75R} = 29.2^\circ$, rpm = 6400.	51

Figure		Page
36	Longitudinal Transient Response. Two Degrees of Freedom, θ-U_f. No Stability Augmentation. $\beta_{.75R}$ = 29.2°, rpm = 6400.	52
37	Longitudinal Transient Response. Two Degrees of Freedom, θ-U_f. No Stability Augmentation. $\beta_{.75R}$ = 29.2°, rpm = 6400.	53
38	Lateral Transient Response. One Degree of Freedom, ϕ. $K_{\dot{\phi}}$ = 0.029 sec. $\beta_{.75R}$ = 25.8°, rpm = 7000.	54
39	Lateral Transient Response. One Degree of Freedom, ϕ. $K_{\dot{\phi}}$ = 0.016 sec. $\beta_{.75R}$ = 25.8°, rpm = 7000.	55
40	Lateral Transient Response. One Degree of Freedom, ϕ. No Stability Augmentation. $\beta_{.75R}$ = 25.8°	56
41	Lateral Transient Response. One Degree of Freedom, ϕ. $K_{\dot{\phi}}$ = 0.029 sec. $\beta_{.75R}$ = 29.2°, rpm = 6400.	57
42	Lateral Transient Response. One Degree of Freedom, ϕ. $K_{\dot{\phi}}$ = 0.016 sec. $\beta_{.75R}$ = 29.2°, rpm = 6400.	58
43	Lateral Transient Response. One Degree of Freedom, ϕ. No Stability Augmentation. $\beta_{.75R}$ = 29.2°, rpm = 6400.	59
44	Lateral Transient Response. One Degree of Freedom, ϕ. $K_{\dot{\phi}}$ = 0.055 sec. $\beta_{.75R}$ = 25.8°, rpm = 6400.	60
45	Lateral Transient Response. One Degree of Freedom, ϕ. $K_{\dot{\phi}}$ = 0.029 sec. $\beta_{.75R}$ = 25.8°, rpm = 6400.	61
46	Lateral Transient Response. One Degree of Freedom, ϕ. $K_{\dot{\phi}}$ = 0.016 sec. $\beta_{.75R}$ = 25.8°, rpm = 6400.	62

Figure		Page
47	Lateral Transient Response. One Degree of Freedom, ϕ. No Stability Augmentation. $\beta_{.75R} = 25.8^{\circ}$, rpm = 6400.	63
48	Lateral Transient Response. One Degree of Freedom, ϕ. $K_{\dot{\phi}} = 0.055$ sec. $\beta_{.75R} = 25.8^{\circ}$, rpm = zero.	64
49	Lateral Transient Response. One Degree of Freedom, ϕ. $K_{\dot{\phi}} = 0.029$ sec. $\beta_{.75R} = 25.8^{\circ}$, rpm = zero.	65
50	Lateral Transient Response. One Degree of Freedom, ϕ. $K_{\dot{\phi}} = 0.016$ sec. $\beta_{.75R} = 25.8^{\circ}$, rpm = zero.	66
51	Lateral Transient Response. One Degree of Freedom, ϕ. No Stability Augmentation. $\beta_{.75R} = 25.8^{\circ}$, rpm = zero.	67
52	Directional Transient Response. One Degree of Freedom, Ψ. $K_{\dot{\Psi}} = 0.083$ sec. $\beta_{.75R} = 25.8^{\circ}$, rpm = 7000.	68
53	Directional Transient Response. One Degree of Freedom, Ψ. No Stability Augmentation. $\beta_{.75R} = 25.8^{\circ}$, rpm = 7000.	69
54	Directional Transient Response. One Degree of Freedom, Ψ. $K_{\dot{\Psi}} = 0.389$ sec. $\beta_{.75R} = 25.8^{\circ}$, rpm = 6400.	70
55	Directional Transient Response. One Degree of Freedom, Ψ. $K_{\dot{\Psi}} = 0.209$ sec. $\beta_{.75R} = 25.8^{\circ}$, rpm = 6400.	71
56	Directional Transient Response. One Degree of Freedom, Ψ. $K_{\dot{\Psi}} = 0.083$ sec. $\beta_{.75R} = 25.8^{\circ}$, rpm = 6400.	72
57	Directional Transient Response. One Degree of Freedom, Ψ. No Stability Augmentation. $\beta_{.75R} = 25.8^{\circ}$, rpm = 6400.	73

Figure		Page
58	Directional Transient Response. One Degree of Freedom, Ψ. $K_{\dot{\psi}}$ = 0.389 sec. $\beta_{.75R}$ = 25.8°, rpm = zero.	74
59	Directional Transient Response. One Degree of Freedom, Ψ. $K_{\dot{\psi}}$ = 0.083 sec. $\beta_{.75R}$ = 25.8°, rpm = zero.	75
60	Directional Transient Response. One Degree of Freedom, Ψ. $K_{\dot{\psi}}$ = 0.209 sec. $\beta_{.75R}$ = 29.2°, rpm = 6400.	76
61	Directional Transient Response. One Degree of Freedom, Ψ. $K_{\dot{\psi}}$ = 0.083 sec. $\beta_{.75R}$ = 29.2°, rpm = 6400.	77
62	Directional Transient Response. One Degree of Freedom, Ψ. No Stability Augmentation. $\beta_{.75R}$ = 29.2°, rpm = 6400.	78
63	Directional Transient Response. One Degree of Freedom, Ψ. No Stability Augmentation. $\beta_{.75R}$ = 29.2°, rpm = zero.	79
64	Lateral/Directional Transient Response. Two Degrees of Freedom, ϕ-v_f. $K_{\dot{\phi}}$ = 0.055 sec. $\beta_{.75R}$ = 25.8°, rpm = 6400.	80
65	Lateral/Directional Transient Response. Two Degrees of Freedom, ϕ-v_f. $K_{\dot{\phi}}$ = 0.029 sec. $\beta_{.75R}$ = 25.8°, rpm = 6400.	81
66	Lateral/Directional Transient Response. Two Degrees of Freedom, ϕ-v_f. $K_{\dot{\phi}}$ = 0.016 sec. $\beta_{.75R}$ = 25.8°, rpm = 6400.	82
67	Lateral/Directional Transient Response. Two Degrees of Freedom, ϕ-v_f. No Stability Augmentation. $\beta_{.75R}$ = 25.8°, rpm = 6400.	83

Figure		Page
68	Lateral/Directional Transient Response. Three Degrees of Freedom, ϕ-Ψ-v_f. K_ϕ = 0.055 sec. $\beta_{.75R}$ = 25.8°, rpm = 6400.	84
69	Lateral Transient Response. Three Degrees of Freedom, ϕ-v_f-w_f. K_ϕ = 0.055 sec. $\beta_{.75R}$ = 25.8°, rpm = 7000.	85
70	Definitions of Space-Fixed and Stability Axis Systems. Variables are Shown in Their Positive Sense.	94
71	Model and Link Mass Arrangements and Reference Systems for Model cg (Pivot Axes)	95

LIST OF SYMBOLS

b	propeller blade chord, feet
C_D	drag coefficient, $C_D = \frac{D}{q_o\ cd}$
C_L	lift coefficient, $C_L = \frac{L}{q_o\ cd}$
C_M	pitching moment coefficient, $C_M = \frac{M}{q_o\ c^2 d}$
c	duct chord, feet
cg	center of gravity of pivoting mass of model
D	drag of isolated ducted propeller model, pounds
d	propeller blade diameter, feet
FS	fuselage station (horizontal reference), inches
g	acceleration due to gravity, feet per second squared
h	altitude, feet
I_x	moment of inertia in roll about principal axis, slug-feet squared
I_y	moment of inertia in pitch about principal axis, slug-feet squared
I_z	moment of inertia in yaw about principal axis, slug-feet squared
I_{xz}	product of inertia, slug-feet squared
i_d	duct incidence, degrees
J	propeller advance ratio, $J = \frac{U_f}{nd}$, or as used in Reference 4, V/nd
$K_{\dot{\theta}}$	feedback gain, proportionality constant between differential blade angle change and angular velocity in pitch, seconds
$K_{\dot{\phi}}$	feedback gain, proportionality constant between differential blade angle change and angular velocity in roll, seconds

$K_{\dot{\psi}}$	feedback gain, proportionality constant between differential blade angle change and angular velocity in yaw, seconds
k_{θ_m}	mechanical spring constant in pitch, foot-pounds per radian
k_{ϕ_m}	mechanical spring constant in roll, foot-pounds per radian
k_{ψ_m}	mechanical spring constant in yaw, foot-pounds per radian
L	lift of isolated ducted propeller model, pounds
L_p, L_r, L_v,	stability derivatives, rate of change of rolling moment divided by inertia I_x with variable indicated in subscript
$L_{\Delta\beta_{ROLL}}$	lateral control effectiveness, rate of change of rolling moment divided by inertia I_x with propeller lateral differential collective pitch, per second squared
$\bar{L}_p$	augmented roll damping stability derivative ($\bar{L}_p = L_p + K_{\dot{\phi}} L_{\Delta\beta_{ROLL}}$), per second
M	pitching moment of isolated ducted propeller model, foot-pounds
M_u, M_w, $M_{\dot{w}}$, $M_{\dot{\theta}}$	stability derivatives, rate of change of pitching moment divided by inertia I_y with variable indicated in subscript
$M_{\Delta\beta_{PITCH}}$	longitudinal control effectiveness, rate of change of pitching moment divided by inertia I_y with propeller longitudinal differential collective pitch, per second squared
$\bar{M}_{\dot{\theta}}$	augmented pitch damping stability derivative ($\bar{M}_{\dot{\theta}} = M_{\dot{\theta}} + K_{\dot{\theta}} M_{\Delta\beta_{PITCH}}$), per second
m	mass accelerated by the model when translating vertically, slugs ($m = m_p + m_v = 1.60$ slugs)
m_h	mass of horizontal travel link, slugs ($m_h = 0.11$ slugs)
m_p	pivoting mass of model, slugs ($m_p = 1.48$ slugs)

m_t	total mass accelerated by the model when translating horizontally, slugs ($m_t = m + m_h = 1.71$ slugs)
m_v	mass of vertical travel link, slugs ($m_v = 0.12$ slugs)
$\frac{m}{m_t}$	ratio of vertical mass to horizontal mass ($\frac{m}{m_t} = 0.936$)
N_p, N_r, N_v,	stability derivatives, rate of change of yawing moment divided by inertia I_z with variable indicated in subscript
$N_{\Delta\delta}$	directional control effectiveness, rate of change of yawing moment divided by inertia I_z with lateral differential elevon deflection, per second squared
$\bar{N}_r$	augmented yaw damping stability derivative ($\bar{N}_r = N_r + K_{\dot{\psi}} N_{\Delta\delta}$), per second
n	propeller rotational speed, revolutions per second
p	model angular velocity in roll about principal axis, Figure 11, radians per second or degrees per second ($p = \dot{\phi}$)
q	angular velocity in pitch, radians per second
q_o	free-stream dynamic pressure, pounds per square foot ($q_o = \frac{1}{2} \rho U_f^2$)
R	propeller blade radius, feet
r	distance along propeller radius (measured from axis of rotation), feet; or model angular velocity in yaw about principal axis, Figure 11, radians per second or degrees per second ($r = \dot{\Psi} \cos \phi \approx \dot{\Psi}$)
$\frac{r}{R}$	propeller blade radial station
rpm	model propeller rotational speed, revolutions per minute
T	thrust of isolated ducted propeller model, pounds
t	propeller blade thickness, feet
U	aircraft velocity along body-fixed X axis (stability axis system), feet per second ($U = U_o + u$)

U_f	aircraft and isolated ducted propeller model horizontal velocity (space-fixed axis system), feet per second ($U_f = U_{o_f} + u_f$)
U_o	aircraft initial velocity along flight path (stability axis system), feet per second
U_{o_f}	aircraft initial horizontal velocity (space-fixed axis system), feet per second
u	aircraft perturbation velocity along body-fixed X axis (stability axis system), feet per second
u_f	aircraft horizontal perturbation velocity (space-fixed axis system), feet per second
V	free-stream velocity in tests of Reference 4, feet per second
V_f	aircraft lateral velocity (space-fixed axis system), feet per second ($V_f = V_{o_f} + v_f$)
V_{o_f}	aircraft initial lateral velocity (space-fixed axis system), feet per second
v	aircraft lateral perturbation velocity along body-fixed Y axis, feet per second
v_f	aircraft lateral perturbation velocity (space-fixed axis system), feet per second
W	model gross weight, pounds
W_f	aircraft vertical velocity (space-fixed axis system), feet per second ($W_f = W_{o_f} + w_f$)
W_p	model pivoting weight, pounds (W_p = 47.5 lb)
W_{o_f}	aircraft initial vertical velocity (space-fixed axis system), feet per second
w	aircraft perturbation velocity along body-fixed Z axis (stability axis system), feet per second
w_f	aircraft vertical perturbation velocity (space-fixed axis system), feet per second
WL	fuselage water line (vertical reference station), inches

X	body-fixed longitudinal axis, initially aligned into the relative wind (stability axis system), Figure 70
X_f	longitudinal horizontal axis (space-fixed axis system), Figure 70
$\bar{X}_f$	longitudinal space axis, Figures 9 and 11
X_u, X_w, $X_{\dot{\theta}}$	stability derivatives, rate of change of longitudinal horizontal force divided by mass m with variable indicated in subscript
x_{PIVOT}	longitudinal position of model pivot axis referenced to FS 0, inches (model scale unless noted)
$\bar{x}$	axial coordinate distance from duct leading edge, inches (full scale)
Y_f	lateral axis (space-fixed axis system), Figure 10
$\bar{Y}_f$	lateral space axis, Figure 11
Y_v	stability derivative, rate of change of lateral horizontal force divided by mass m with lateral velocity, per second
$\bar{y}$	radial coordinate distance from duct center line, inches (full scale)
Z	body-fixed vertical axis, initially aligned perpendicular to the relative wind in the vertical plane (stability axis system), Figure 70
Z_f	vertical axis (space-fixed axis system), aligned with gravity, Figure 70
Z_u, Z_w, $Z_{\dot{\theta}}$	stability derivatives, rate of change of vertical force divided by mass m with variable indicated in subscript
$\bar{Z}_f$	vertical space axis, Figures 9 and 11
z_{PIVOT}	vertical position of model pivot axis referenced to WL 0, inches (model scale unless noted)
α	angle of attack of isolated ducted propeller model, degrees
β	local propeller blade angle (Figure 4), degrees

$\beta_{.75R}$ average propeller blade angle required for vertical force trim (collective pitch) measured at the three-quarter radius and averaged for four propellers, degrees

ΔL_{ϕ_m} additional stability derivative, due to mechanical spring in roll, per second squared $\left(\Delta L_{\phi_m} = - \frac{k_{\phi_m}}{I_x}\right)$

ΔM_{θ_m} additional stability derivative, due to mechanical spring in pitch, per second squared $\left(\Delta M_{\theta_m} = - \frac{k_{\theta_m}}{I_y}\right)$

ΔN_{ψ_m} additional stability derivative, due to mechanical spring in yaw, per second squared $\left(\Delta N_{\psi_m} = - \frac{k_{\psi_m}}{I_z}\right)$

$\Delta\beta$ change in propeller blade angle, degrees (positive for blade trailing edge down with duct at 90° incidence)

$\Delta\beta_{PITCH}$ longitudinal control input due to stability augmentation system, degrees $\left(\Delta\beta_{PITCH} = \frac{\Delta\beta_{RS} + \Delta\beta_{RP}}{4} - \frac{\Delta\beta_{FS} + \Delta\beta_{FP}}{4}\right)$

$\Delta\beta_{ROLL}$ lateral control input due to stability augmentation system, degrees $\left(\Delta\beta_{ROLL} = \frac{\Delta\beta_{FS} + \Delta\beta_{RS}}{4} - \frac{\Delta\beta_{FP} + \Delta\beta_{RP}}{4}\right)$

$\Delta\delta$ elevon directional control input due to stability augmentation system, degrees $\left(\Delta\delta = \frac{\delta_{FS} + \delta_{RS}}{4} - \frac{\delta_{FP} + \delta_{RP}}{4}\right)$

δ elevon deflection, degrees (positive for elevon trailing edge forward with duct at 90° incidence)

η angle between model principal axis and fuselage reference line, Figure 9, degrees (positive for principal axis inclined downward)

θ fuselage pitch angle, degrees or radians (positive nose up)

λ_L linear scale factor $\lambda_L = \frac{\text{model length}}{\text{full-scale length}}$

ρ ambient air mass density, slugs per cubic foot

ϕ	roll angle about model gimbal roll axis, degrees or radians
Ψ	yaw angle about model gimbal yaw axis, degrees or radians
$(\dot{})$	differentiation with respect to time
$(\,)'$	perturbed locations of axes
$(\,)''$	
$(\,)_{FP}$	control deflection associated with front port duct or elevon
$(\,)_{FS}$	control deflection associated with front starboard duct or elevon
$(\,)_{RP}$	control deflection associated with rear port duct or elevon
$(\,)_{RS}$	control deflection associated with rear starboard duct or elevon
$(\,)_o$	initial or trim condition

INTRODUCTION

A series of experiments to determine the dynamic stability characteristics of a quad configuration, four-duct V/STOL aircraft near hover were conducted on the Princeton Dynamic Model Track. The results presented in this report are for Phase I of a three-phase investigation and consist of measurements of the longitudinal and lateral hovering stability characteristics. Succeeding reports will pertain to Phase II, the longitudinal dynamics of the same configuration at four forward-speed trim conditions, and Phase III, the lateral/directional dynamics at the same trim conditions.

The dynamic model employed in these tests is shown in Figure 1. The model was designed as a general research model with variable geometry and a lifting system configuration such that a variety of quad V/STOL configurations could be simulated. In the configuration selected for the tests described here, the model closely resembles a 0.145-scale dynamic model of the Bell X-22A V/STOL research aircraft. The model differs from the actual aircraft (as given in Reference 1) in certain minor details, which are described in the section Description of Apparatus under Model.

The test program consisted of two parts. In the first part, the lift, drag, and pitching moment acting on an isolated duct from the model were measured as a function of advance ratio and duct angle of attack. These static data are presented in comparison with full-scale duct data. The experiments were conducted to determine the nature and magnitude of possible scale effects on the duct. Comparison of these data did not indicate any appreciable scale effect present on the model duct. The second part, comprising the majority of the experiments in Phase I, was concerned with the measurement of the transient response characteristics of the dynamic model in various degrees of freedom, both laterally and longitudinally, with initial conditions of hovering flight. To enhance the usefulness of the data, responses of the model with various levels of rate feedback are presented along with the transient response characteristics of the basic model. Also, data are presented in various degrees of freedom to assist in analysis of the data for stability derivatives. A summary of the transient response test conditions is presented in Table I.

All data are presented in model scale, and they may be interpreted in terms of the full-scale vehicle (which the model closely resembles) using the conversion factors given in Table II.

DESCRIPTION OF APPARATUS

TEST FACILITY

The Princeton University Dynamic Model Track is a facility designed expressly for the study of the dynamic motions of helicopter and V/STOL models at equivalent flight speeds of up to 60 knots (for a one-tenth scale model). Basic components of the facility include a servo-driven carriage riding on a track 750 feet long, located in a building with a cross section of 30 by 30 feet; the carriage has an acceleration potential of 0.6g and a maximum speed of 40 feet per second. A detailed description of the facility and the testing techniques employed may be found in Reference 2.

A model can be attached to the carriage by one of several booms. The mount used to conduct longitudinal investigations is shown in Figure 1. This mount permits relative displacements of the model with respect to the carriage in horizontal and vertical directions. The model is supported on a three-axis gimbal system that allows selection of any or all of the three angular degrees of freedom. Horizontal relative motion of the model with respect to the carriage is sensed and used to command the carriage to follow the model in a closed-loop fashion. Similarly, vertical displacement of the model with respect to the carriage commands the boom to move vertically. This servo operation of the carriage allows the model to fly "free", with no restraints on the dynamic motions being investigated. This method of testing may be considered to be similar to dynamic flight testing, but considerably more control over the experiment is possible.

The dynamic tests conducted for this program were two- and three-degree-of-freedom motions. For the longitudinal tests, the model was mounted as shown in Figure 1; the transient response in two degrees of freedom, fuselage pitch angle and horizontal velocity, was measured. The lateral/directional hovering experiments were conducted by rotating the model about the yaw axis 90 degrees, such that side velocity of the model corresponded to motion of the carriage down the track. Two-degree-of-freedom (roll and side velocity) and three-degree-of-freedom (roll, yaw, and side velocity) motions were measured. Since the model motions were in general quite unstable, no predetermined inputs were used to excite the motions.

MODEL

A photograph of the model on the dynamic testing apparatus is shown in Figure 2, and a three-view drawing is presented in Figure 3. The model's pertinent dimensions and inertia characteristics are listed in Table III. The model was designed as a general research model for investigation of the dynamic stability characteristics of various quad configuration V/STOL aircraft as described in Reference 3.

This dynamic model is powered by a 200-volt, 400-cycle, 3-phase electric motor. The motor drives the four ducted propellers through a central transmission and various right-angle gearboxes. The aerodynamic shape of the model is obtained through the use of a Fiberglas skin with Styrofoam stiffeners. The propeller blades are made with a plastic foam core and Fiberglas skin. The geometric characteristics of the propeller are shown in Figure 4, and the duct geometry and elevon are shown in Figures 5 and 6. The duct shape is identical to that of the Bell X-22A aircraft.

Model control positions are set from a control console on the carriage. The blade pitch angles of each of the four propellers are electrically controllable. Also, the deflection angles of the elevons are electrically controllable. All of these control systems are closed-loop position controls and are used as such in the portions of the experiments involving feedback to alter the transient motions of the model. The dynamic characteristics of these feedback loops are such that the time response of the control is negligible in the frequency range of interest. Although the control servo loops are nonlinear, using polarized relays for power amplification, they can be characterized as having a closed-loop natural frequency of approximately 10 cycles per second with a damping ratio of approximately seven-tenths. The servo gear ratios were selected so that the rate limits arising from the rpm limitations of the control drive motors were equal to or greater than scaled rate limits determined from full-scale Bell X-22A values.

This research model differs from the Bell X-22A in the following particulars:

1. The elevon on the model differs from that on the full-scale aircraft. The model elevon has no movable surface forward of the hinge line, and its hinge line is located below the trailing edge of the duct as shown in Figure 6. While these differences would affect the control effectiveness and the control loads, they would not be expected to have any significant effect on the dynamic motions.

2. The duct rotation point is at a different location on the model (84 percent c) than on the full-scale aircraft (55 percent c).

   With the ducts at 90 degrees incidence, the propeller hubs and the cg on the model are at the same location relative to fuselage reference points as on the full-scale aircraft.

3. The vertical tail is smaller on the model than on the full-scale vehicle as shown in Figure 3. This difference in vertical tail area would not have a significant effect on the hovering dynamic stability characteristics.

This model was planned as a general research model; numerous other quad configuration layouts can be simulated through the use of interchangeable parts as described in Reference 3. No attempt was made in the design stage to simulate the X-22A precisely. However, the modifications described above will not result in appreciable differences in the model dynamic stability characteristics.

EXPERIMENTAL RESULTS AND DISCUSSION

The experimental program consisted of two parts:

1. Measurement of the static forces and moment acting on an isolated duct.

2. Measurement of the transient response characteristics of the complete vehicle in various longitudinal and lateral degrees of freedom near hover.

STATIC DATA - Isolated Duct

The lift, drag, and pitching moment characteristics of an isolated ducted propeller from the model were measured as a function of angle of attack and advance ratio at a fixed blade angle of 19.1 degrees. The axis system used for the reduction of the isolated ducted propeller static tests is shown in Figure 7; the moment center location is identical to that of Reference 4. The measured forces and moments were then compared to the full-scale duct measurements of Reference 4 to determine the importance of Reynolds number effect on the aerodynamic characteristics of this particular duct. The results of this comparison are shown in Figure 8. Data were taken on the basic duct as well as on a modified duct with a circular duct inlet slat. The circular slat had no noticeable effect on the duct aerodynamics; therefore, data with the slat are not included.

There is considerable scatter in the lift and pitching moment data measured on the full-scale duct at the lowest advance ratio (J equal to 0.14) for angles of attack greater than 60 degrees. The model data generally fall among the scatter of the full-scale data in these ranges. No consistent differences appear in the data; therefore, the model duct is considered to be a good representation of the full-scale duct for the test conditions of interest.

DYNAMIC TESTS - Complete Model

The model Reference Stations and the location of the model cg-axes systems for the dynamic tests are given in Figure 9. Figures 10 and 11 show pictorially the axes systems for the longitudinal and the lateral/directional dynamic tests respectively.

The test conditions examined in the transient response tests are given in Table I. In the longitudinal tests, one-degree-of-freedom experiments were conducted both with and without stability augmentation. The two-degree-of-freedom longitudinal experiments were conducted only without stability augmentation, and inputs were not necessary to excite the transient motion since the instability of the basic motion was easily excited by random disturbances. The longitudinal transient response time histories are presented in Figures 12 through 37.

Three longitudinal hovering test conditions representing different blade angle and propeller rpm settings were investigated. Two of the test conditions utilize different combinations of blade angle and rpm to produce the same total thrust (vertical force equal to the weight of the model): $\beta_{.75R}$ equal to 25.8 degrees, rpm equal to 7000; and $\beta_{.75R}$ equal to 29.2 degrees, rpm equal to 6400. These two test conditions were selected for comparison of experimental results with theoretical prediction of the hovering dynamics. Comparison of test results for these two blade angle and rpm combinations (producing the same thrust) will show the importance of matching the full-scale blade angle in conducting model tests. The third test condition uses another combination of blade angle and rpm, resulting in lower total thrust than the previous cases: $\beta_{.75R}$ equal to 25.8 degrees, rpm equal to 6400 (vertical force equal to less than the total weight of the model in order to match a desired equivalent full-scale gross weight). Operation at 6400 rpm and a propeller blade angle of 25.8 degrees produces a hover thrust of 43.1 pounds, as contrasted with 51.5 pounds under the other two test conditions. The lower value of thrust corresponds to a scaled gross weight of 14,000 pounds for the Bell X-22A.

The lateral/directional dynamic tests were somewhat more extensive, encompassing the measurement of the transient response characteristics with various levels of roll rate feedback. The dynamic model incorporates features that permit longitudinal and lateral differential blade angle changes proportional to pitch and roll rate, respectively. The addition of feedback is a valuable aid in analyzing the transient motions for stability derivatives of a vehicle with unstable dynamic characteristics. The lateral/directional dynamic test data are presented in Figures 38 through 69. Lateral/directional data were taken with yaw angle fixed as well as yaw angle free to determine what variations, if any, exist between the roll, side velocity response and the roll, yaw, side velocity response. Differences would be indicative of coupling between the roll, side velocity motion and the yaw freedom. One run is also presented in Figure 69 to show the roll, side velocity and vertical velocity motion.

In addition to the two- and three-degree-of-freedom measurements, various single-degree-of-freedom measurements were made to evaluate the angular damping derivatives in hover; these measurements are shown in Figures 38 through 51 and 52 through 63. Mechanical springs were added to the model about one axis at a time to provide a linear restoring moment such that the angular, single-degree-of-freedom motions of the model were oscillatory. Experiments of this kind produce the time histories that are more readily analyzed for angular damping derivatives. The spring constant and model inertia, noted in Table III , were selected to provide a natural frequency of these single-degree-of-freedom, second-order systems that would be near the frequency of the transient response of the model in three degrees of freedom. Data are presented for the model motor running and for the model motor off, with rpm equal to zero. The model motor off runs are used to determine the mechanical damping arising from gimbal bearing friction. The mechanical damping determined from the runs with the model motor off should be subtracted from the model-motor-running data

to determine the aerodynamic damping. In general, it may be noted that the mechanical damping is very small compared to the aerodynamic damping.

The general nature of the dynamic data indicates unstable oscillations of similar character in the longitudinal and lateral degrees of freedom, as would be expected from the general layout of the vehicle. The unstable oscillation is characteristic of V/STOL vehicles of most types in hovering flight. The model has a period of about four seconds in both the lateral and longitudinal modes.

TABLE I. SUMMARY OF HOVERING TEST CONDITIONS

Degrees of Freedom	Total Vertical Force Hover Thrust (lb)	Average Propeller Blade Angle $\beta_{.75R}$ (deg)	Propeller Rotational Speed (rpm)	Stability Augmentation $K_{\dot{\theta}}$ (sec)	Run Nos.	Fig. Nos.
$\theta^{*,**}$	51.5	25.8	7000	0.044	289,290,291,292	12
				0.030	284,285,286	13
				none	277,278,280,281	14
		29.2	6400	0.044	310,311,312,313	15
				0.030	304,305,306,308	16
				none	300,301,302,303	17
	43.1	25.8	6400	0.044	261,262,263	18
				0.030	251,258,259	19
				none	245,255,256	20
	0	25.8	0	0.044	260	21
				0.030	257	22
				none	254	23

TABLE I - Continued

Degrees of Freedom	Total Vertical Force Hover Thrust (lb)	Average Propeller Blade Angle $\beta_{.75R}$ (deg)	Propeller Rotational Speed (rpm)	Stability Augmentation $K_{\dot{\theta}}$ (sec)	Run Nos.	Fig. Nos.
θ-U_f	51.5	25.8	7000	none	363	24
					364	25
					366	26
					368	27
	43.1	25.8	6400	none	370	28
					389	29
					391	30
					396	31
	51.5	29.2	6400	none	402	32
					403	33
					410	34
					421	35
					425	36
					434	37

TABLE I - Continued

Degrees of Freedom	Total Vertical Force Hover Thrust (lb)	Average Propeller Blade Angle $\beta_{.75R}$ (deg)	Propeller Rotational Speed (rpm)	Stability Augmentation $K_{\dot{\phi}}$ (sec)	Run Nos.	Fig. Nos.
ϕ*	51.5	25.8	7000	0.029	548,549,551	38
				0.016	544,545,546	39
				none	538,540	40
	0	25.8	0	none	535	
	51.5	29.2	6400	0.029	506,507,509	41
				0.016	502,503,504	42
				none	493,496,497,498	43
	43.1	25.8	6400	0.055	531,532,533,534	44
				0.029	526,527,528,529	45
				0.016	521,522,523,524	46
				none	516,517,518	47
	0	25.8	0	0.055	530	48
				0.029	547	49
				0.016	542	50
				none	492	51

TABLE I - Continued

Degrees of Freedom	Total Vertical Force Hover Thrust (lb)	Average Propeller Blade Angle $\beta_{.75R}$ (deg)	Propeller Rotational Speed (rpm)	Stability Augmentation $K_{\dot{\Psi}}$ (sec)	Run Nos.	Fig. Nos.
Ψ*	51.5	25.8	7000	0.083	460,461,462	52
				none	444,445,446	53
	43.1	25.8	6400	0.389	464,465,466,467	54
				0.209	471	55
				0.083	475,476,477	56
				none	440,441,442,443	57
	0	25.8	0	0.389	463	58
				0.083	458	59
	51.5	29.2	6400	0.209	485,487	60
				0.083	489,490	61
				none	436,437,438	62
	0	29.2	0	none	435	63

TABLE I - Continued

Degrees of Freedom	Total Vertical Force Hover Thrust (lb)	Average Propeller Blade Angle $\beta_{.75R}$ (deg)	Propeller Rotational Speed (rpm)	Stability Augmentation $K_{\dot{\phi}}$ (sec)	Run Nos.	Fig. Nos.
ϕ-v_f	43.1	25.8	6400	0.055	137,139	64
				0.029	141,142,143	65
				0.016	145,146	66
				none	147,149,155	67
ϕ-Ψ-v_f	43.1	25.8	6400	0.055	188,189	68
ϕ-v_f-w_f	51.5	25.8	7000	0.055	219	69

*Mechanical spring in place. See Table III for spring rate.

**I_y = 2.52 slug-ft^2 for single-degree-of-freedom, θ runs only.

TABLE II. SCALE FACTORS FOR DYNAMIC MODEL SIMILARITY

Multiply full-scale property by scale factor to obtain model property.

		For $\lambda_L = 0.1453$
Linear dimension	λ_L	0.1453
Area	λ_L^2	2.112×10^{-2}
Volume, mass, force	λ_L^3	3.071×10^{-3}
Moment	λ_L^4	4.463×10^{-4}
Moment of inertia	λ_L^5	6.487×10^{-5}
Linear velocity	$\lambda_L^{0.5}$	0.3812
Linear acceleration	λ_L^0	1.000
Angular velocity	$\lambda_L^{-0.5}$	2.623
Angular acceleration	λ_L	0.1453
Time	$\lambda_L^{0.5}$	0.3812
Frequency	$\lambda_L^{-0.5}$	2.623
Reynolds number	$\lambda_L^{1.5}$	5.541×10^{-2}
Mach number	$\lambda_L^{0.5}$	0.3812

$$\text{where } \lambda_L = \frac{\text{model linear dimension}}{\text{full-scale linear dimension}}$$

TABLE III. MODEL GEOMETRIC AND INERTIA CHARACTERISTICS

Model cg located at pivot axis for all tests

Model	Equivalent Full Scale
W = 51.5 lb	W = 16,770 lb
I_x = 1.41 slug-ft^2	I_x = 21,750 slug-ft^2
I_y = 2.05 slug-ft^2	I_y = 31,600 slug-ft^2
I_z = 2.97 slug-ft^2	I_z = 45,800 slug-ft^2
I_{xz} = 0	I_{xz} = 0
η = 6.1° nose down from fuselage reference line	η = 6.1° nose down from fuselage reference line
Pivot axis located at WL 20.20 FS 45.30	cg located at WL 139 FS 312

$k_{\theta_m} = 21.4 \frac{\text{ft-lb}}{\text{rad}}$ (one-degree-of-freedom, θ runs only)

$k_{\phi_m} = 9.1 \frac{\text{ft-lb}}{\text{rad}}$ (one-degree-of-freedom, ϕ runs only)

$k_{\psi_m} = 7.7 \frac{\text{ft-lb}}{\text{rad}}$ (one-degree-of-freedom, Ψ runs only)

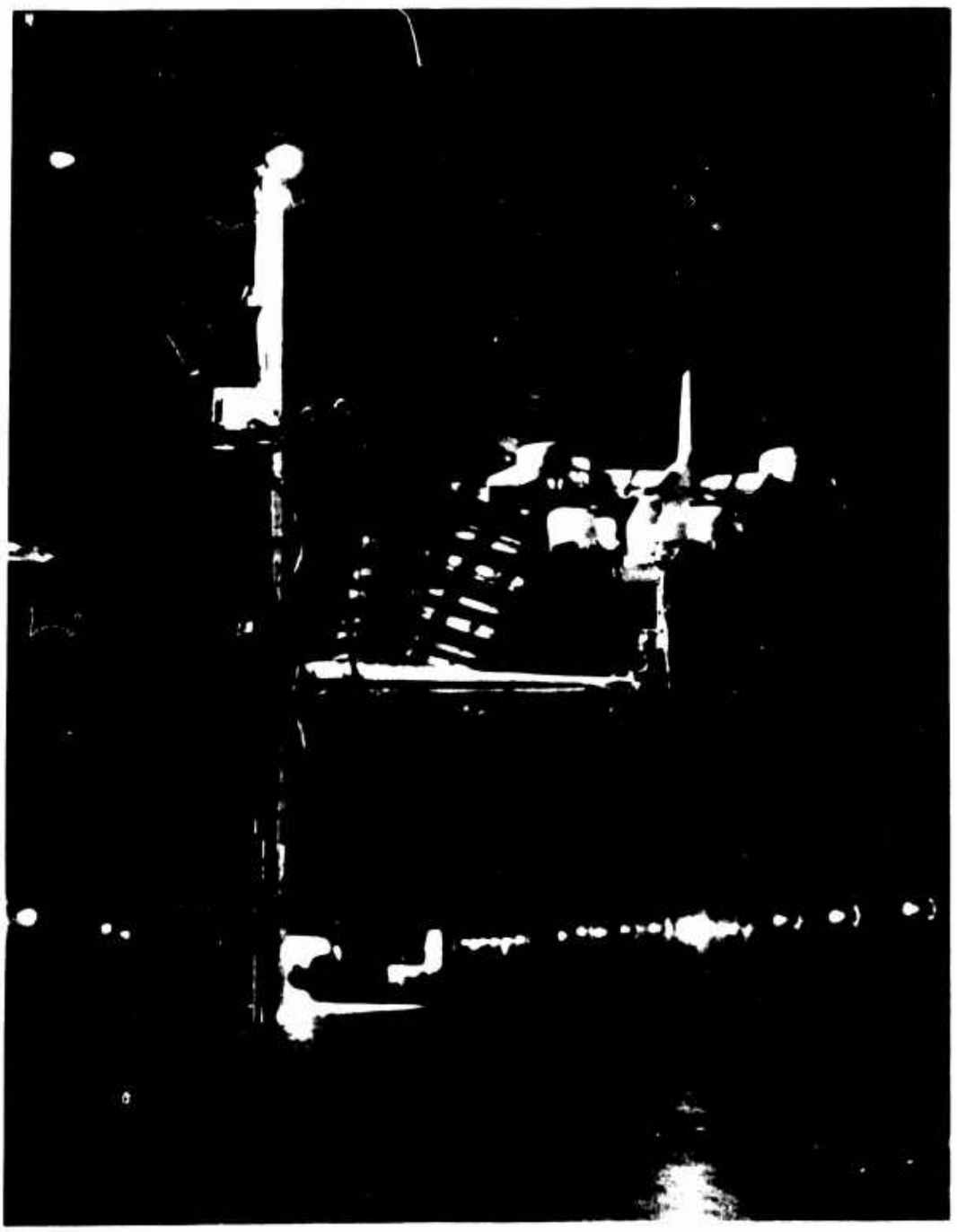

Figure 1. Photograph of Princeton Dynamic Model Track Showing Model Mounted on Longitudinal Dynamic Testing Apparatus.

Figure 2. Photograph of 0.145 Scale Quad Configuration Dynamic Model.

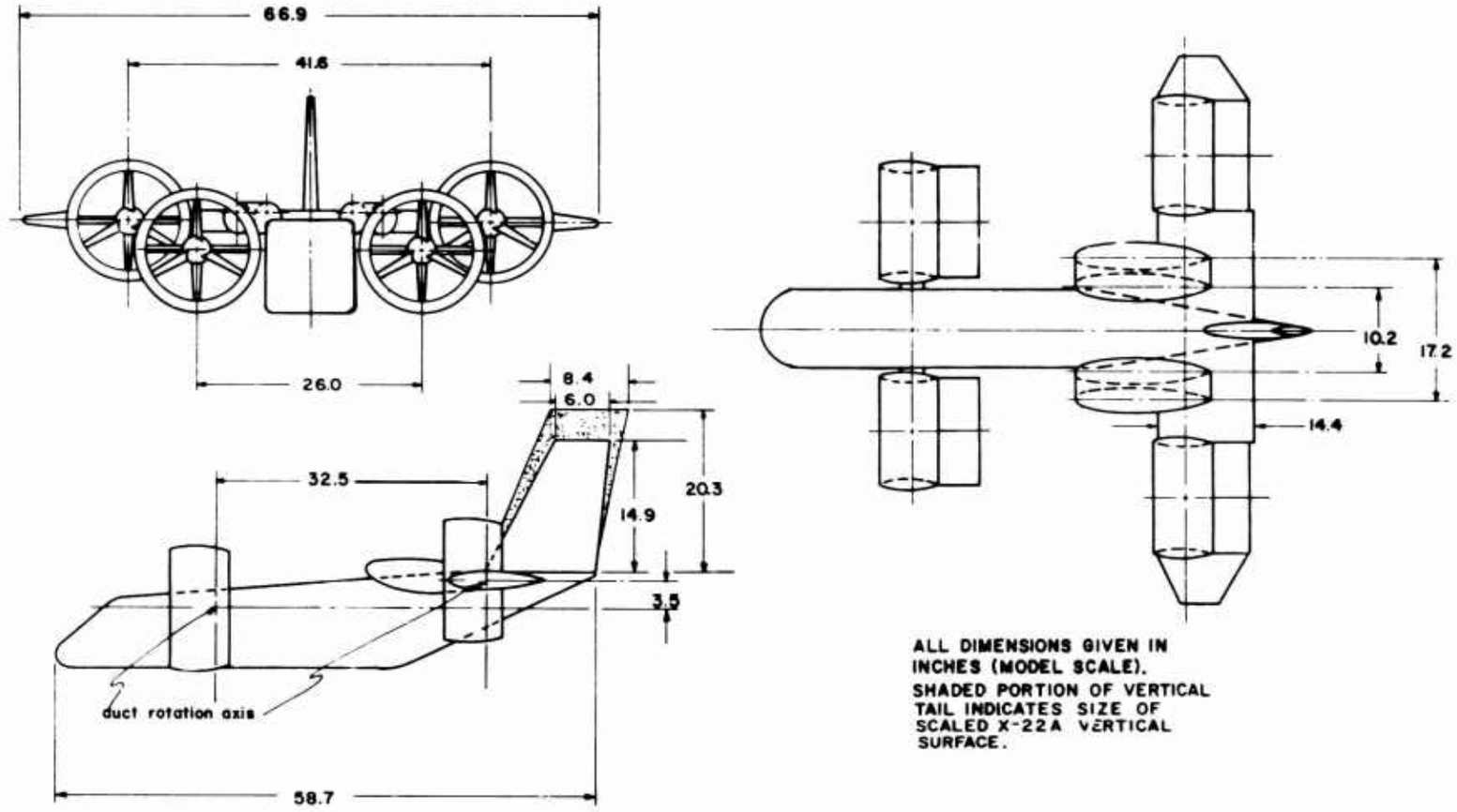

Figure 3. General Arrangement Drawing of Quad Model in X-22A Configuration.

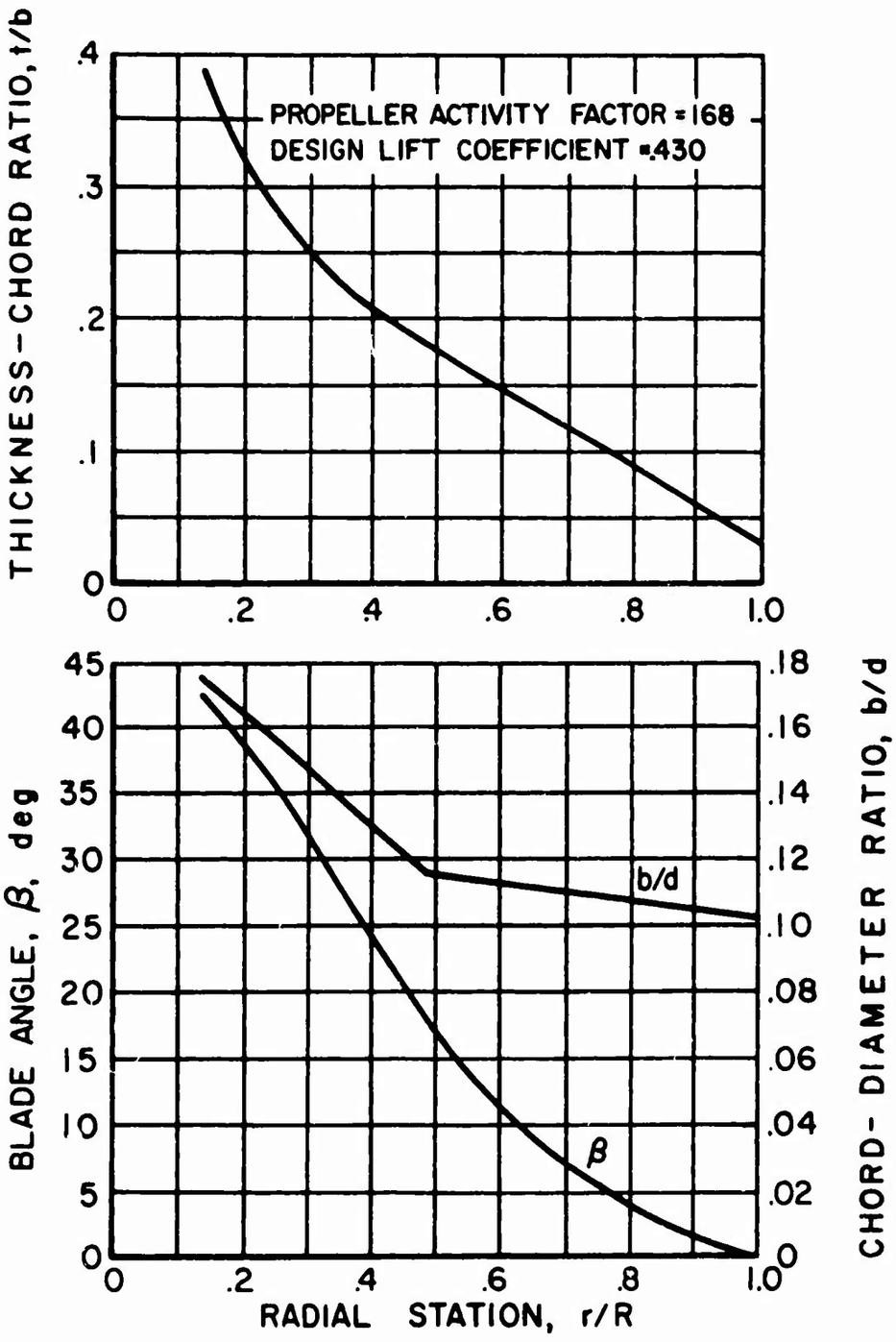

Figure 4. Geometric Characteristics of Three-Bladed Model Propellers.

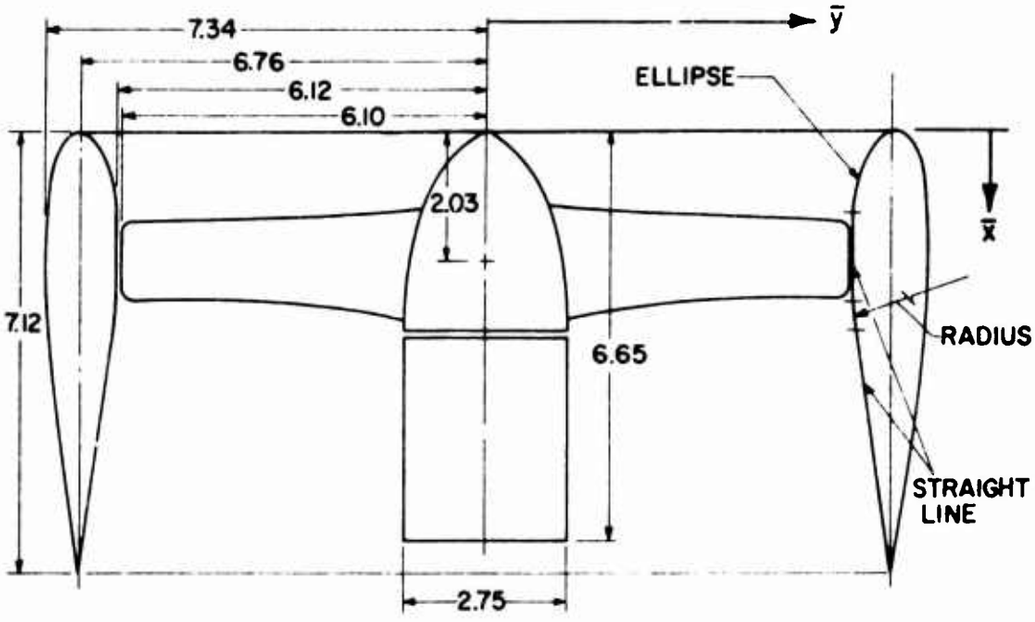

ALL DIMENSIONS ON ABOVE DRAWING IN INCHES (MODEL SCALE)

X-22A DUCT OUTER ORDINATES (FULL SCALE)	
$\bar{x}$	$\bar{y}$
0	47.625
0.613	48.695
1.225	49.096
2.450	49.609
3.675	49.953
4.900	50.205
7.350	50.535
9.800	50.710
10.250	—
12.250	50.779
14.700	50.763
17.750	—
19.600	50.552
23.700	—
24.500	50.164
29.400	49.649
34.300	49.038
39.200	48.344
44.100	47.576
46.550	47.160
49.000	46.722

Figure 5. Geometric Characteristics of Scaled Model Ducts.

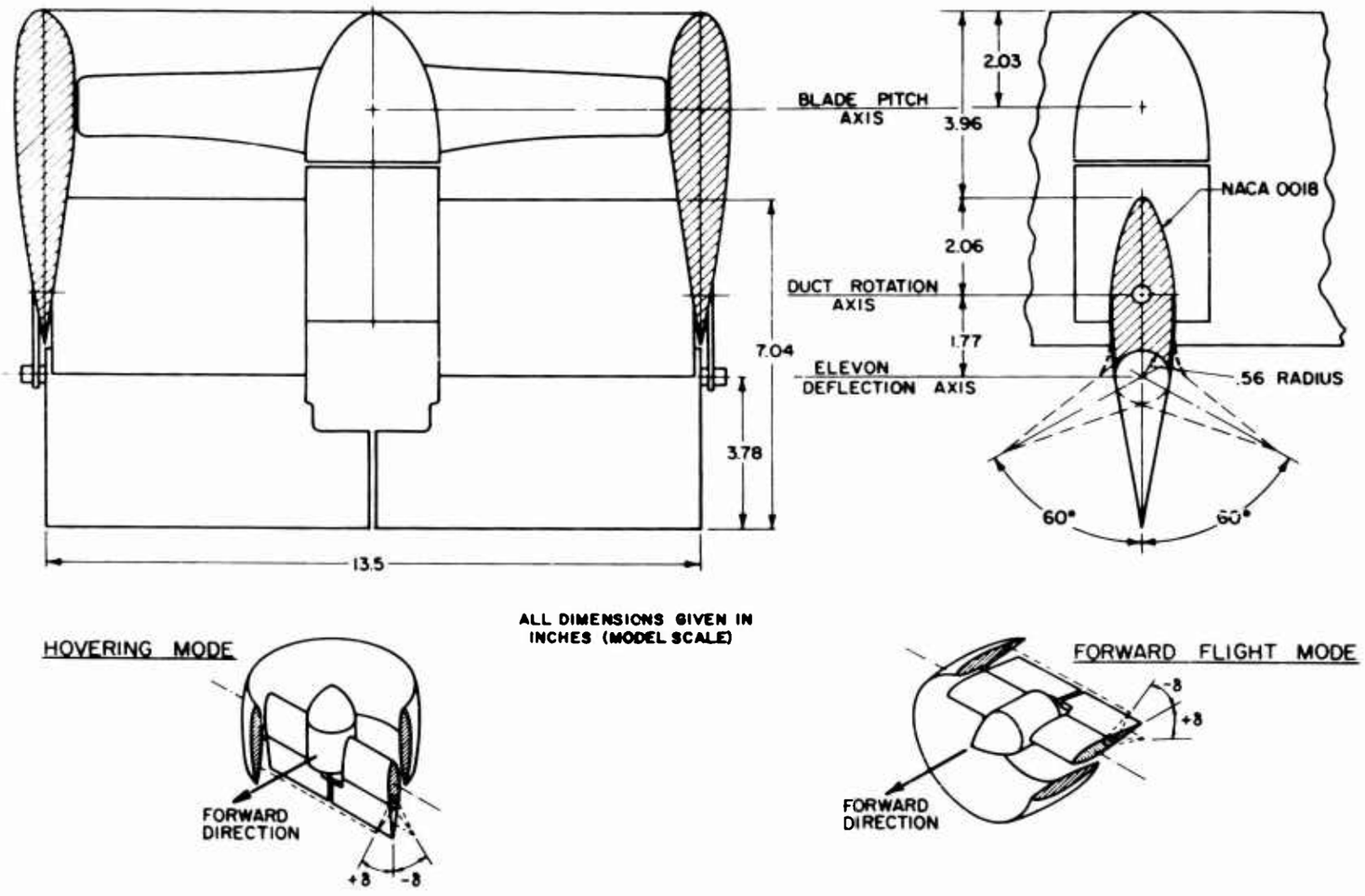

Figure 6. Geometric Characteristics and Reference Locations for Model Duct System.

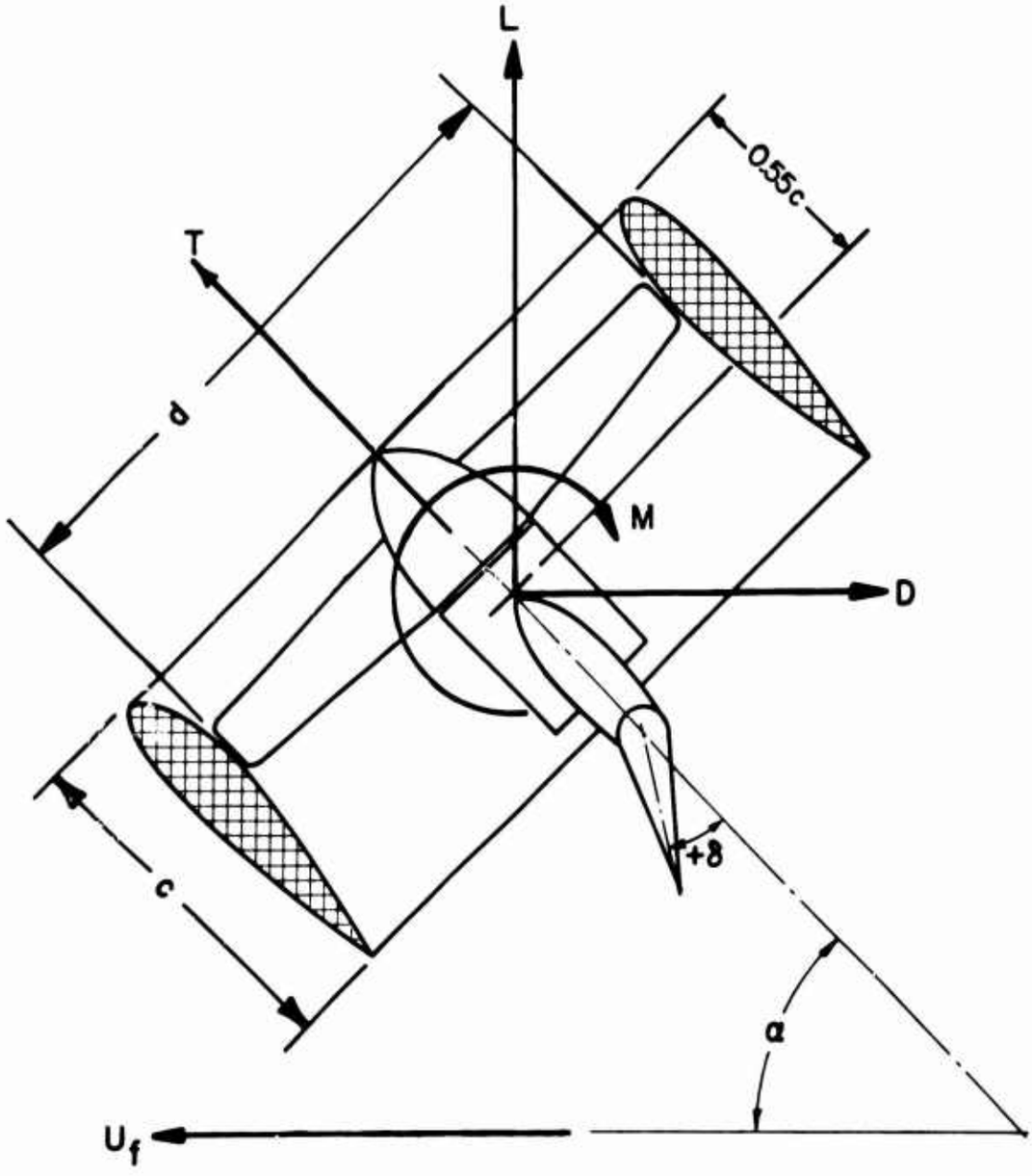

Figure 7. Axis System for Isolated Duct Static Tests.

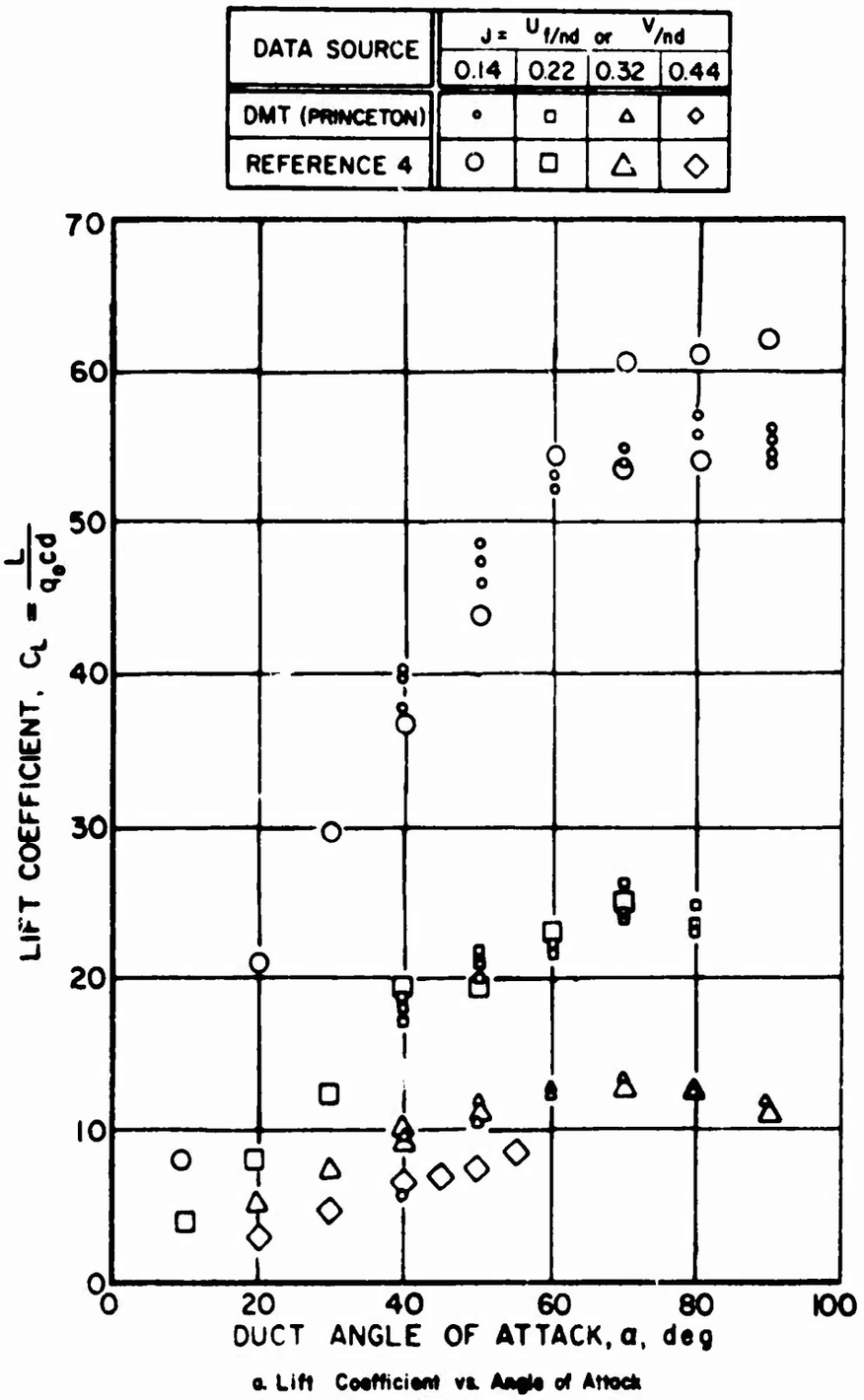

a. Lift Coefficient vs. Angle of Attack

Figure 8. Comparison of Isolated Ducted Propeller Model Data to Full-Scale Data of Reference 4. $\beta_{.75R} = 19.1°$, $\delta = 0$.

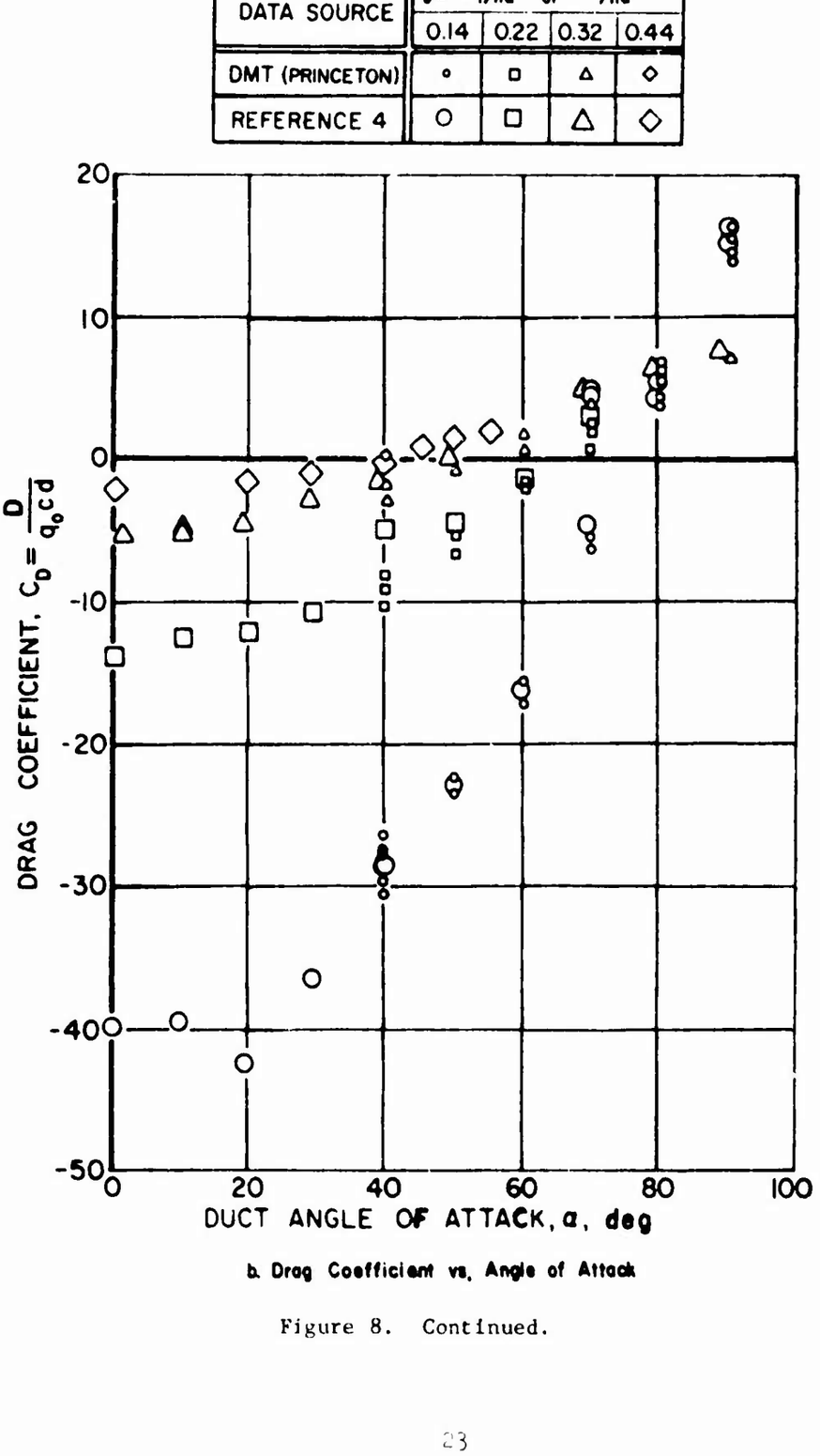

b. Drag Coefficient vs. Angle of Attack

Figure 8. Continued.

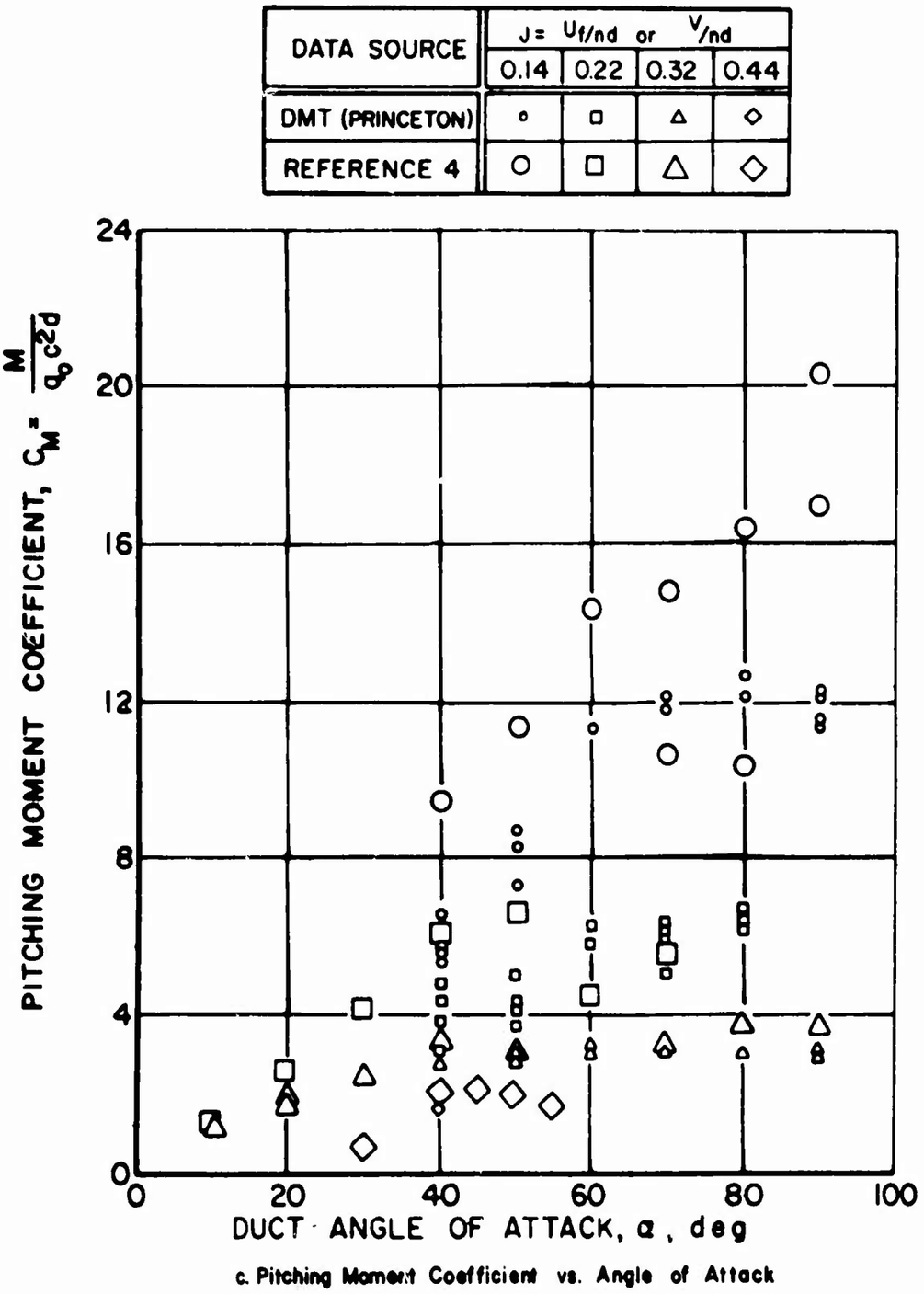

c. Pitching Moment Coefficient vs. Angle of Attack

Figure 8. Concluded.

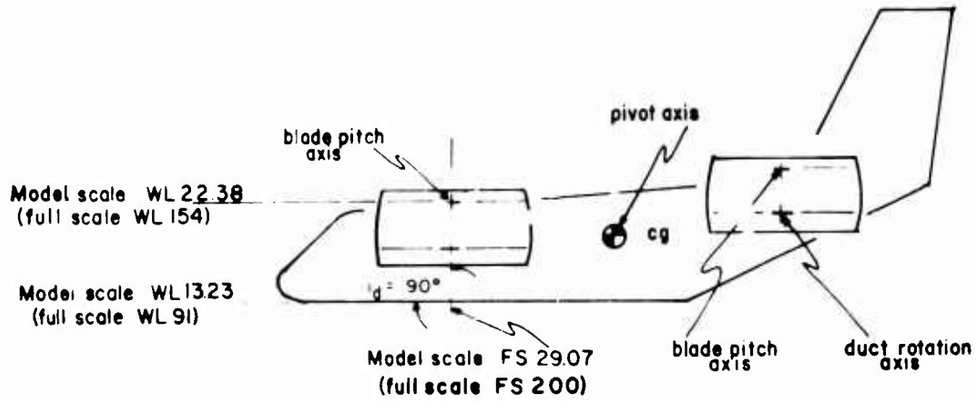

Note: 1.) Reference FS and WL locations shown do not change with duct rotation.

2) Pivot point is reference point for aerodynamic measurements of complete aircraft.

3) Model angular motions measured about pivot point.

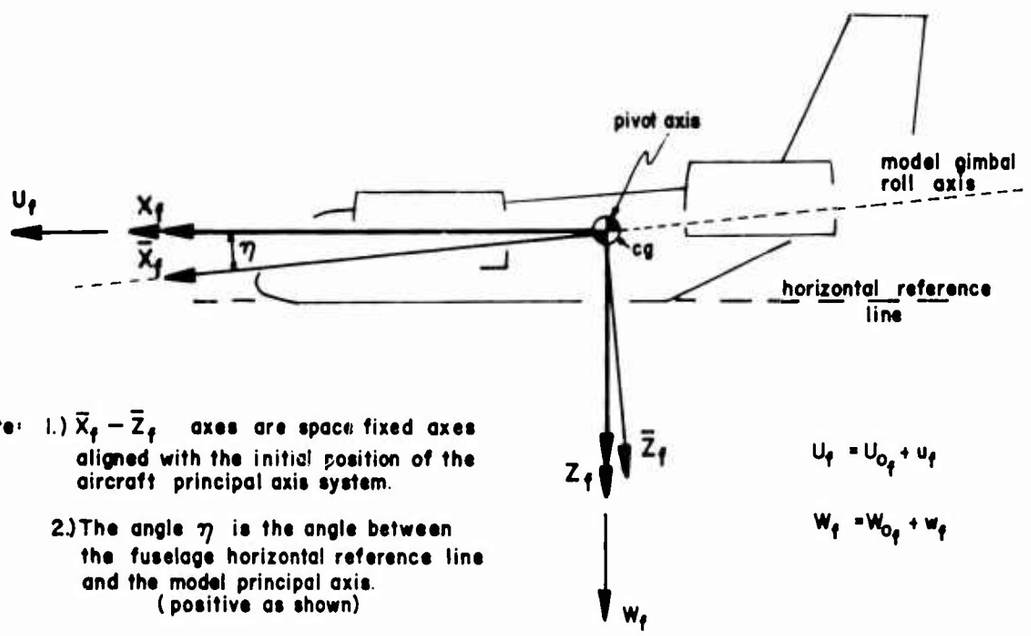

Note: 1.) $\bar{X}_f - \bar{Z}_f$ axes are space fixed axes aligned with the initial position of the aircraft principal axis system.

2.) The angle η is the angle between the fuselage horizontal reference line and the model principal axis. (positive as shown)

Figure 9. Model Reference Stations, Location of Model cg and Axes Systems.

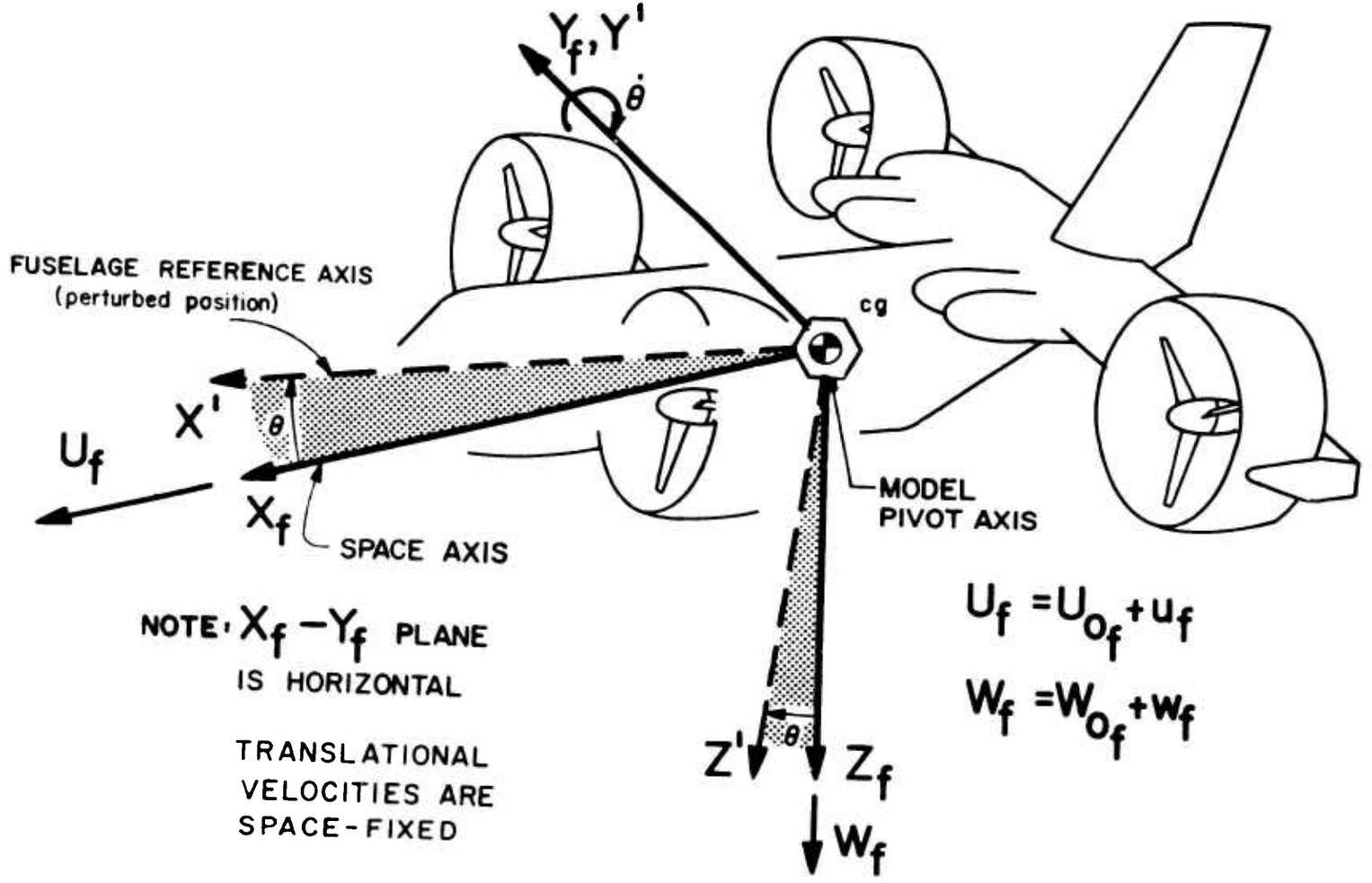

Figure 10. Axis System for Longitudinal Transient Response Data.

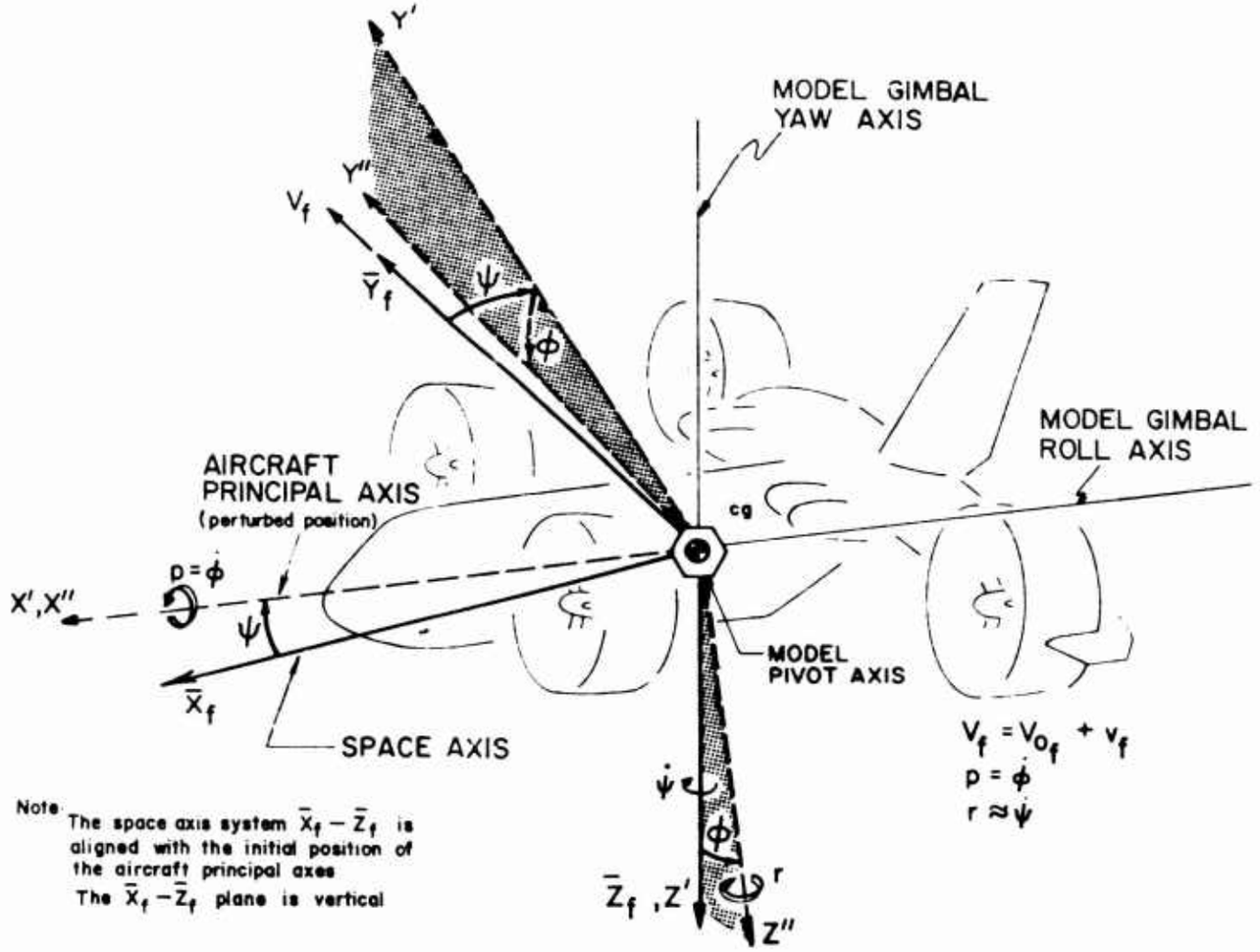

Figure 11. Axis System for Lateral/Directional Transient Response Data.

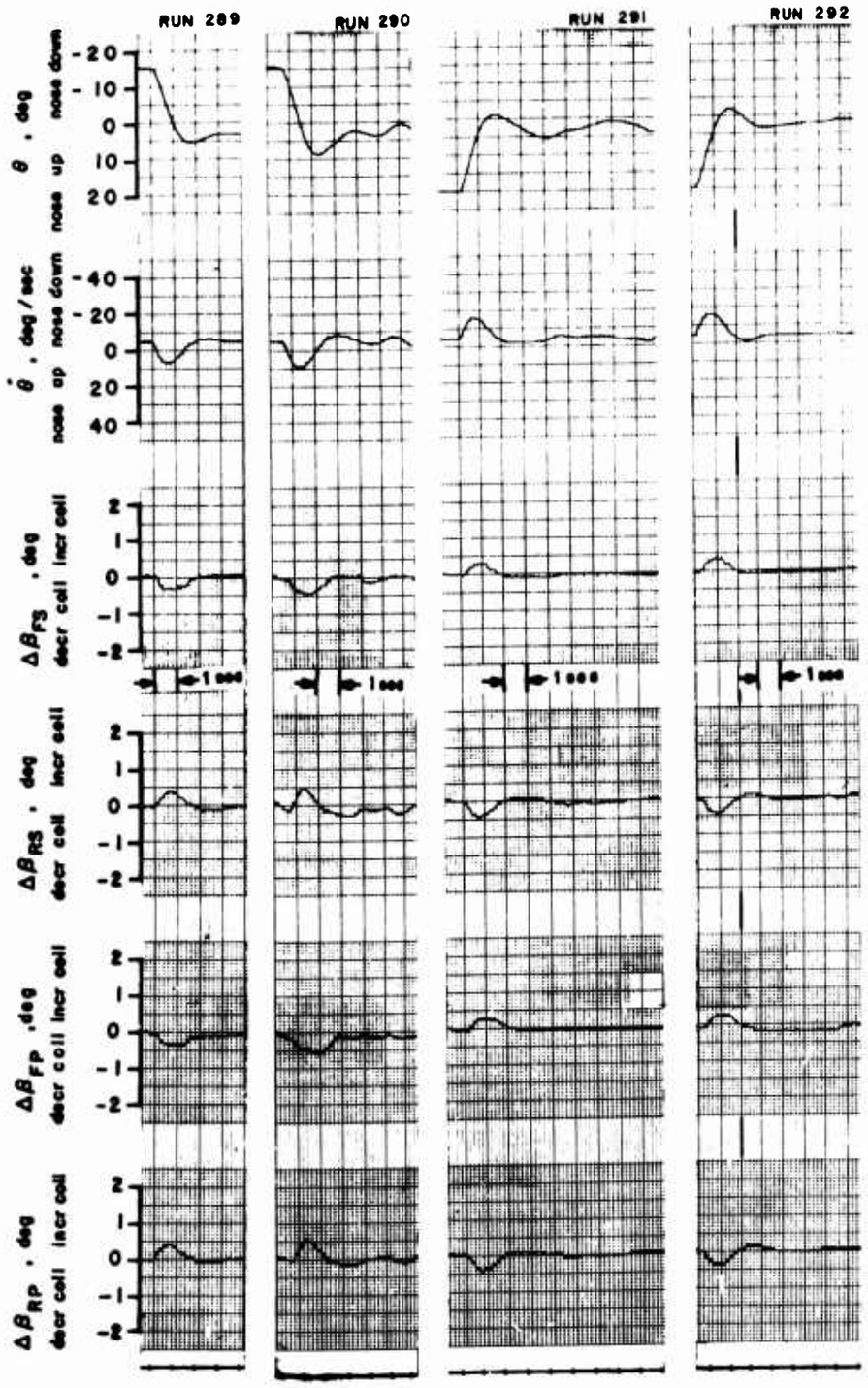

Figure 12. Longitudinal Transient Response. One Degree of Freedom, θ. $K_{\dot{\theta}} = 0.044$ sec .

$\beta_{.75R} = 25.8°$, rpm = 7000.

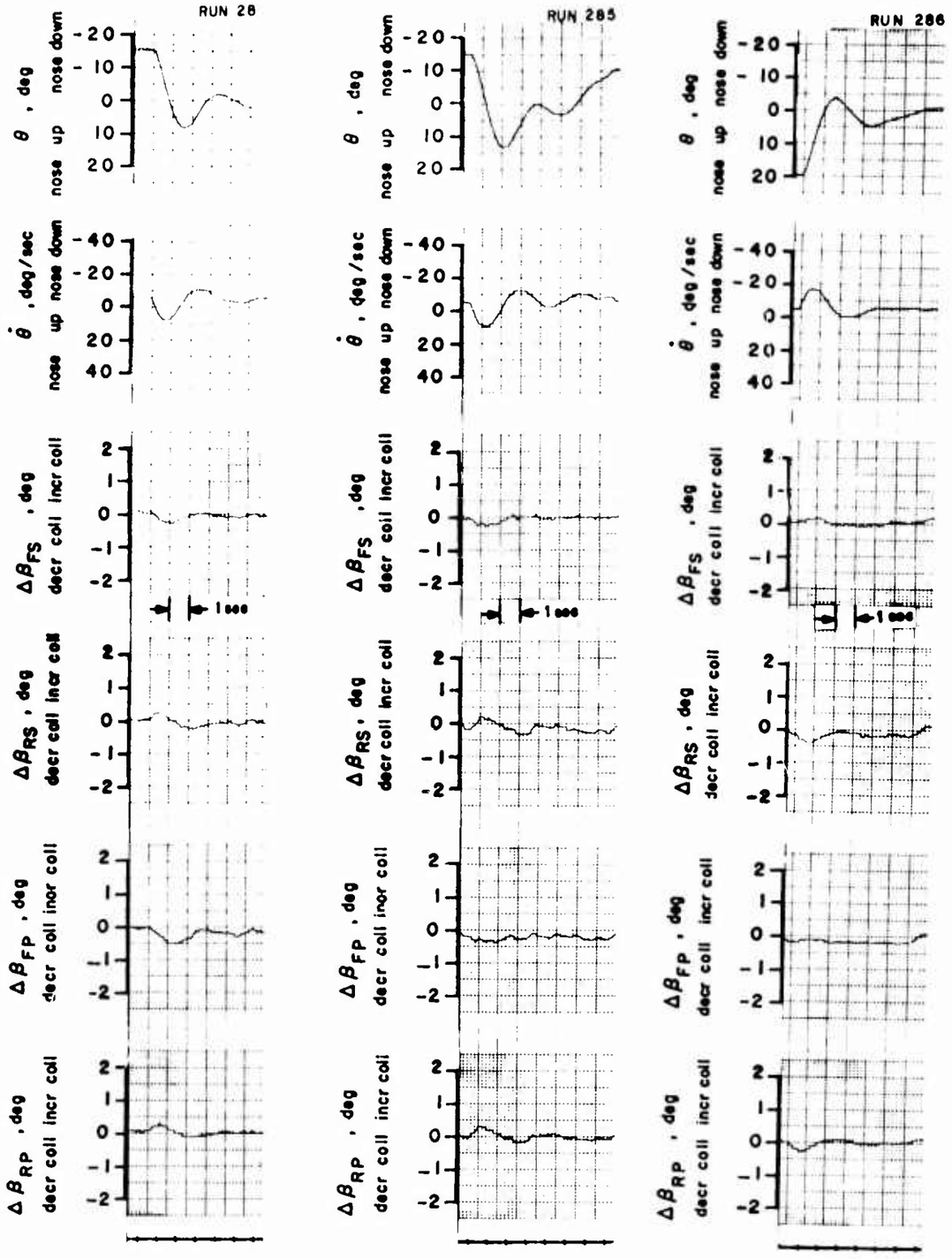

Figure 13. Longitudinal Transient Response. One Degree of Freedom, θ. $K_{\theta}^{\bullet} = 0.030$ sec^{-1}.

$\theta_{.75R} = 25.8°$, rpm = 7000.

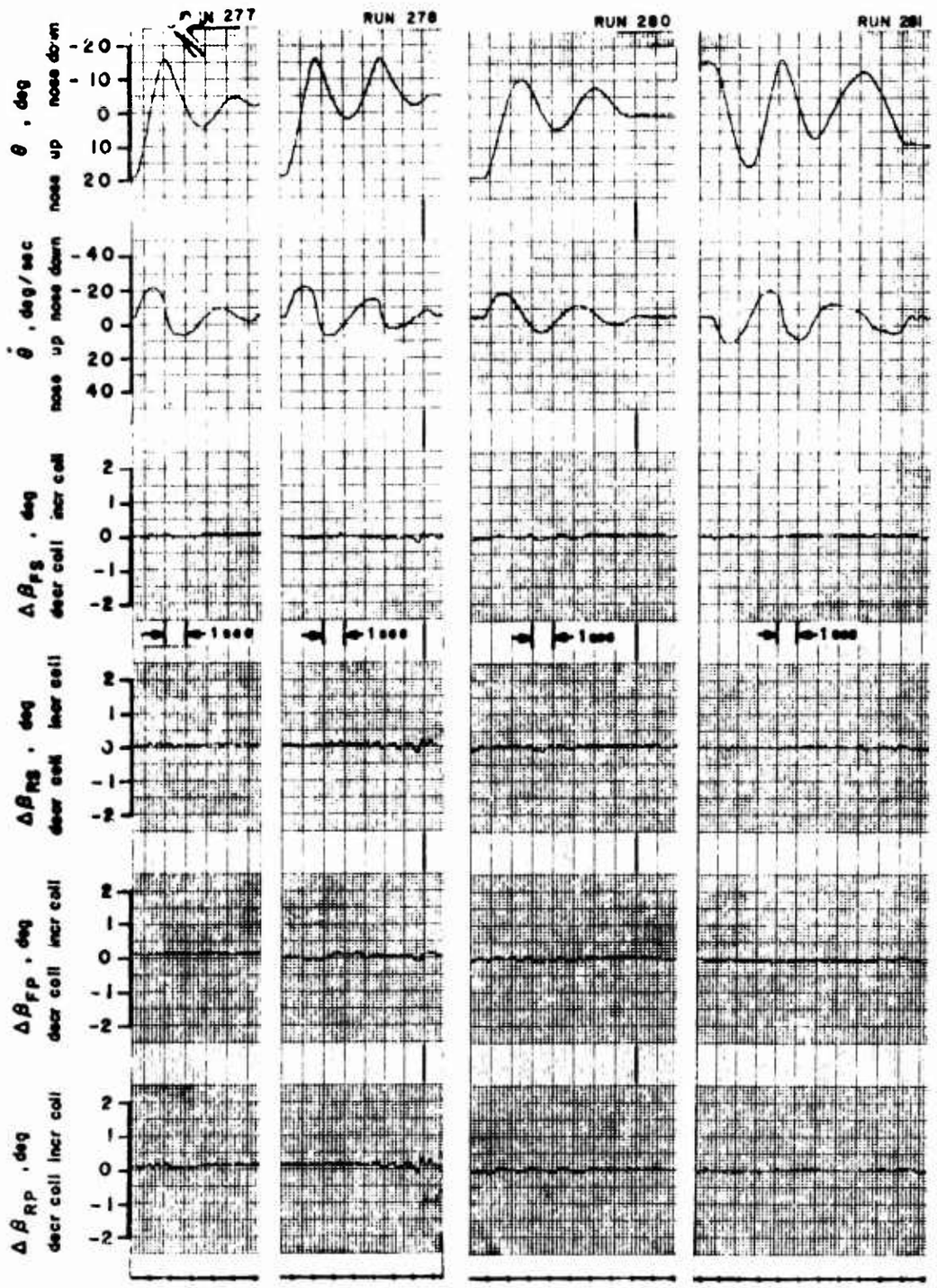

Figure 14. Longitudinal Transient Response. One Degree of Freedom, θ. No Stability Augmentation.
$\delta_{.75R}$ = 25.8°, rpm = 7000.

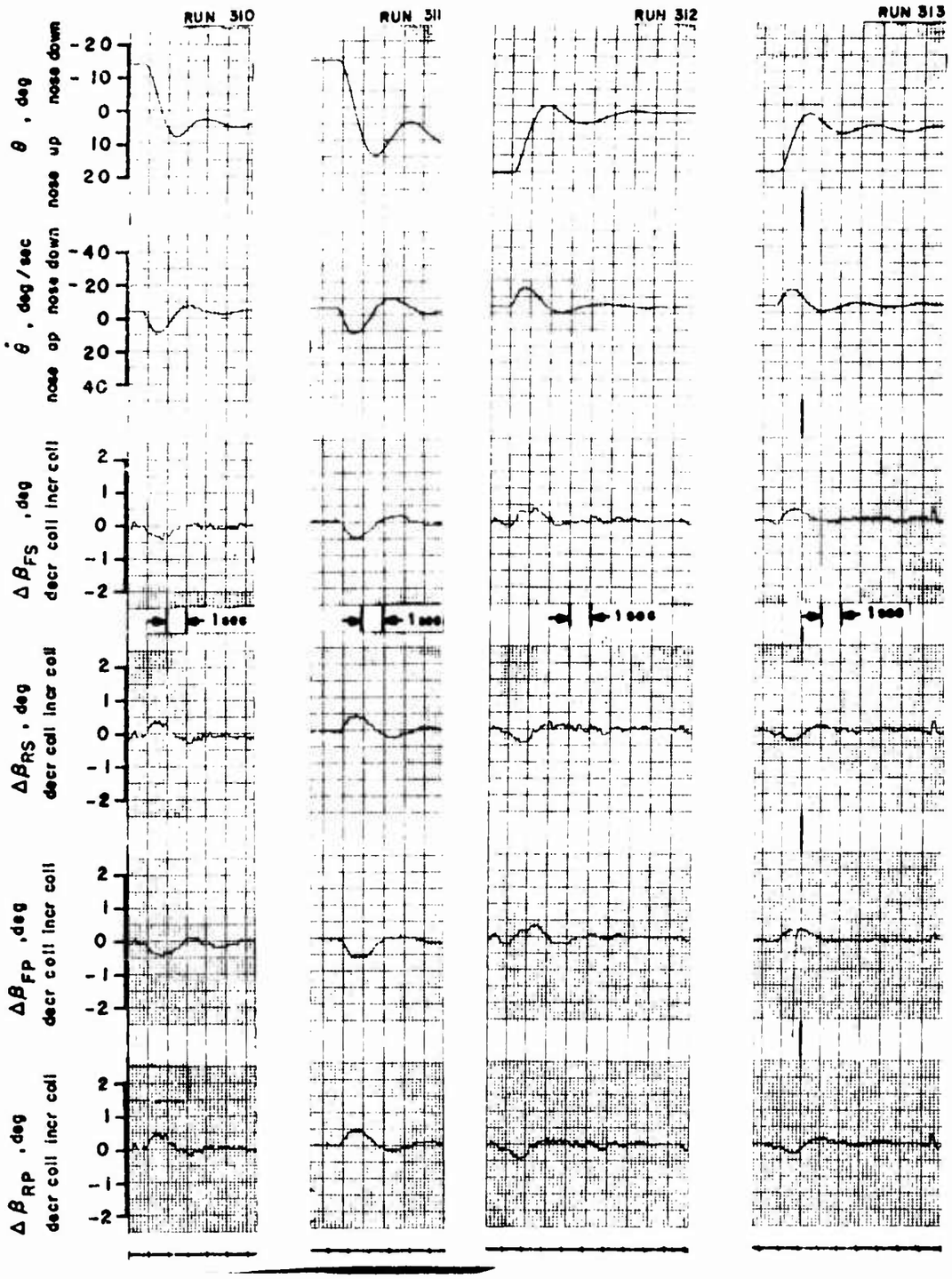

Figure 15. Longitudinal Transient Response. One Degree of Freedom, θ.
$K_{\dot{\theta}}$ = 0.044 sec .
$\beta_{.75R}$ = 29.2°, rpm = 6400.

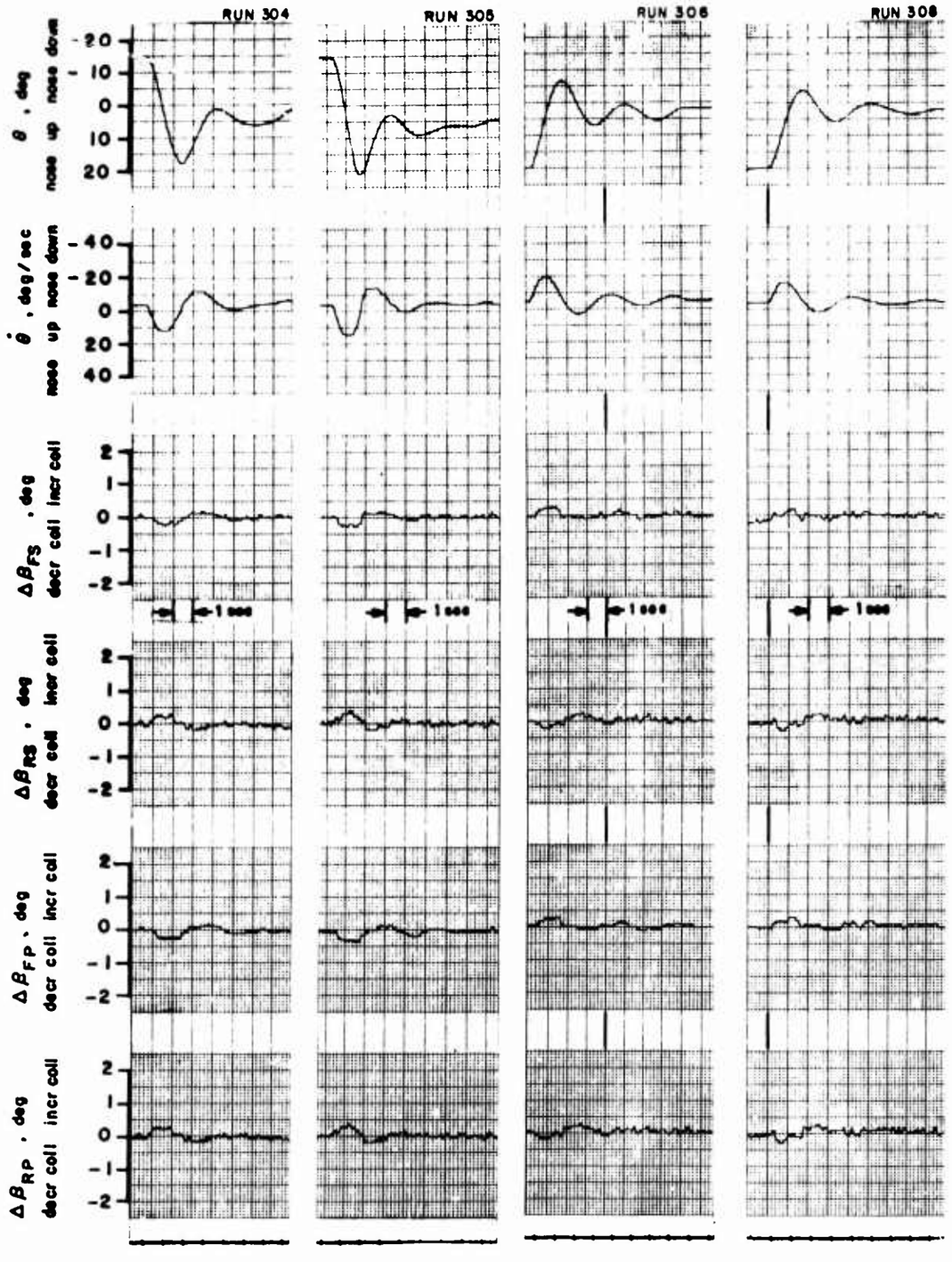

Figure 16. Longitudinal Transient Response. One Degree of Freedom, θ.
$K_{\dot{\theta}}^{*} = 0.030$ sec .
$\beta_{.75R} = 29.2°$, rpm = 6400.

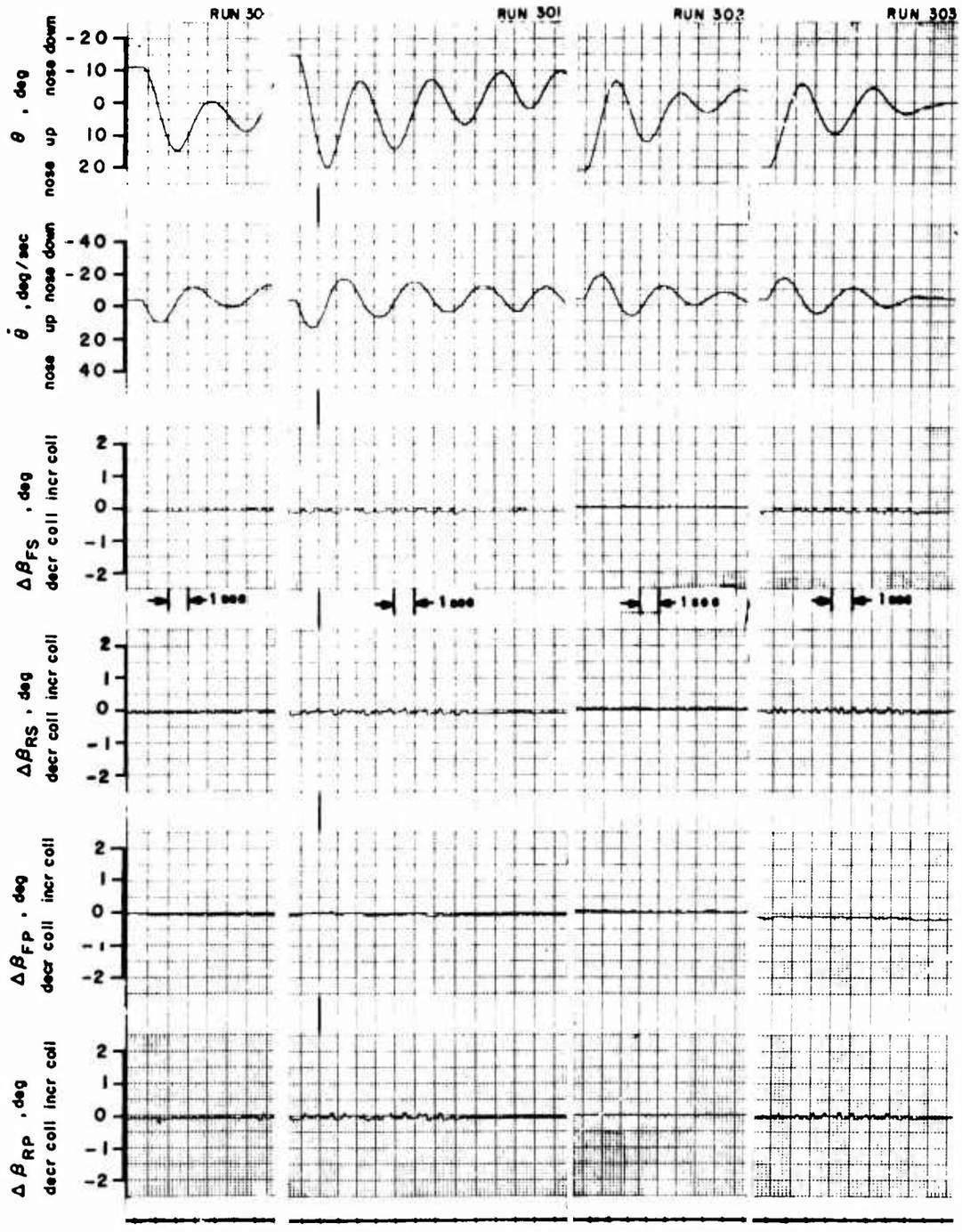

Figure 17. Longitudinal Transient Response. One Degree of Freedom, θ. No Stability Augmentation.
$\beta_{.75R}$ = 29.2°, rpm = 6400.

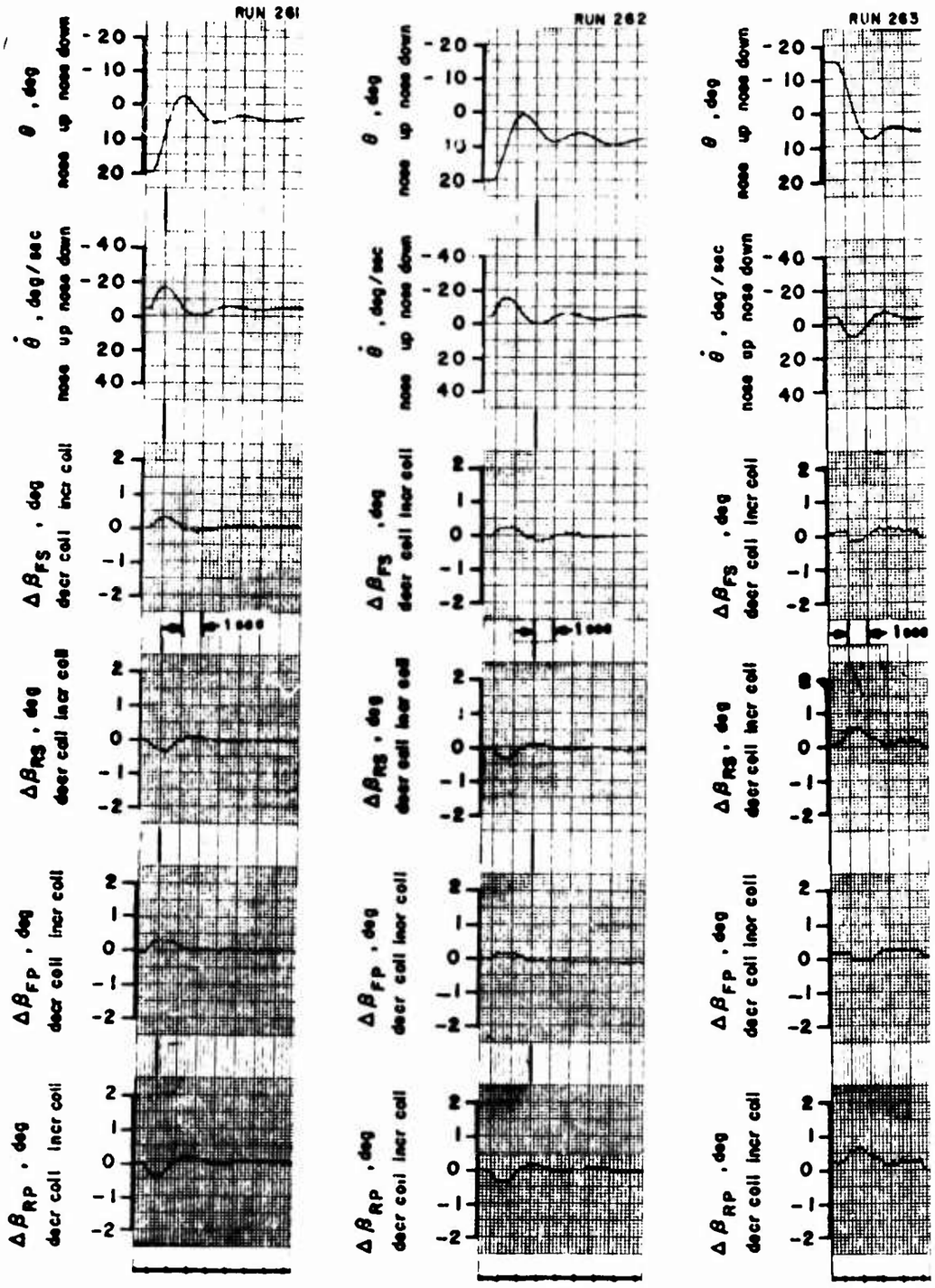

Figure 18. Longitudinal Transient Response. One Degree of Freedom, θ.
$K_{\dot{\theta}}$ = 0.044 sec .
$\theta_{.75R}$ = 25.8°, rpm = 6400.

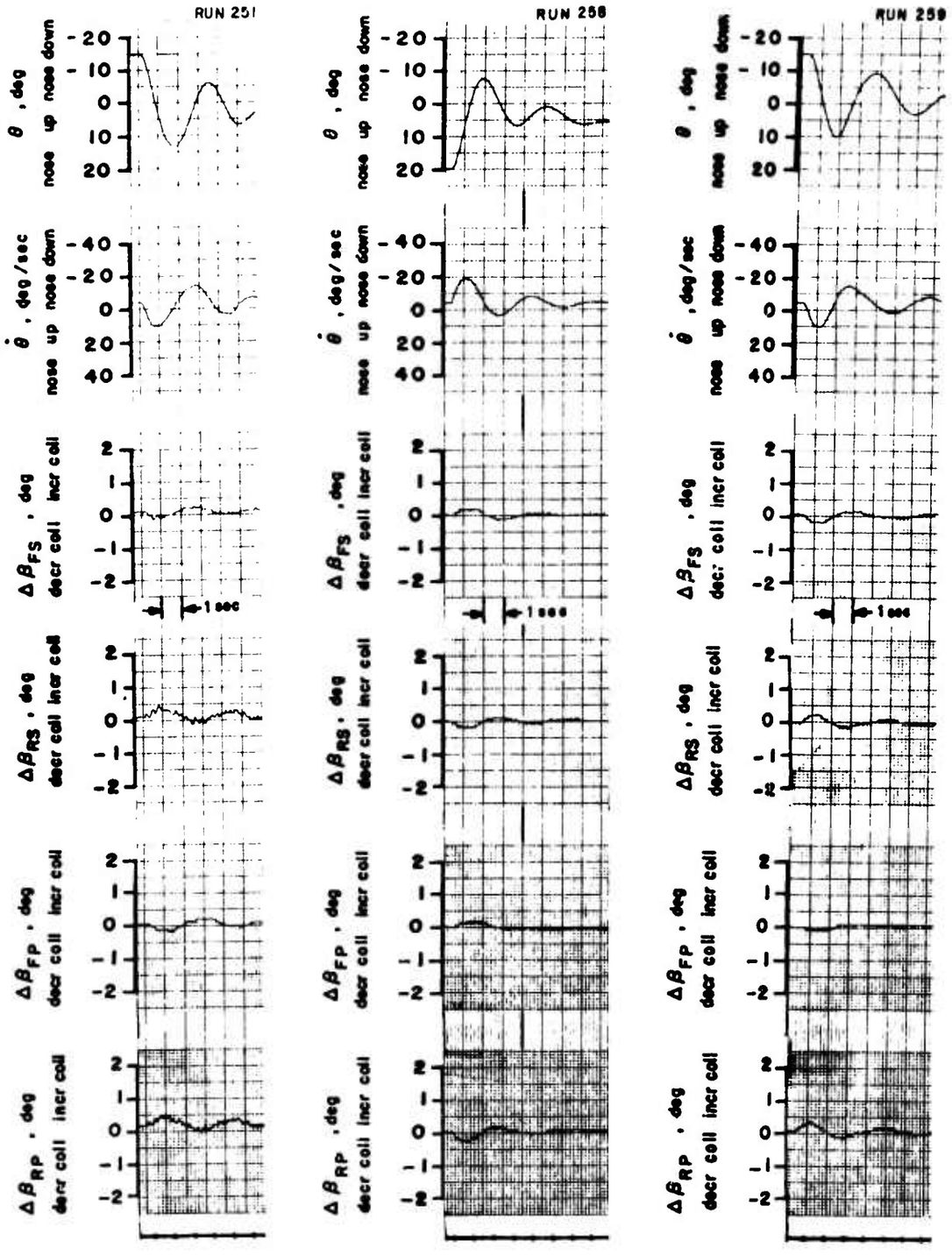

Figure 19. Longitudinal Transient Response. One Degree of Freedom, θ. $K_{\dot{\theta}}$ = 0.030 sec .

$\beta_{.75R}$ = 25.8°, rpm = 6400.

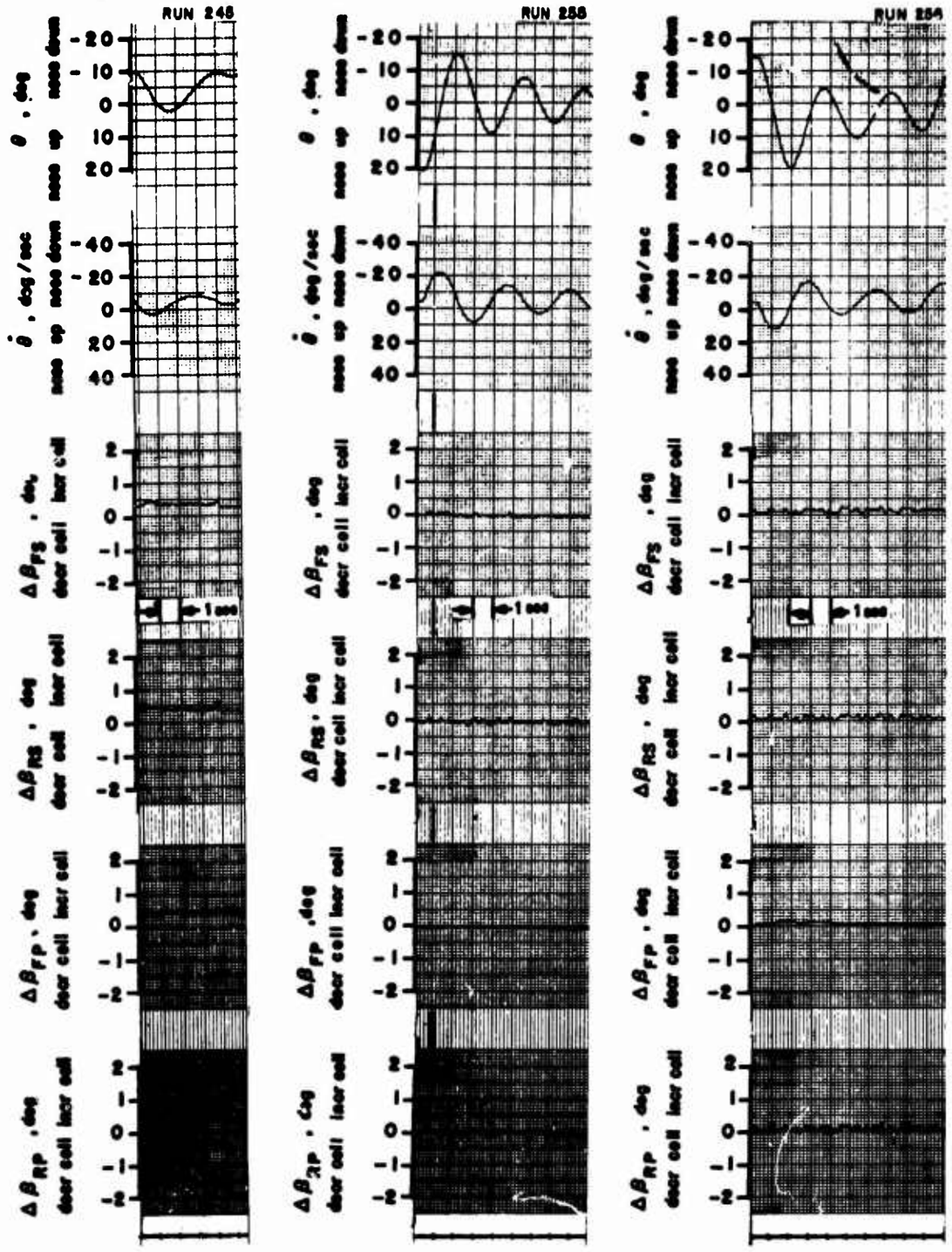

Figure 20. Longitudinal Transient Response. One Degree of Freedom, θ. No Stability Augmentation.
$\beta_{.75R}$ = 25.8°, rpm = 6400.

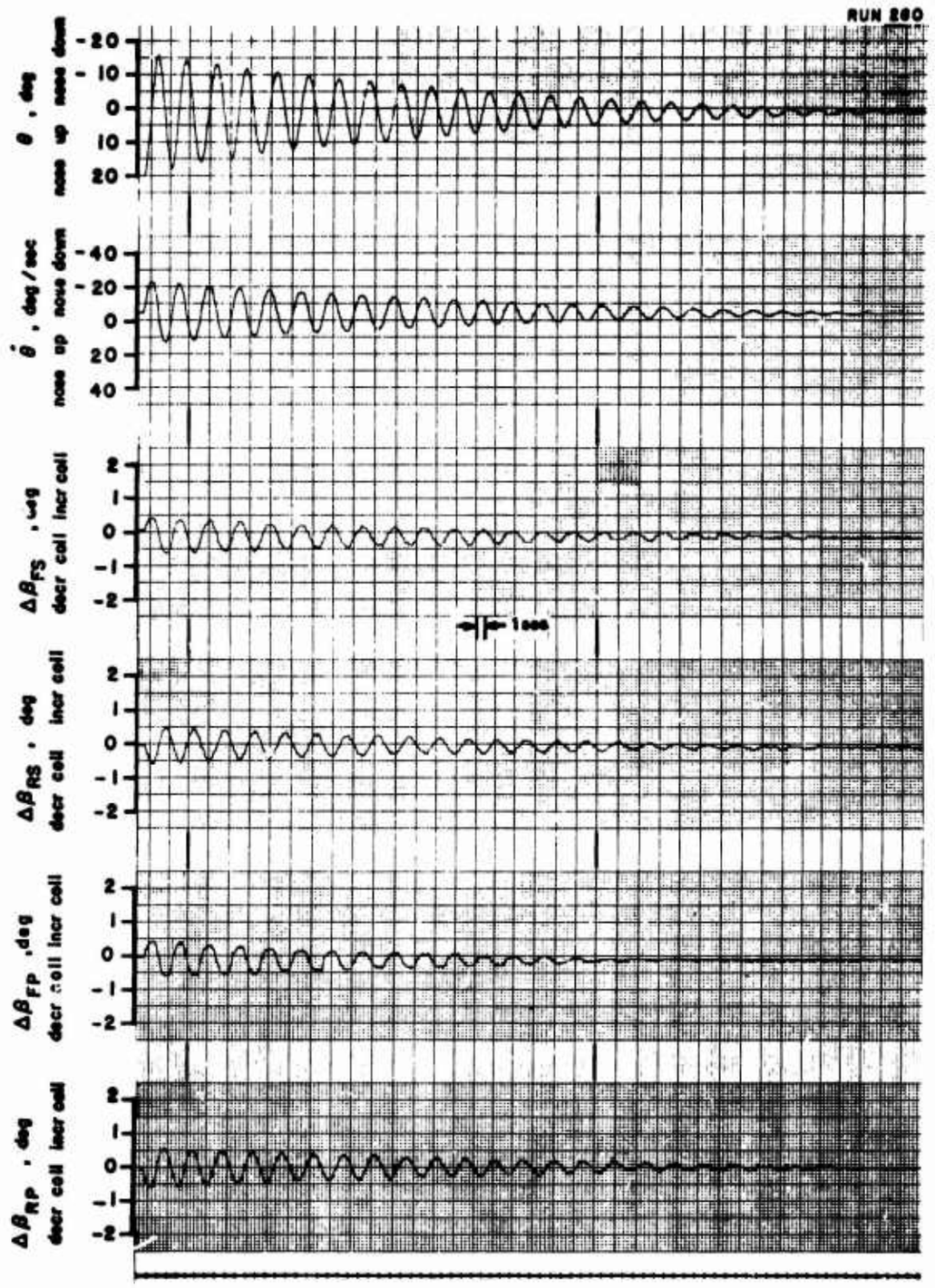

Figure 21. Longitudinal Transient Response. One Degree of Freedom, θ.
$K_{\theta}^{\cdot} = 0.044$ sec .
$\beta_{.75R} = 25.8°$, rpm = zero.

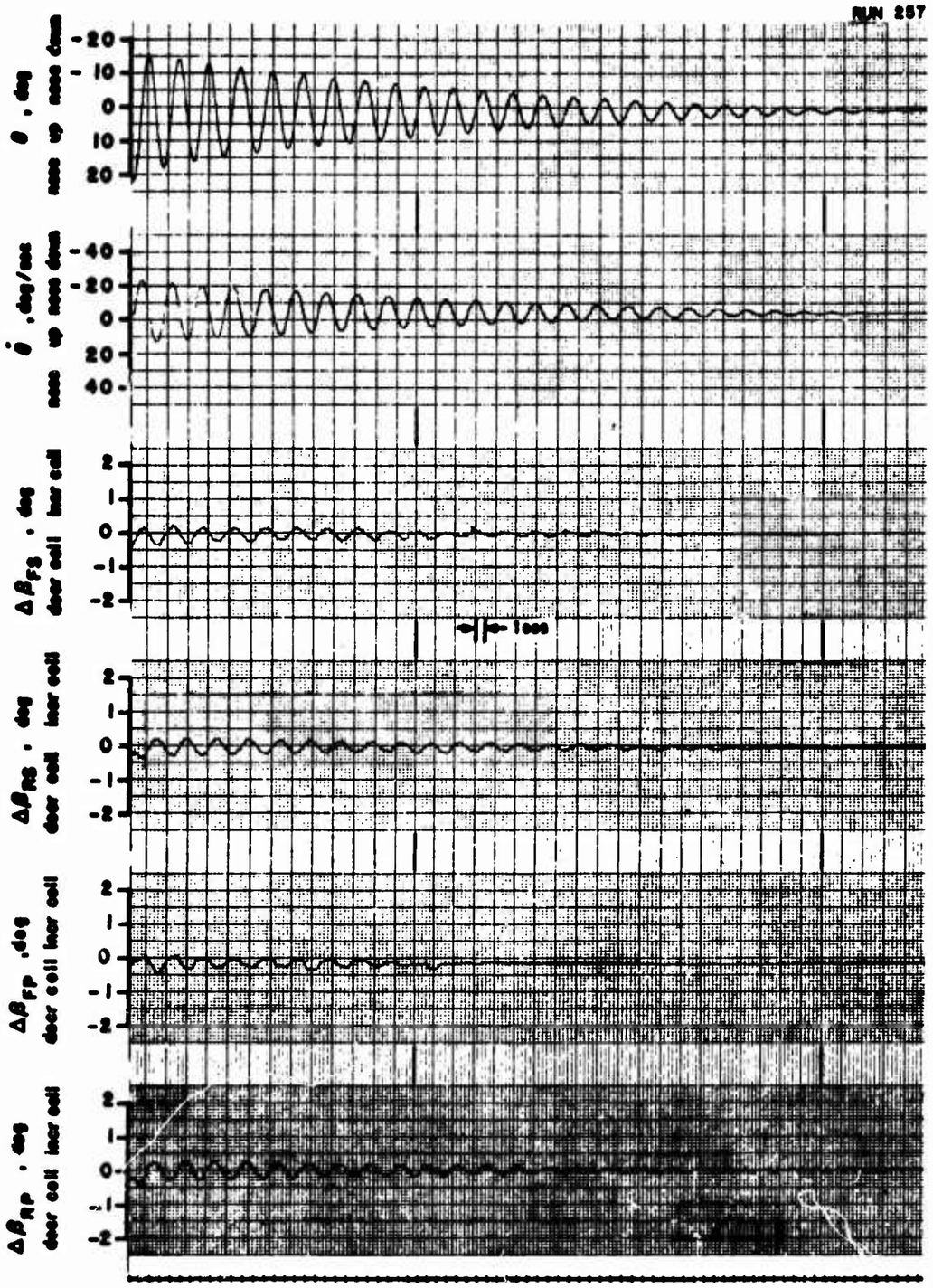

Figure 22. Longitudinal Transient Response. One Degree of Freedom, θ.
$K_{\dot{\theta}}$ = 0.030 sec .
$\beta_{.75R}$ = 25.8°, rpm = zero.

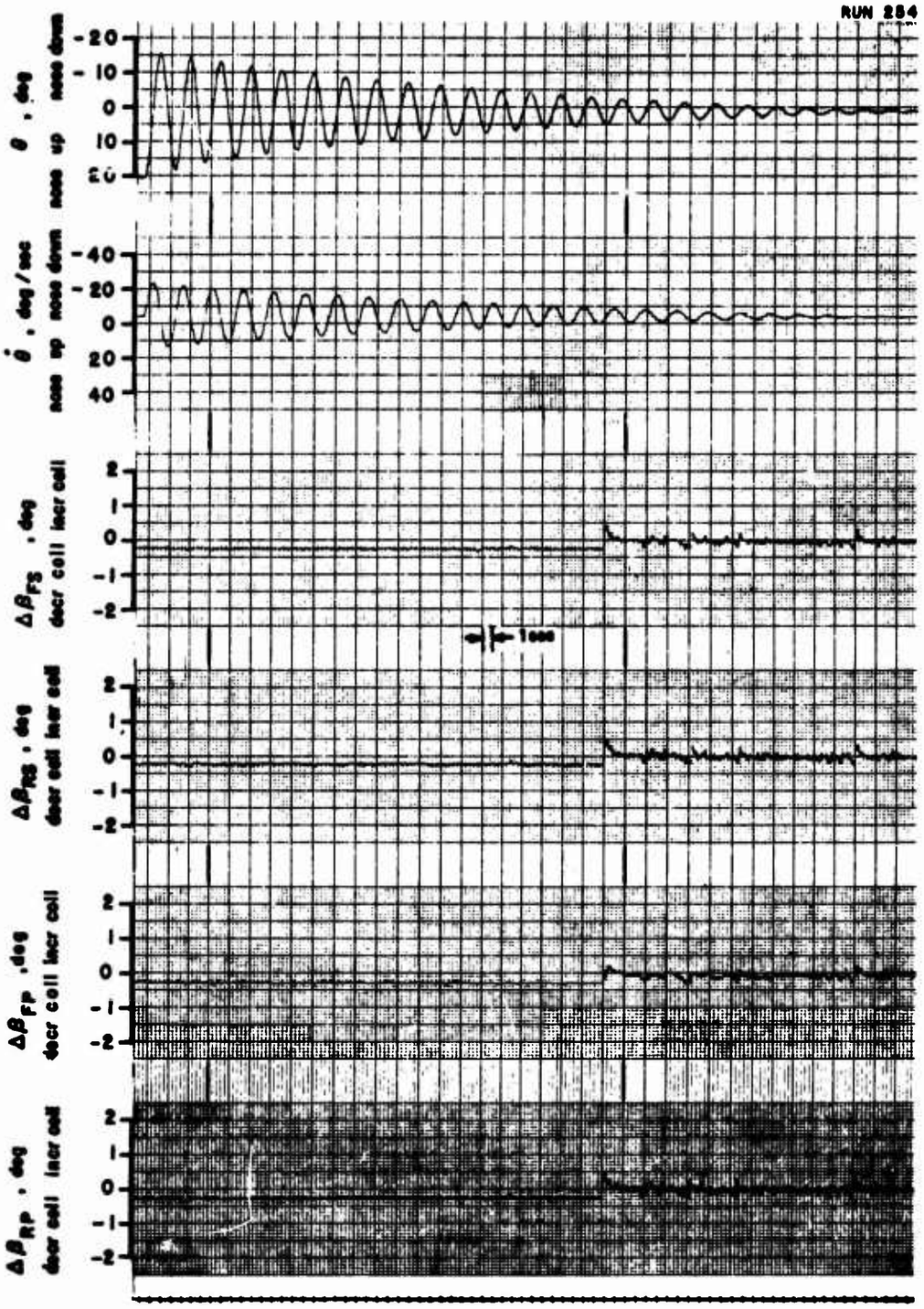

Figure 23. Longitudinal Transient Response. One Degree of Freedom, θ. No Stability Augmentation. $\beta_{.75R}$ = 25.8°, rpm = zero.

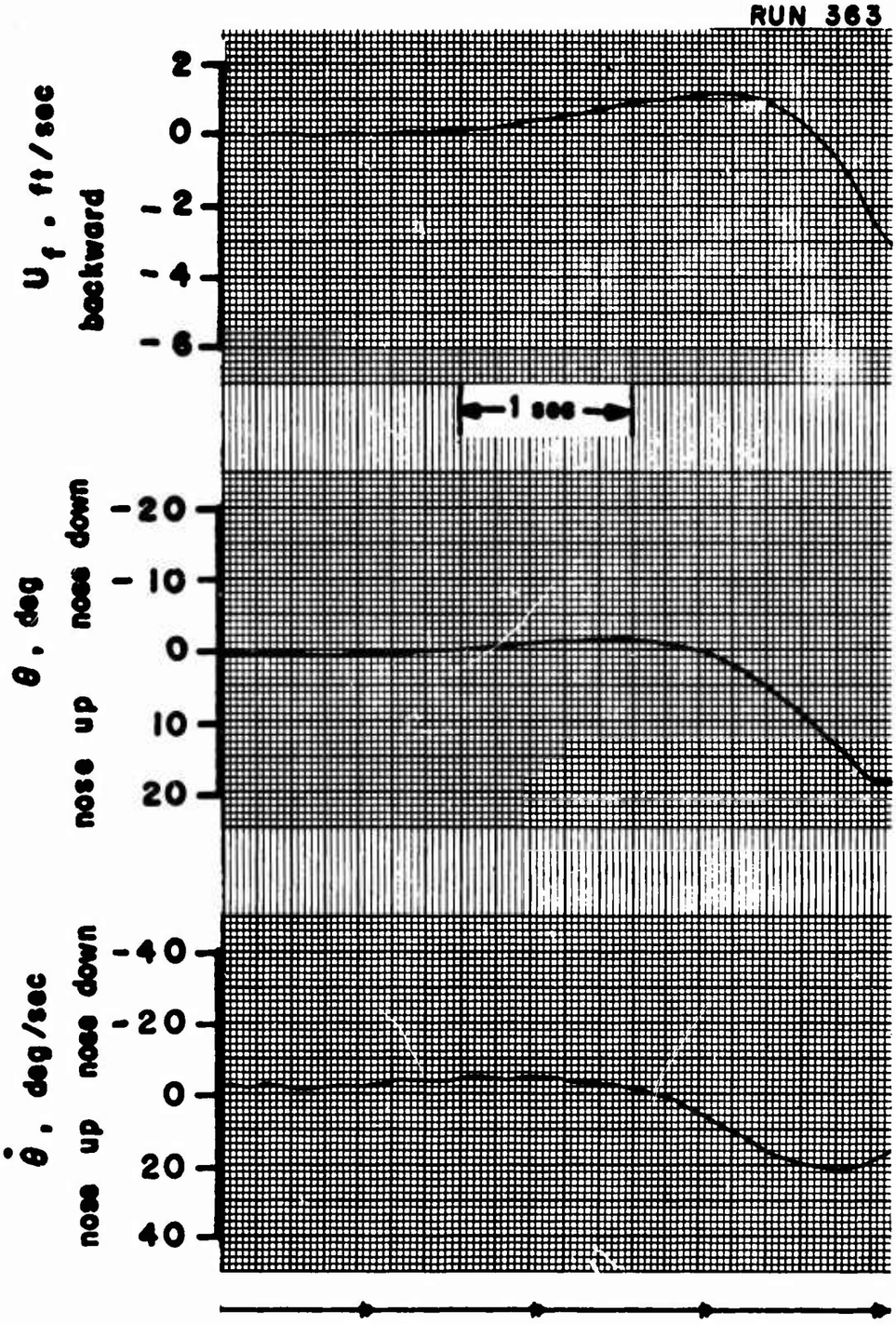

Figure 24. Longitudinal Transient Response. Two Degrees of Freedom, θ-U_f. No Stability Augmentation. $\beta_{.75R}$ = 25.8°, rpm = 7000.

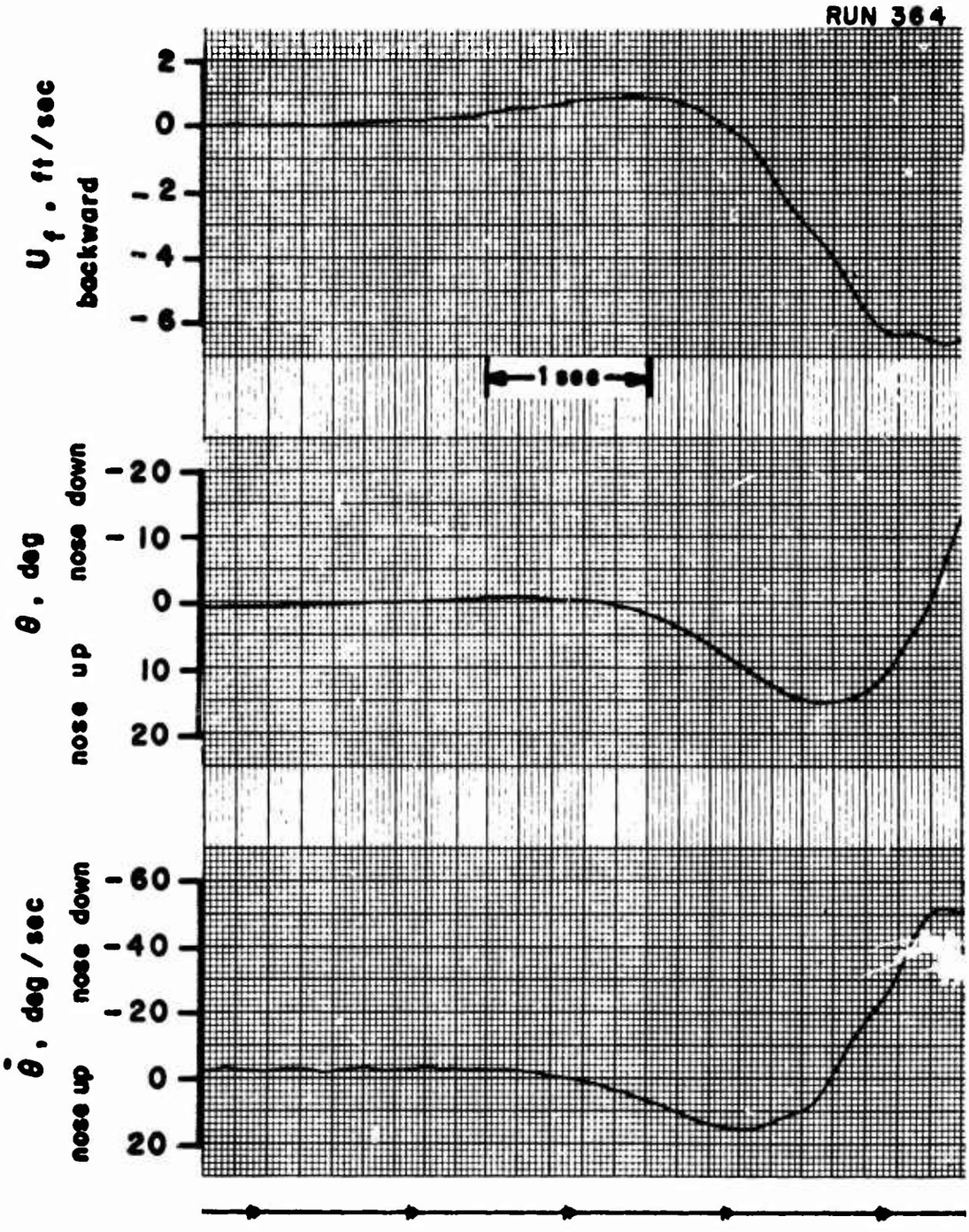

Figure 25. Longitudinal Transient Response. Two Degrees of Freedom, θ-U_f. No Stability Augmentation.
$\beta_{.75R}$ = 25.8°, rpm = 7000.

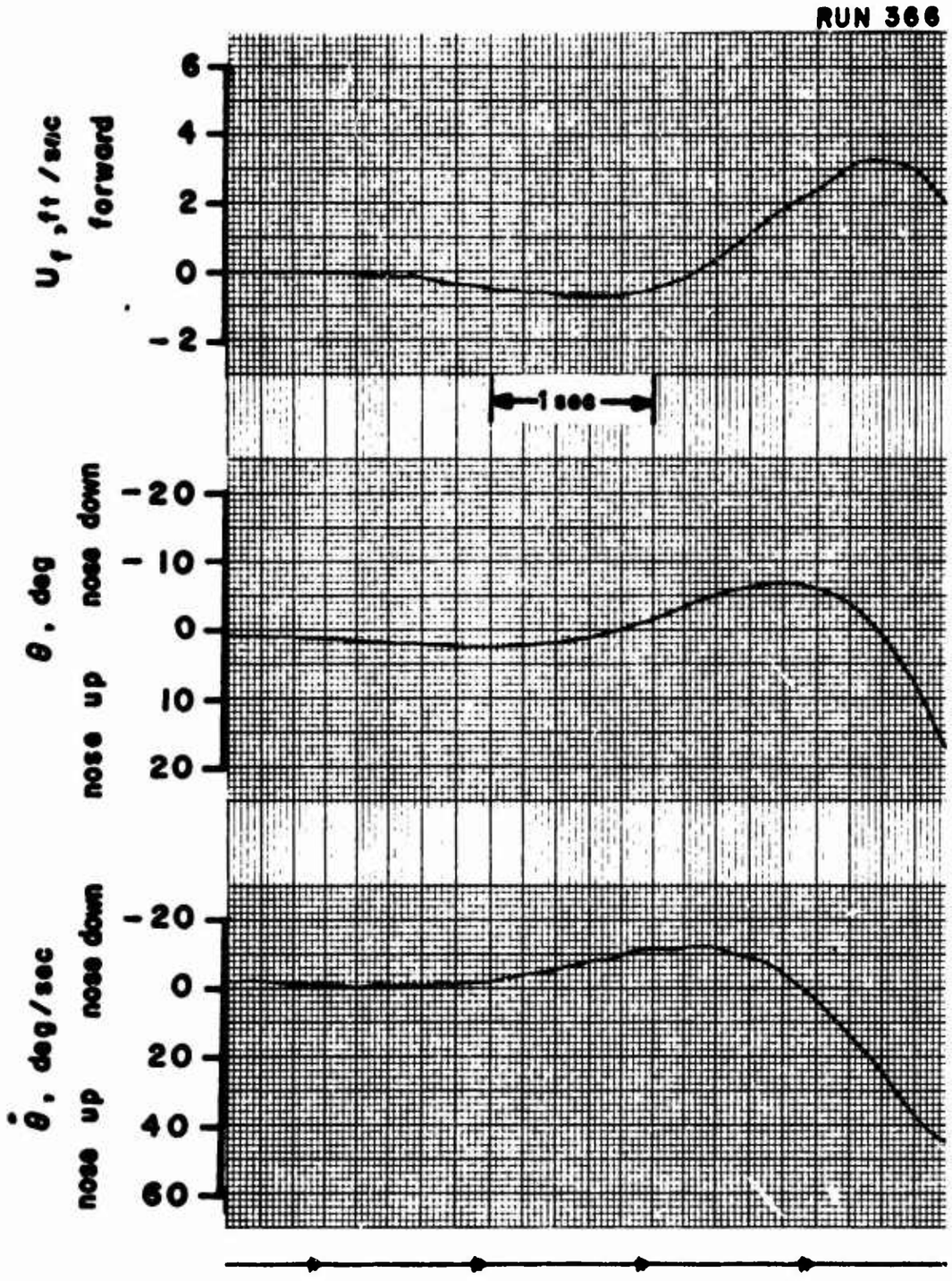

Figure 26. Longitudinal Transient Response. Two Degrees of Freedom, θ-U_f. No Stability Augmentation.
$\beta_{.75R}$ = 25.8°, rpm = 7000.

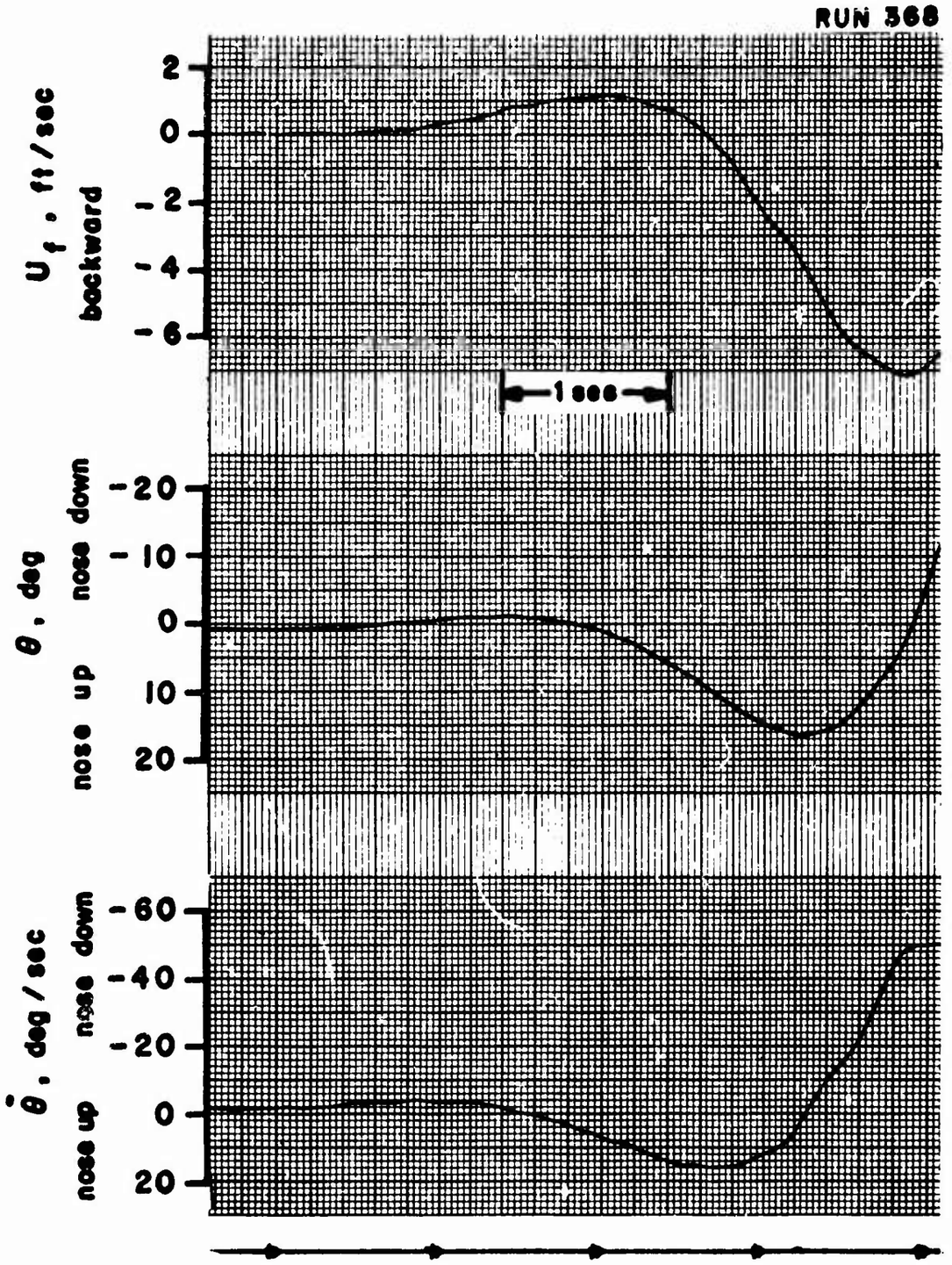

Figure 27. Longitudinal Transient Response. Two Degrees of Freedom, θ-U_f. No Stability Augmentation.
$\beta_{.75R}$ = 25.8°, rpm = 7000.

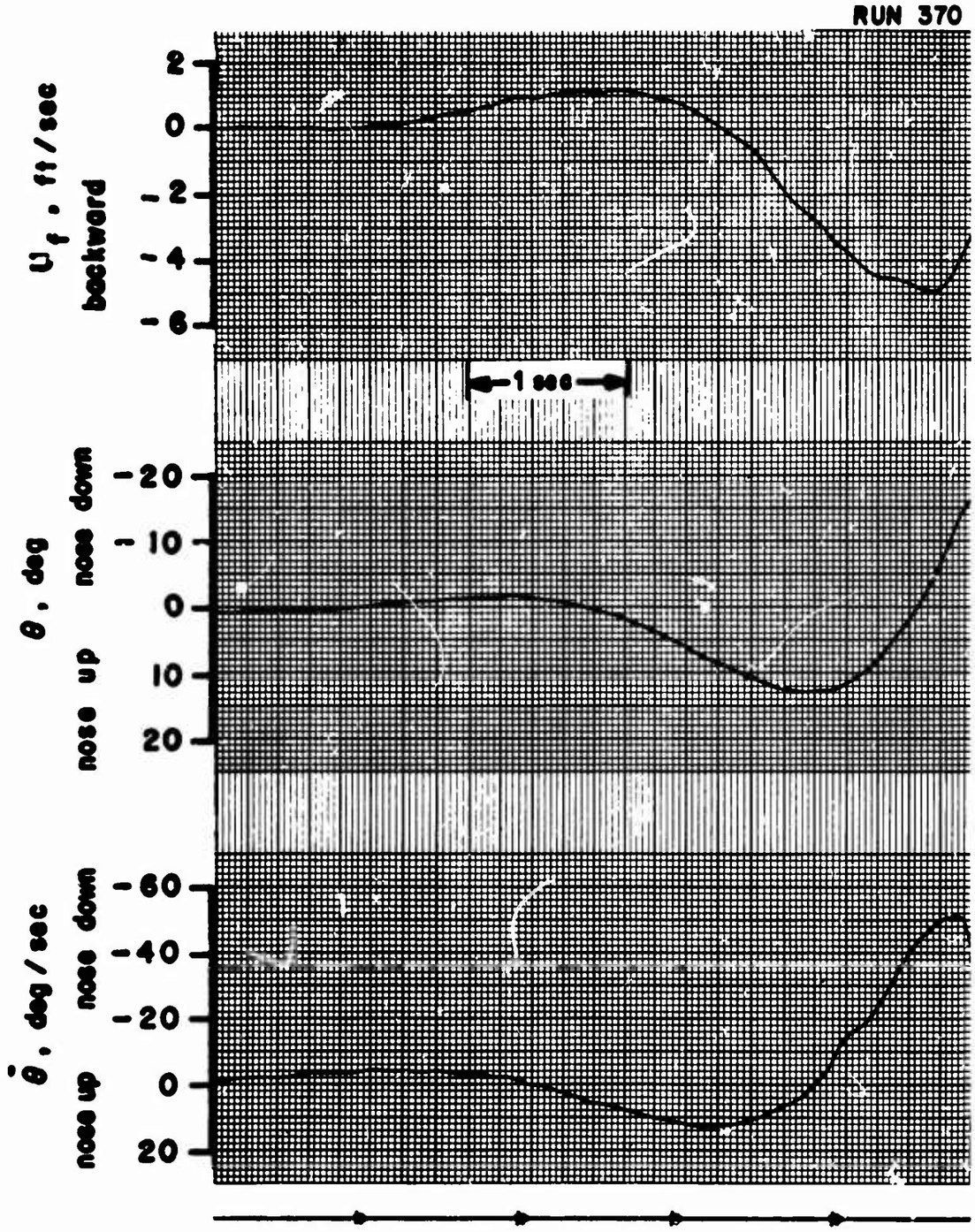

Figure 28. Longitudinal Transient Response. Two Degrees of Freedom, θ-U_f. No Stability Augmentation.

$\beta_{.75R}$ = 25.8°, rpm = 6400.

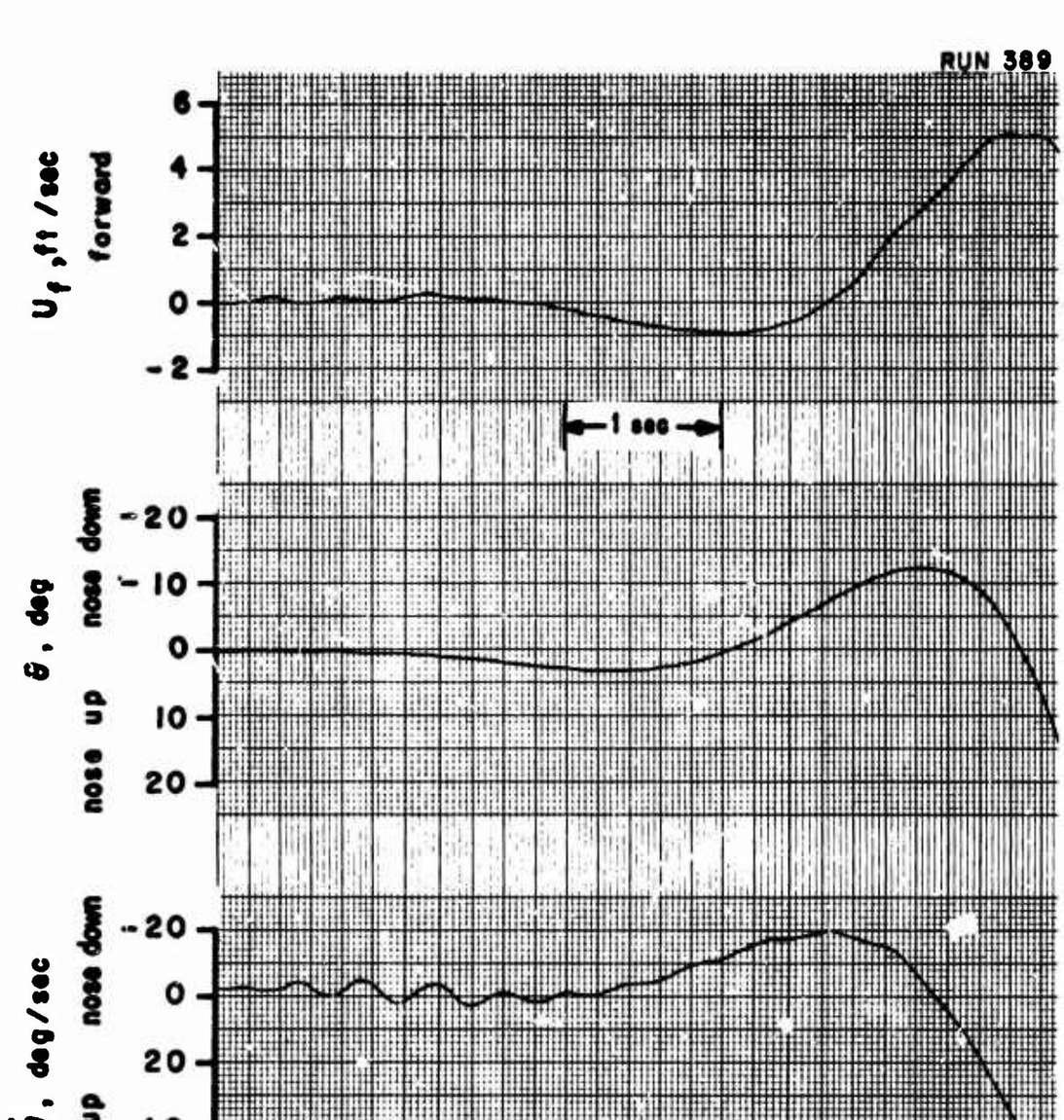

Figure 29. Longitudinal Transient Response. Two Degrees of Freedom, θ-U_f. No Stability Augmentation.
$\beta_{.75R}$ = 25.8°, rpm = 6400.

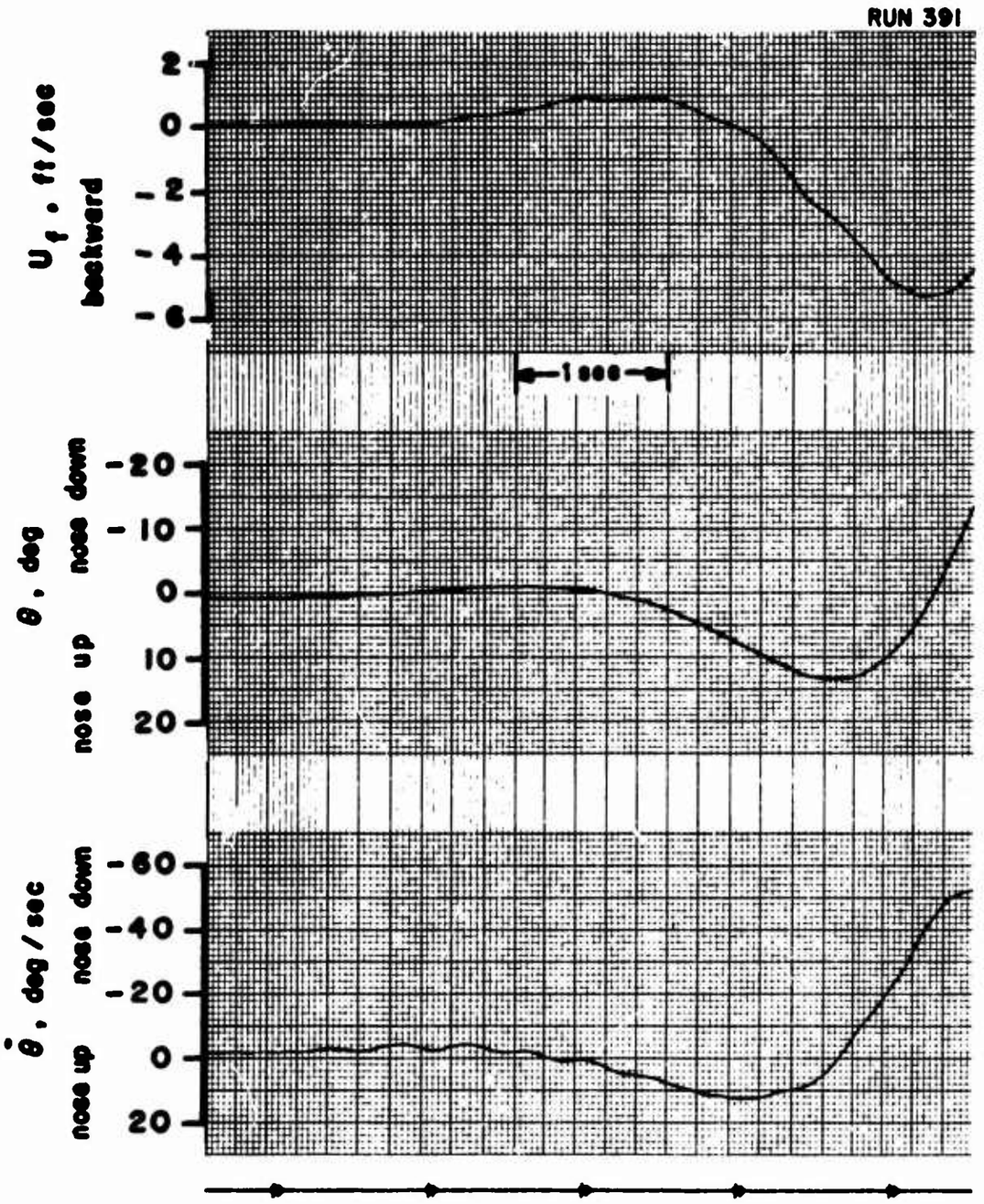

Figure 30. Longitudinal Transient Response. Two Degrees of Freedom, θ-U_f. No Stability Augmentation.
$\beta_{.75R}$ = 25.8°, rpm = 6400.

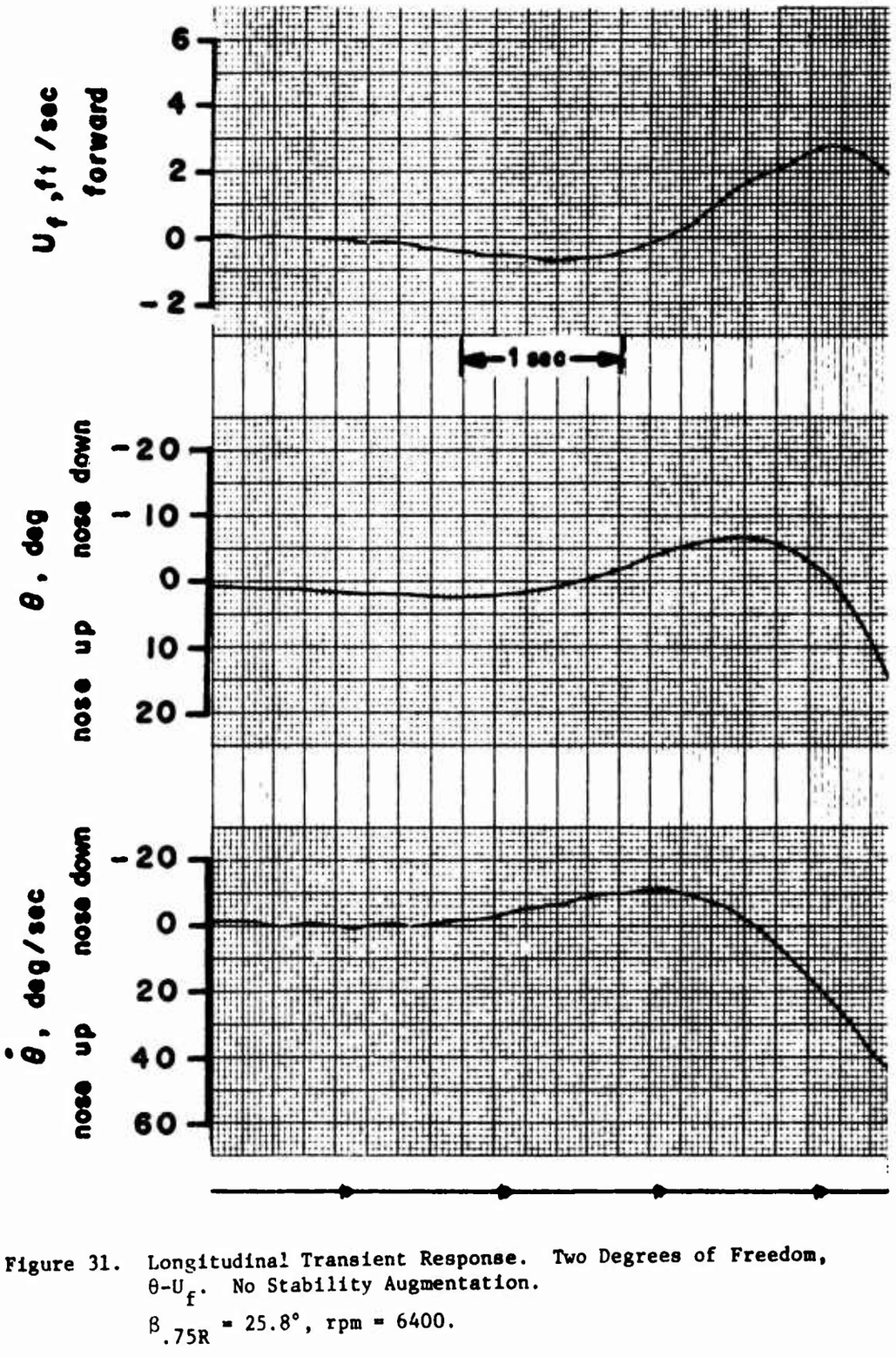

Figure 31. Longitudinal Transient Response. Two Degrees of Freedom, θ-U_f. No Stability Augmentation.
$\beta_{.75R}$ = 25.8°, rpm = 6400.

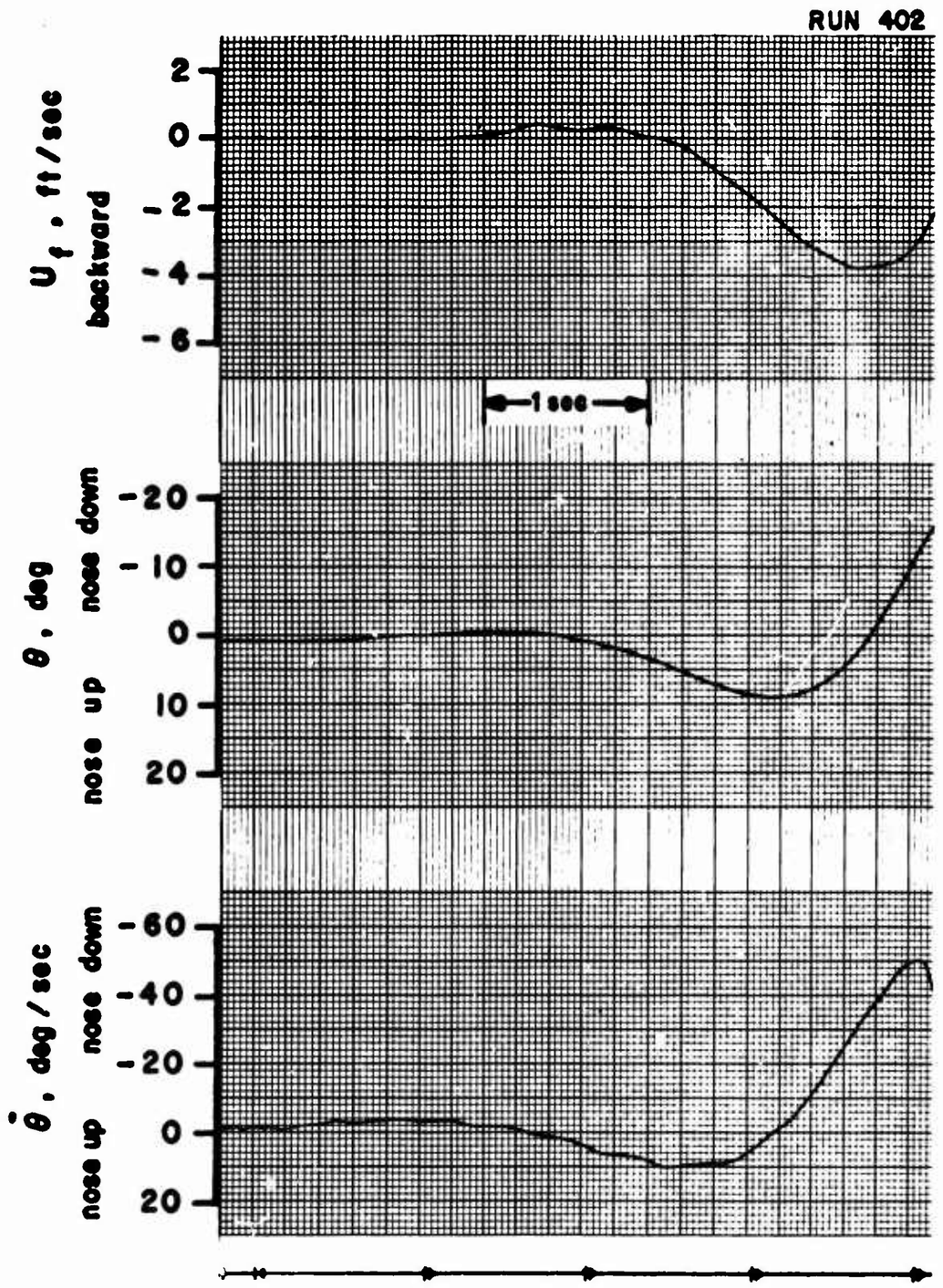

Figure 32. Longitudinal Transient Response. Two Degrees of Freedom, θ-U_f. No Stability Augmentation.
$\beta_{.75R}$ = 29.2°, rpm = 6400.

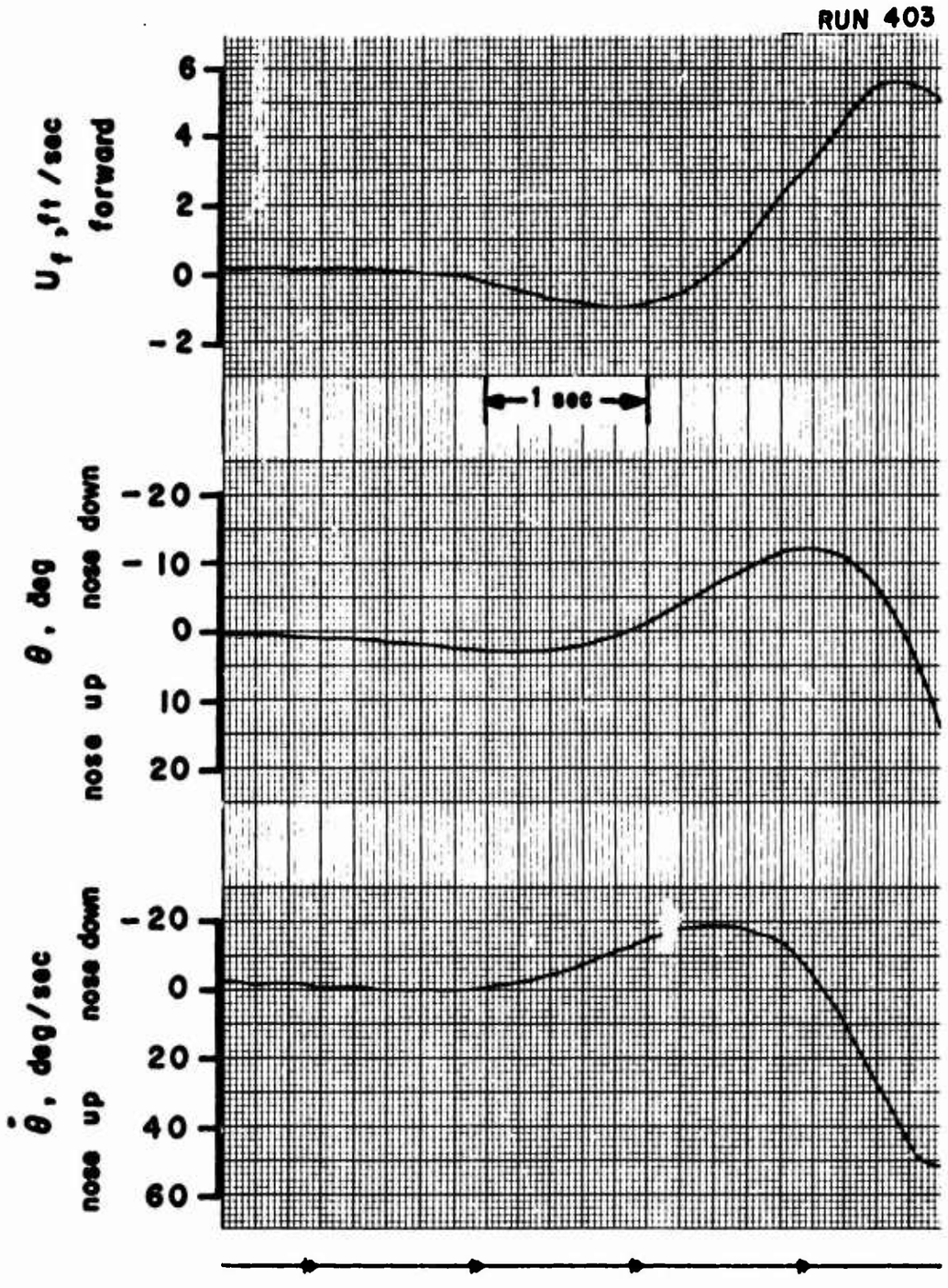

Figure 33. Longitudinal Transient Response. Two Degrees of Freedom, θ-U_f. No Stability Augmentation.
$\beta_{.75R}$ = 29.2°, rpm = 6400.

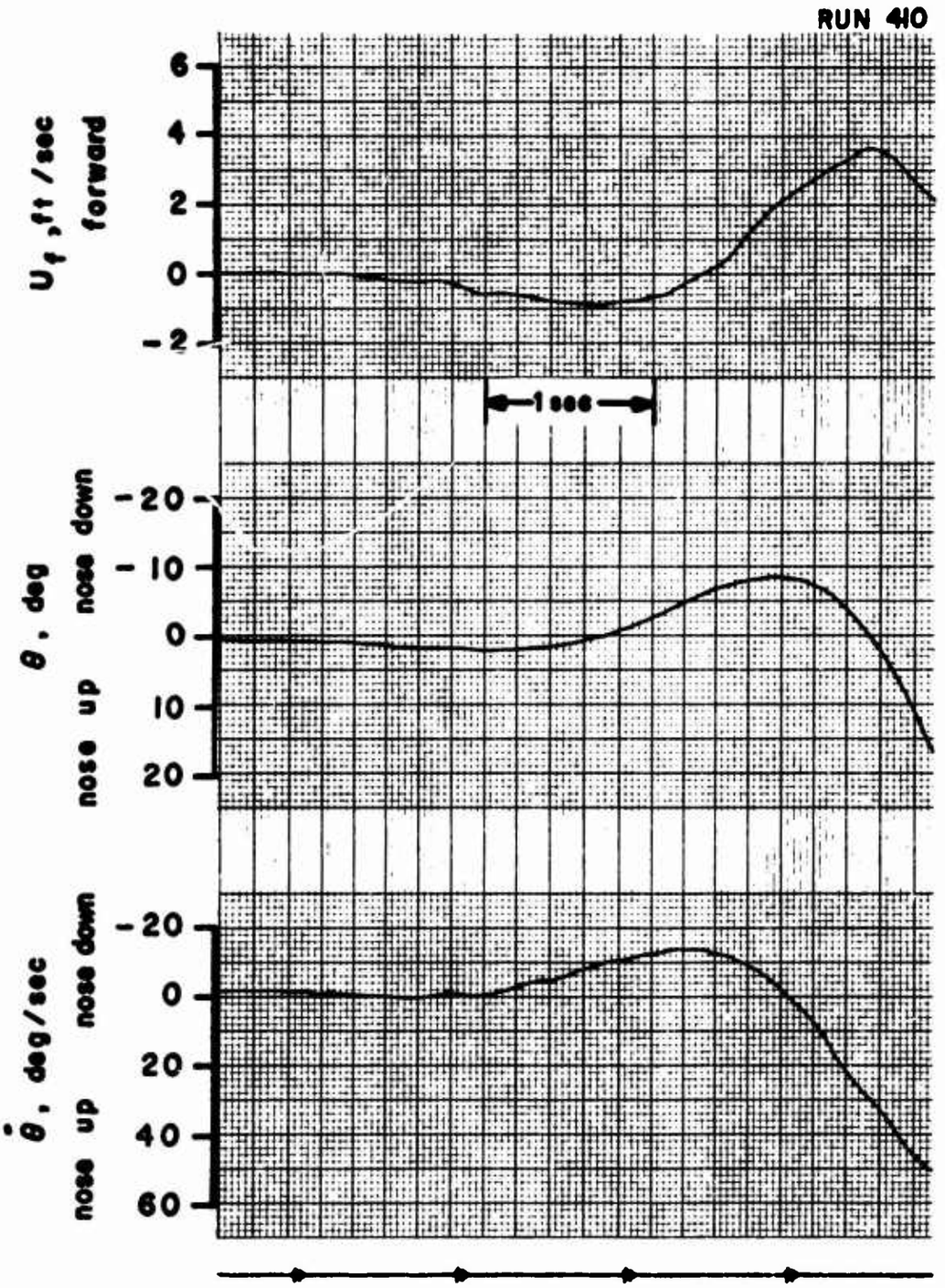

Figure 34. Longitudinal Transient Response. Two Degrees of Freedom, θ-U_f. No Stability Augmentation.
$\beta_{.75R}$ = 29.2°, rpm = 6400.

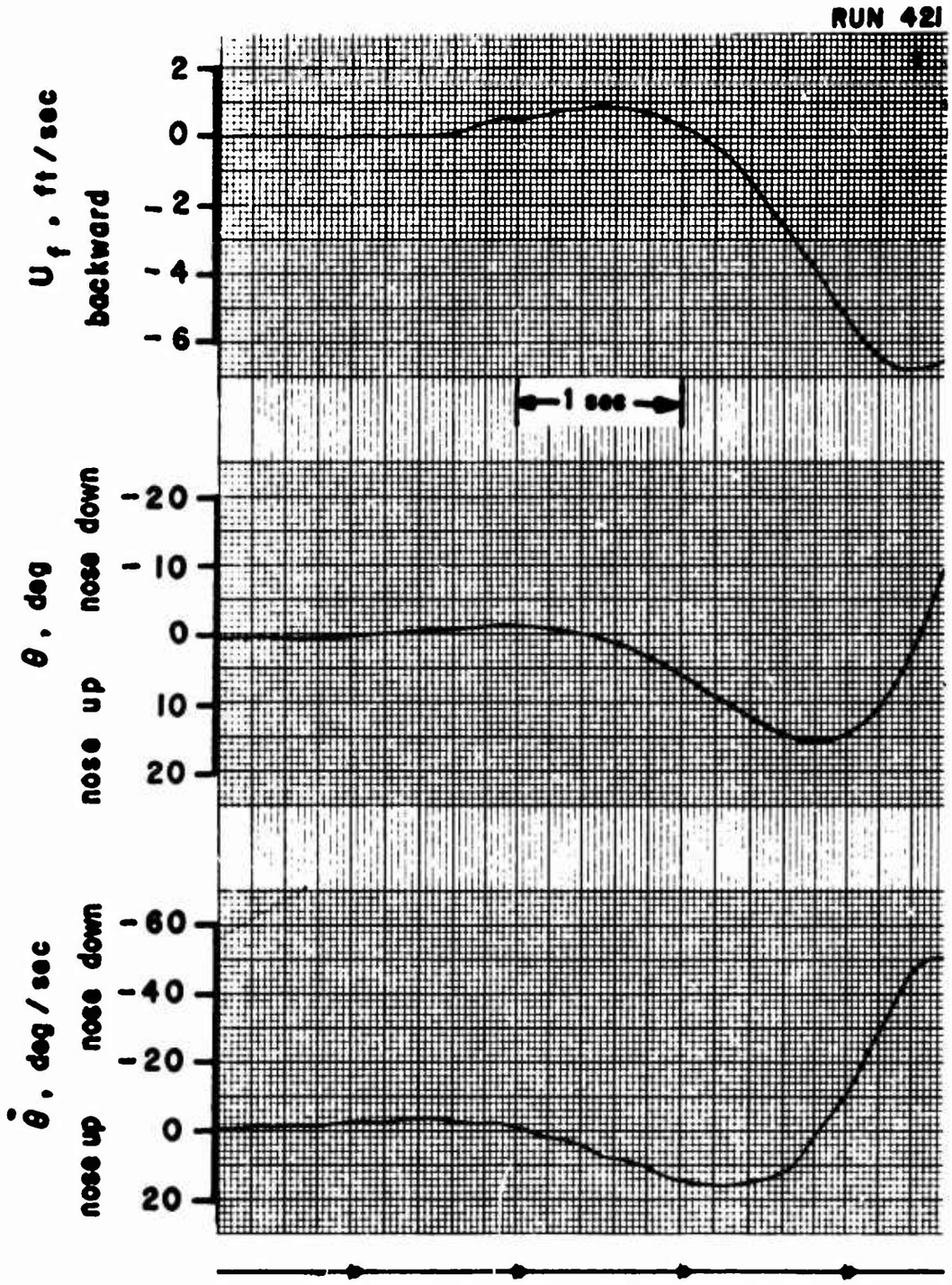

Figure 35. Longitudinal Transient Response. Two Degrees of Freedom, θ-U_f. No Stability Augmentation.
$\beta_{.75R}$ = 29.2°, rpm = 6400.

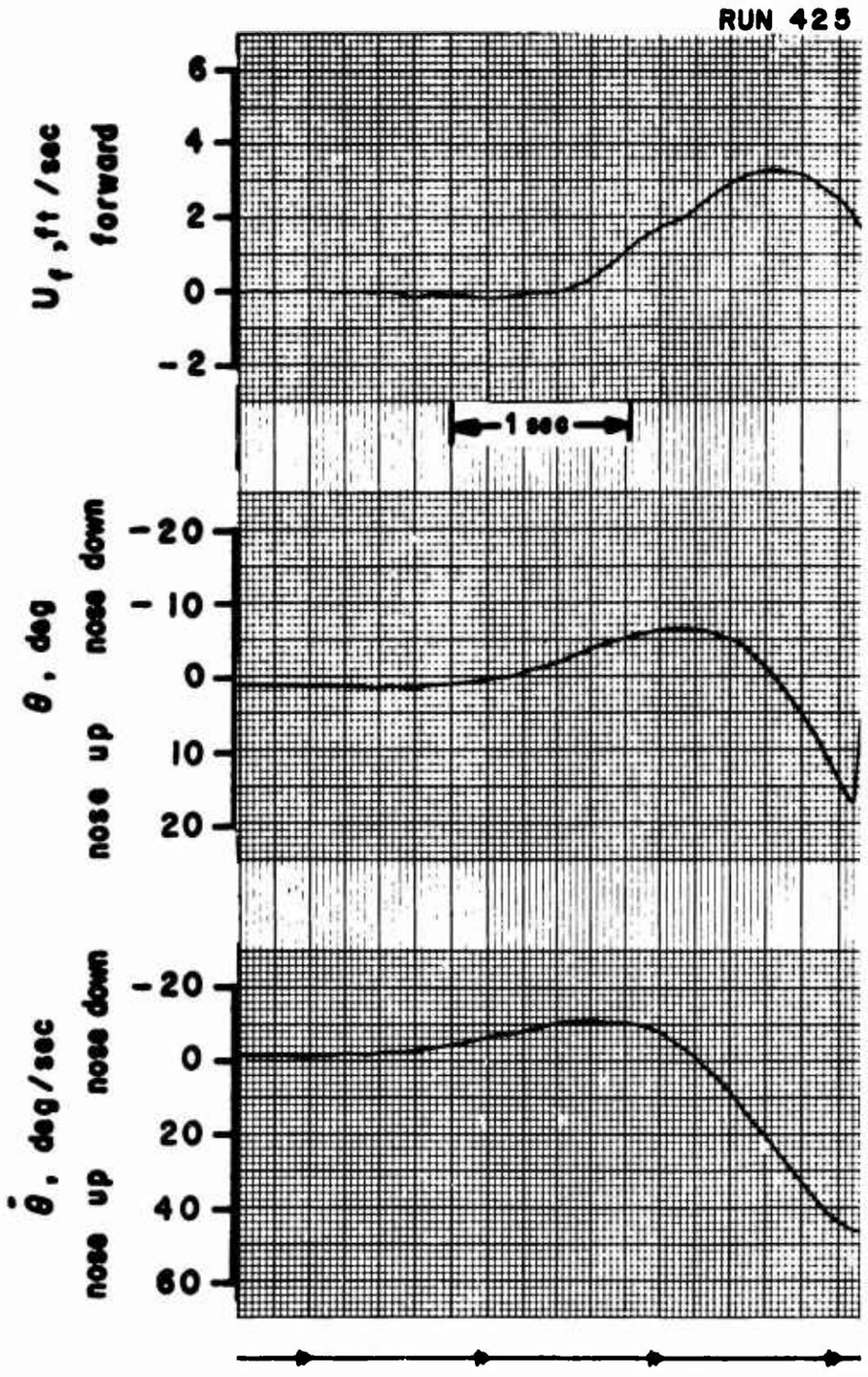

Figure 36. Longitudinal Transient Response. Two Degrees of Freedom, θ-U_f. No Stability Augmentation.
$\beta_{.75R}$ = 29.2°, rpm = 6400.

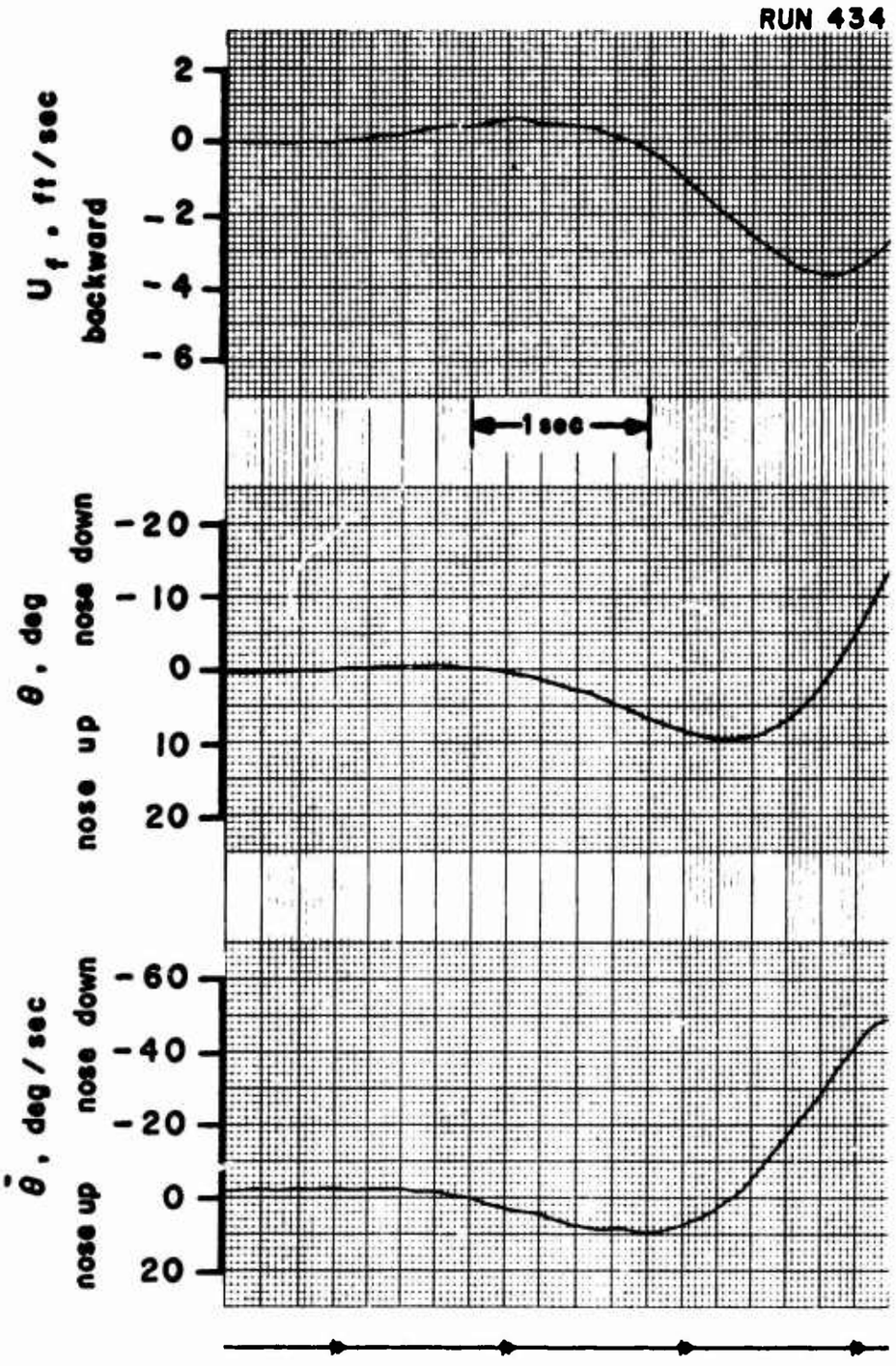

Figure 37. Longitudinal Transient Response. Two Degrees of Freedom, θ-U_f. No Stability Augmentation.

$\beta_{.75R}$ = 29.2°, rpm = 6400.

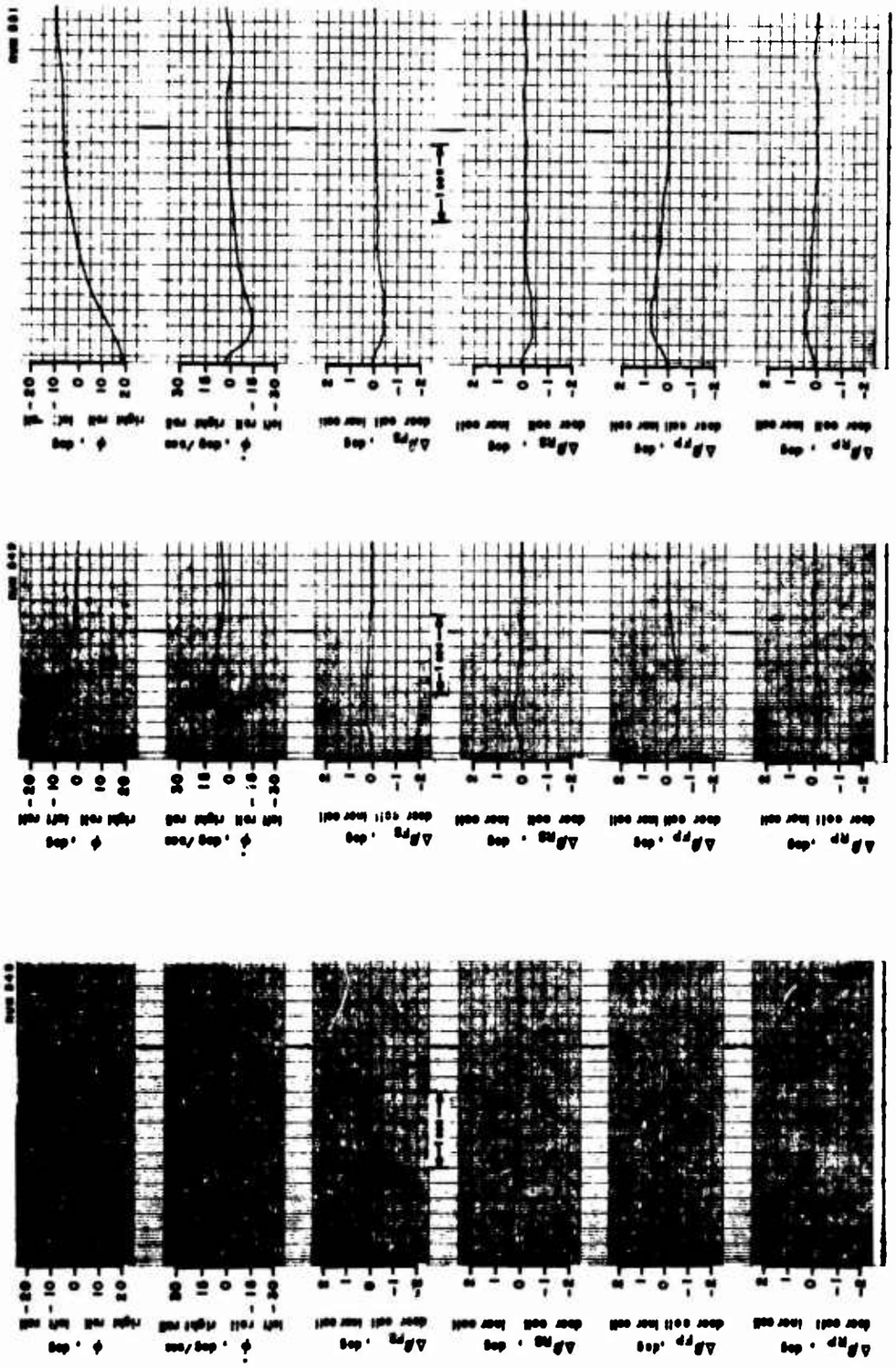

Figure 38. Lateral Transient Response. One Degree of Freedom, ϕ.
$K_{\dot{\phi}} = 0.029$ sec .
$\beta_{.75R} = 25.8°$, rpm = 7000.

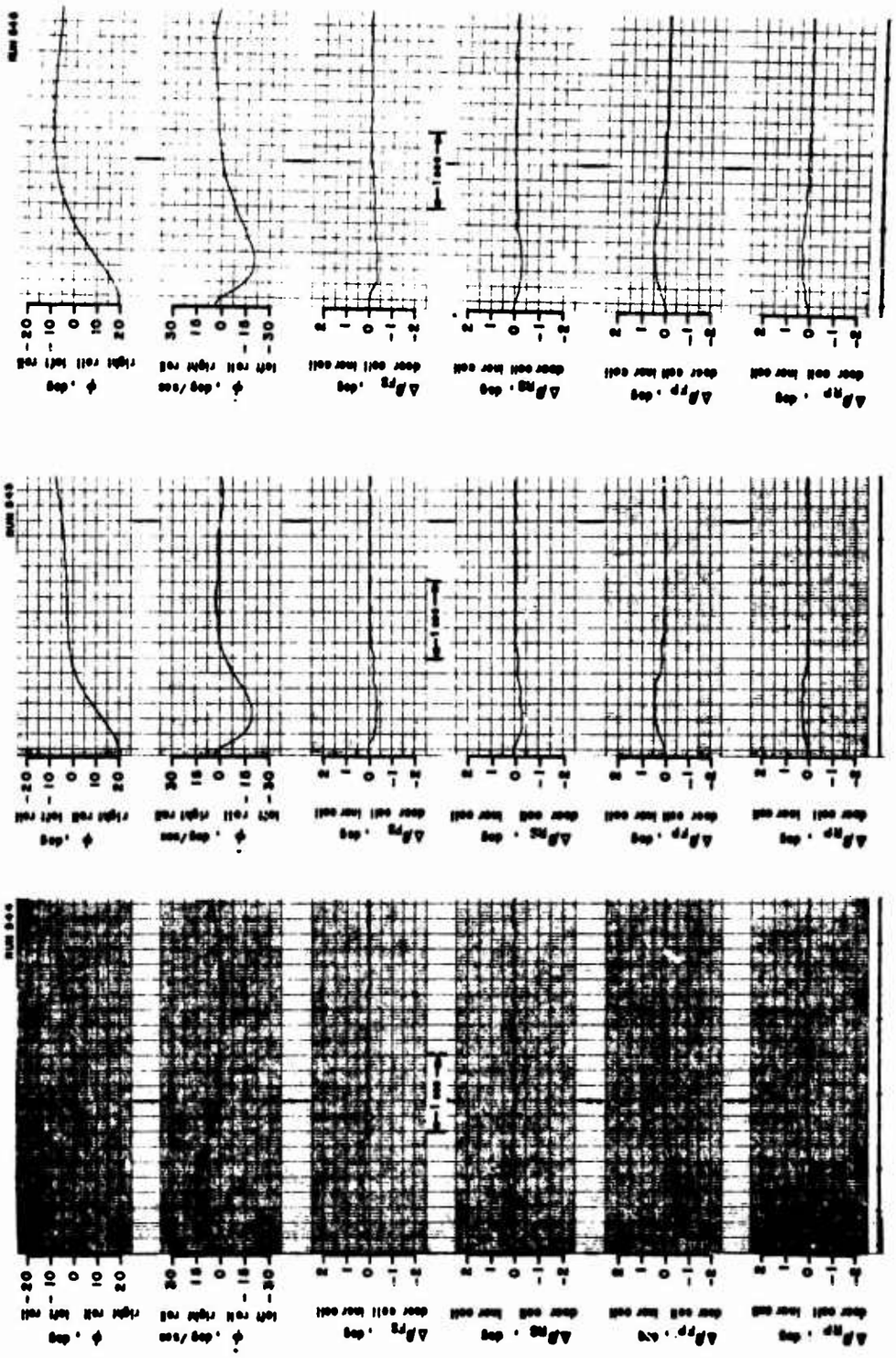

Figure 39. Lateral Transient Response. One Degree of Freedom, ϕ.
$K_{\dot{\phi}}$ = 0.016 sec .
$\beta_{.75R}^{\phi}$ = 25.8°, rpm = 7000.

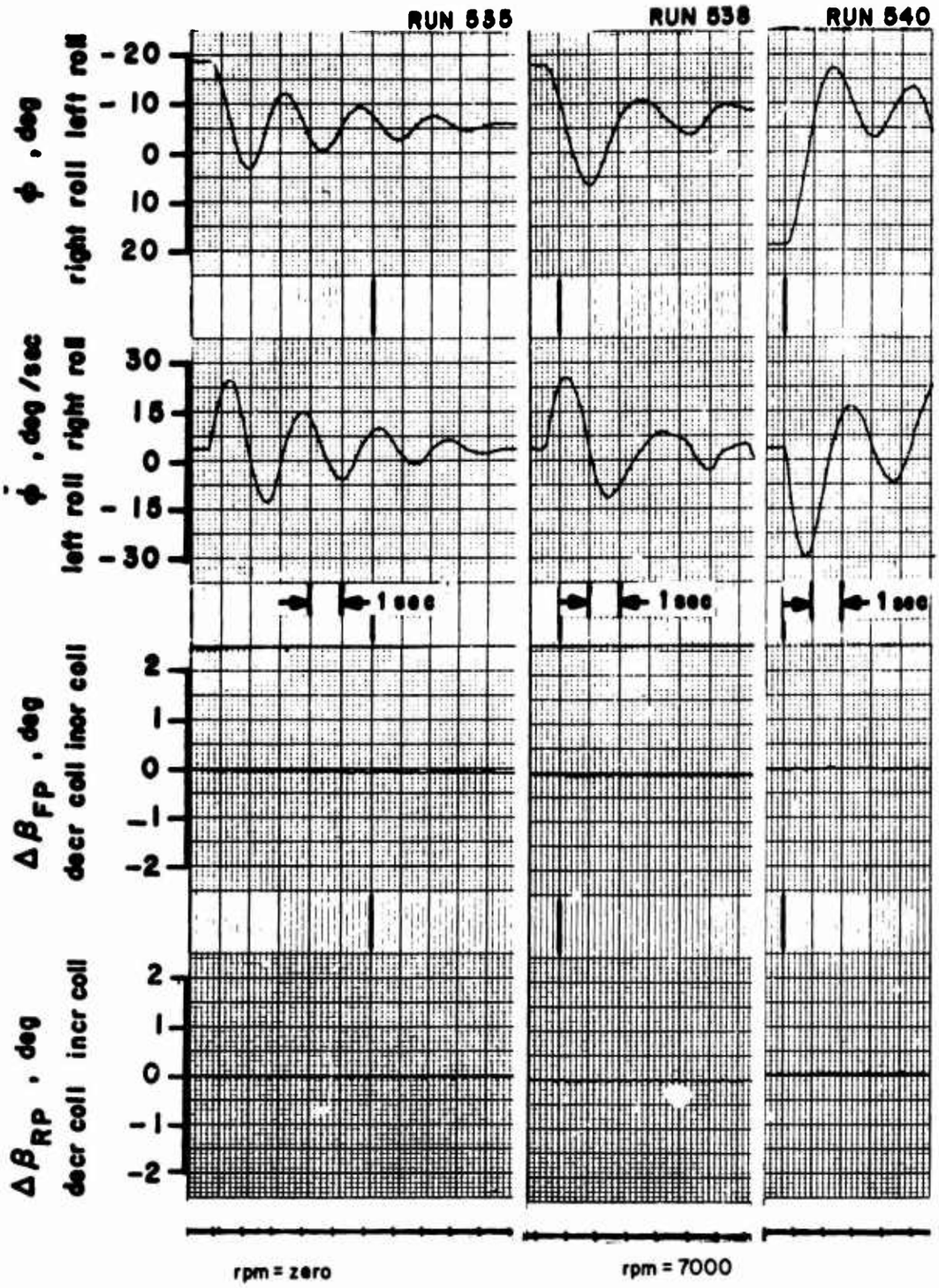

Figure 40. Lateral Transient Response. One Degree of Freedom, ϕ. No Stability Augmentation. $\beta_{.75R} = 25.8°$.

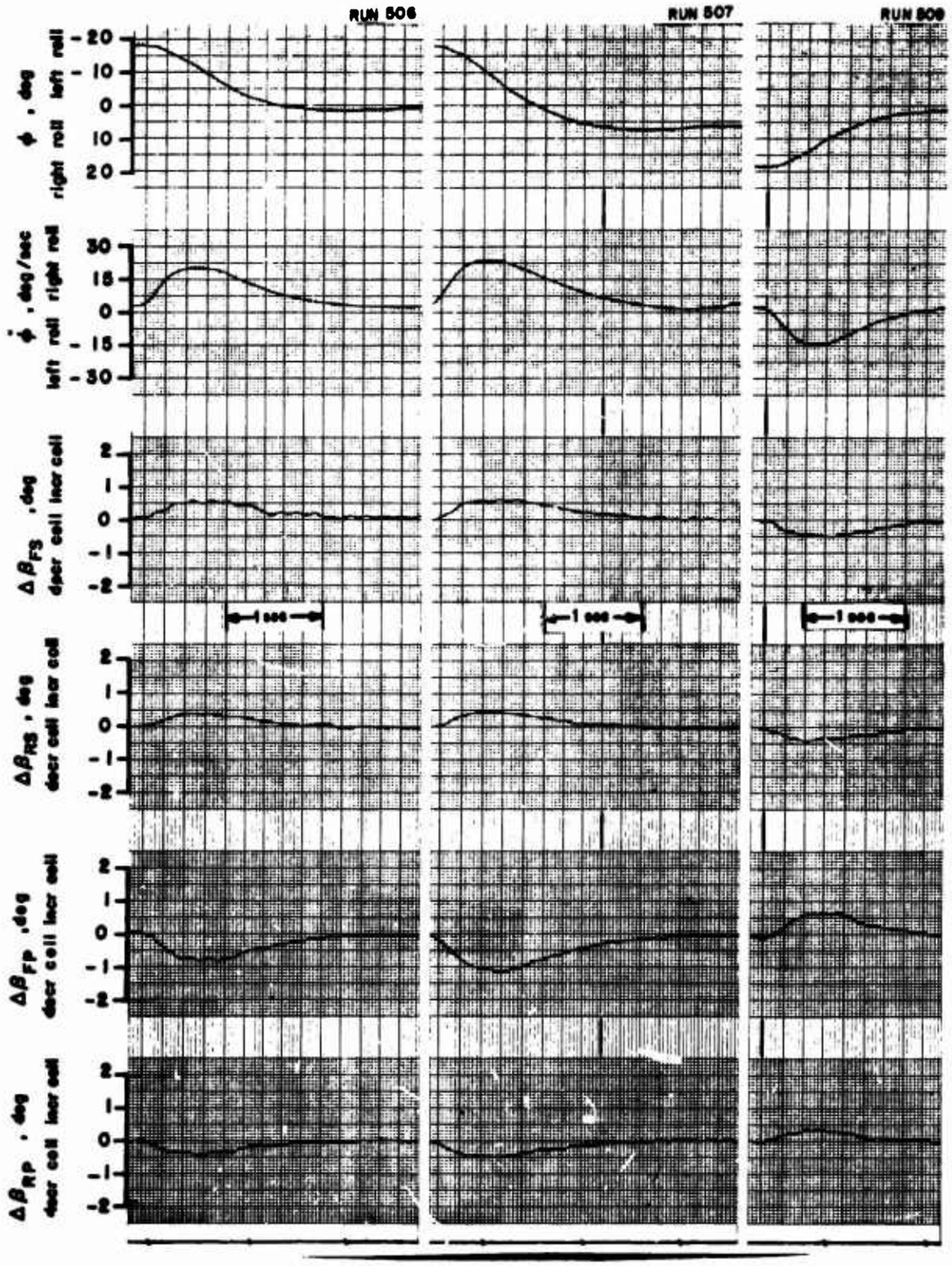

Figure 41. Lateral Transient Response. One Degree of Freedom, ϕ.
$K_{\dot{\phi}} = 0.029$ sec .
$\beta_{.75R} = 29.2°$, rpm = 6400.

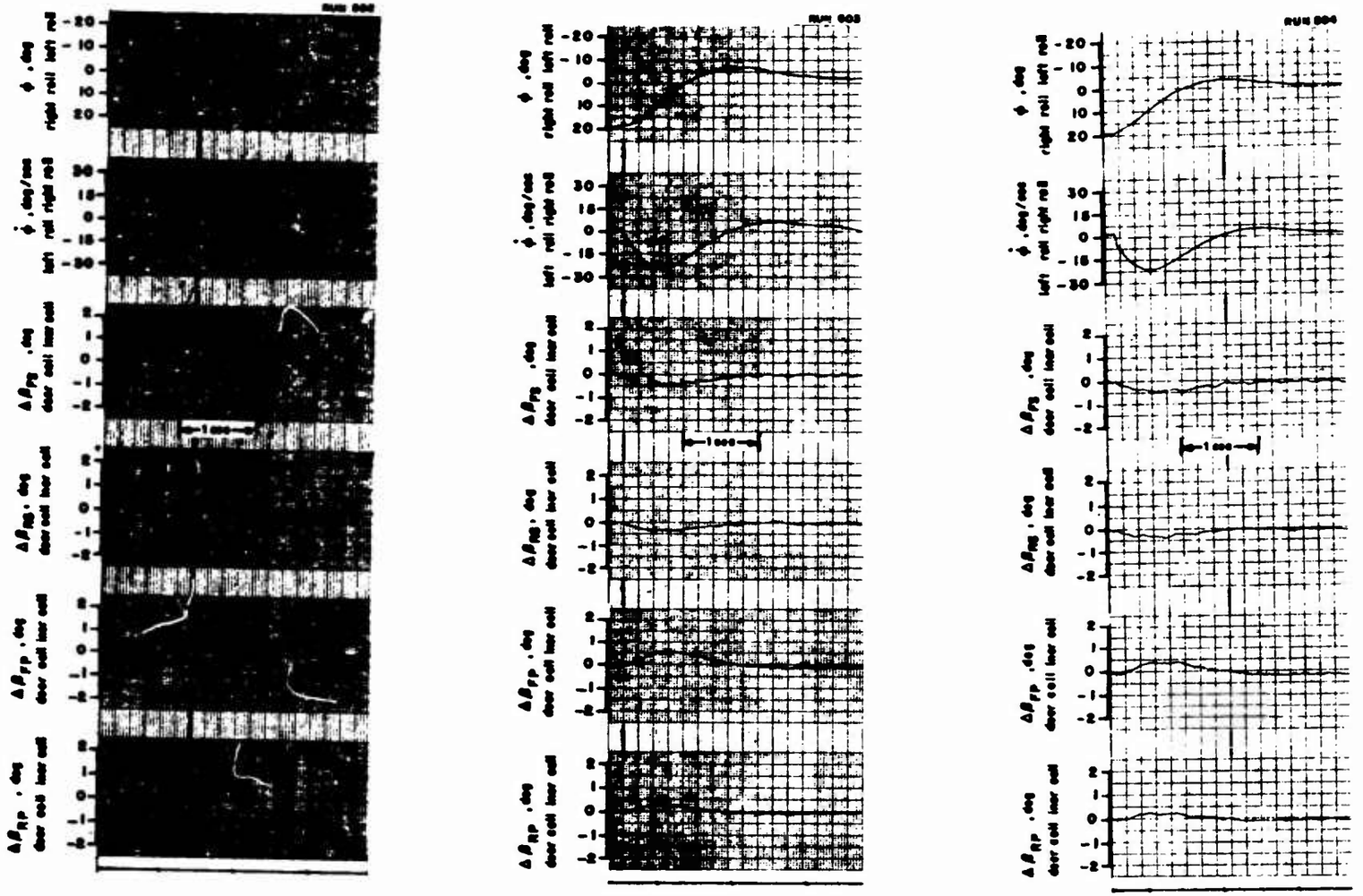

Figure 42. Lateral Transient Response. One Degree of Freedom, ϕ.
$K_{\dot{\phi}}$ = 0.016 sec .
$\beta_{.75R}$ = 29.2°, rpm = 6400.

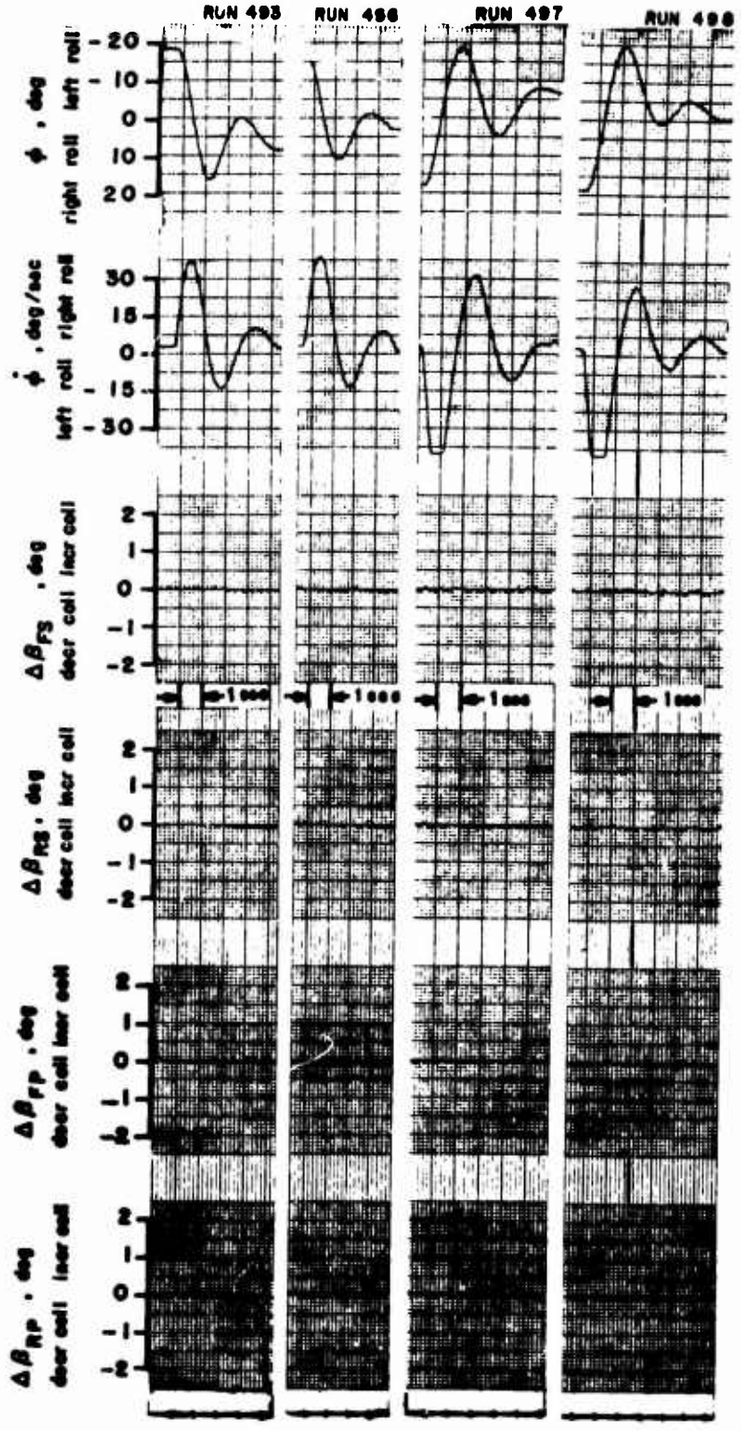

Figure 43. Lateral Transient Response. One Degree of Freedom, ϕ. No Stability Augmentation. $\beta_{.75R}$ = 29.2°, rpm = 6400.

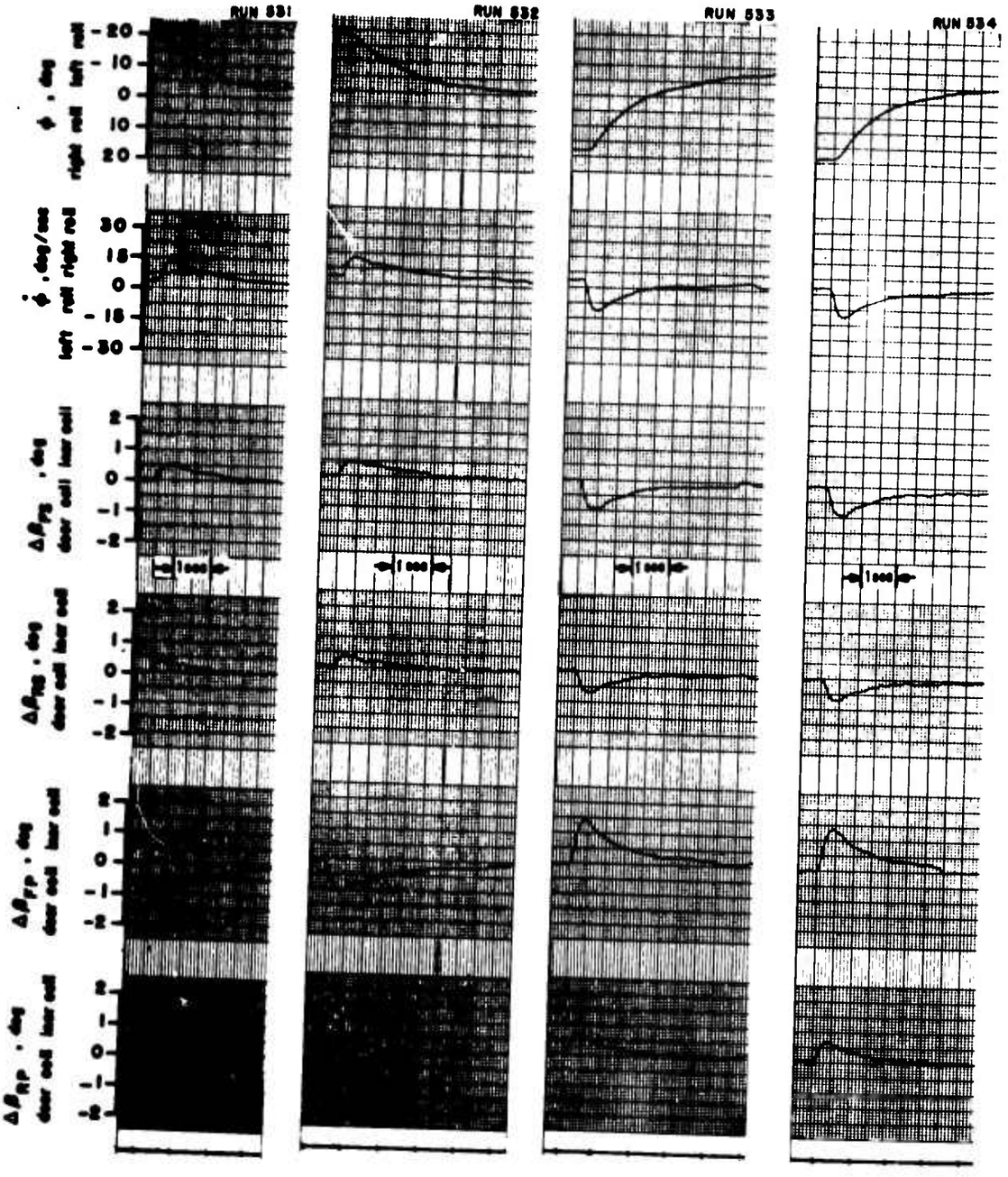

Figure 44. Lateral Transient Response. One Degree of Freedom, ϕ.
$K_{\dot{\phi}}$ = 0.055 sec .
$\beta_{.75R}$ = 25.8°, rpm = 6400.

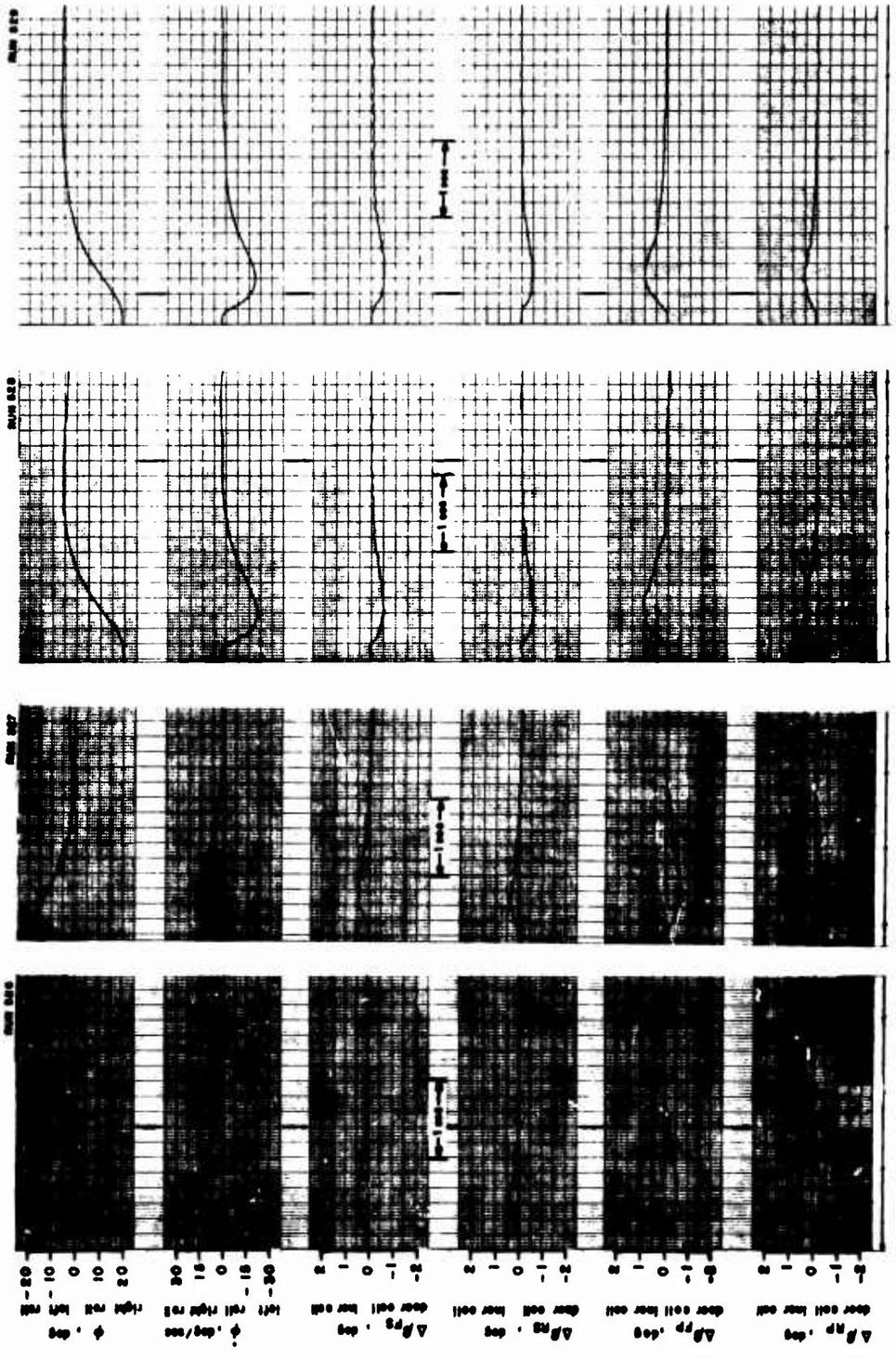

Figure 45. Lateral Transient Response. One Degree of Freedom, ϕ.
$K_{\dot{\phi}}' = 0.029$ sec .
$\beta_{.75R} = 25.8°$, rpm = 6400.

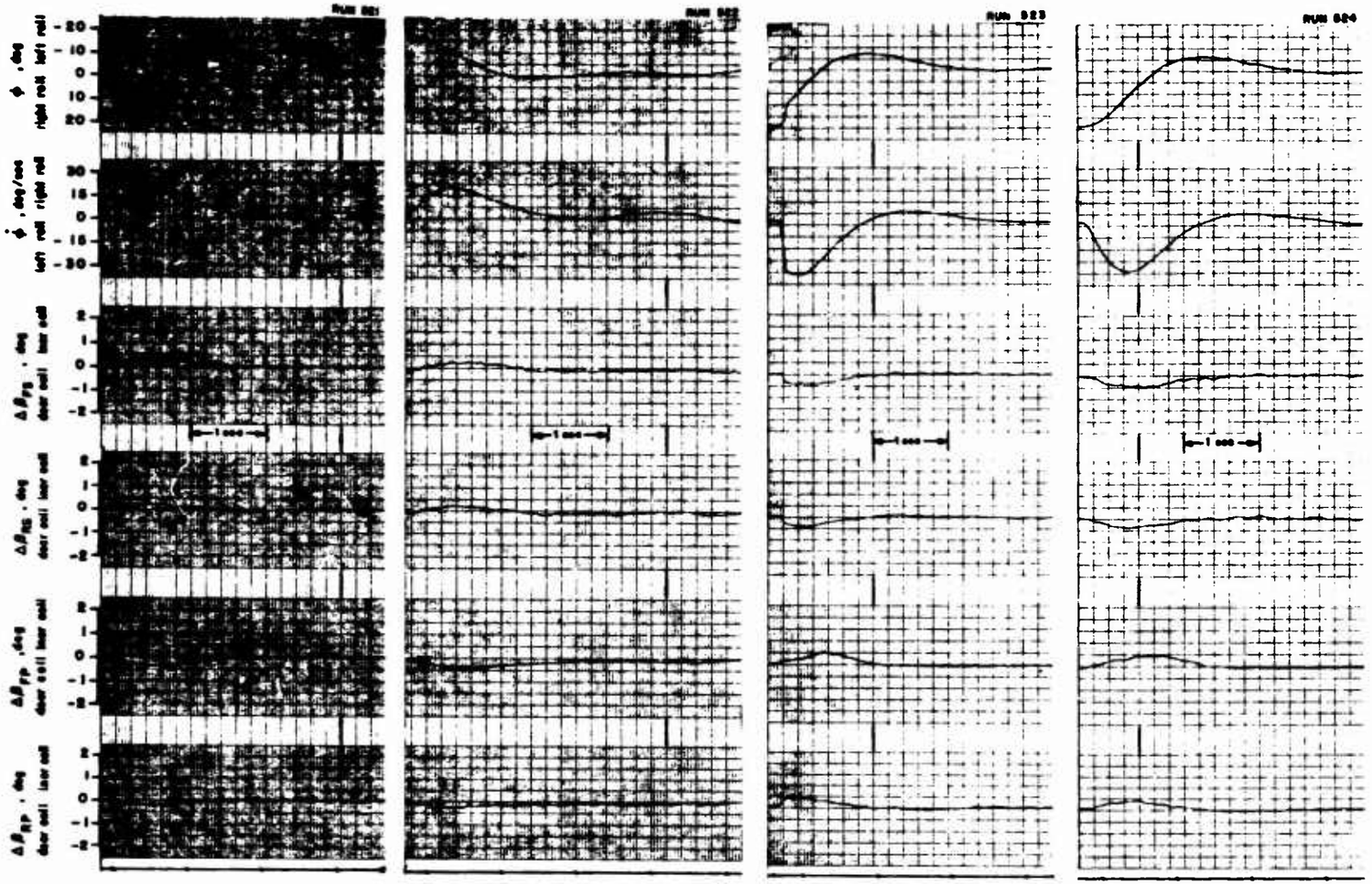

Figure 46. Lateral Transient Response. One Degree of Freedom, ϕ.
$K_{\dot{\phi}}$ = 0.016 sec .
$\beta_{.75R}$ = 25.8°, rpm = 6400.

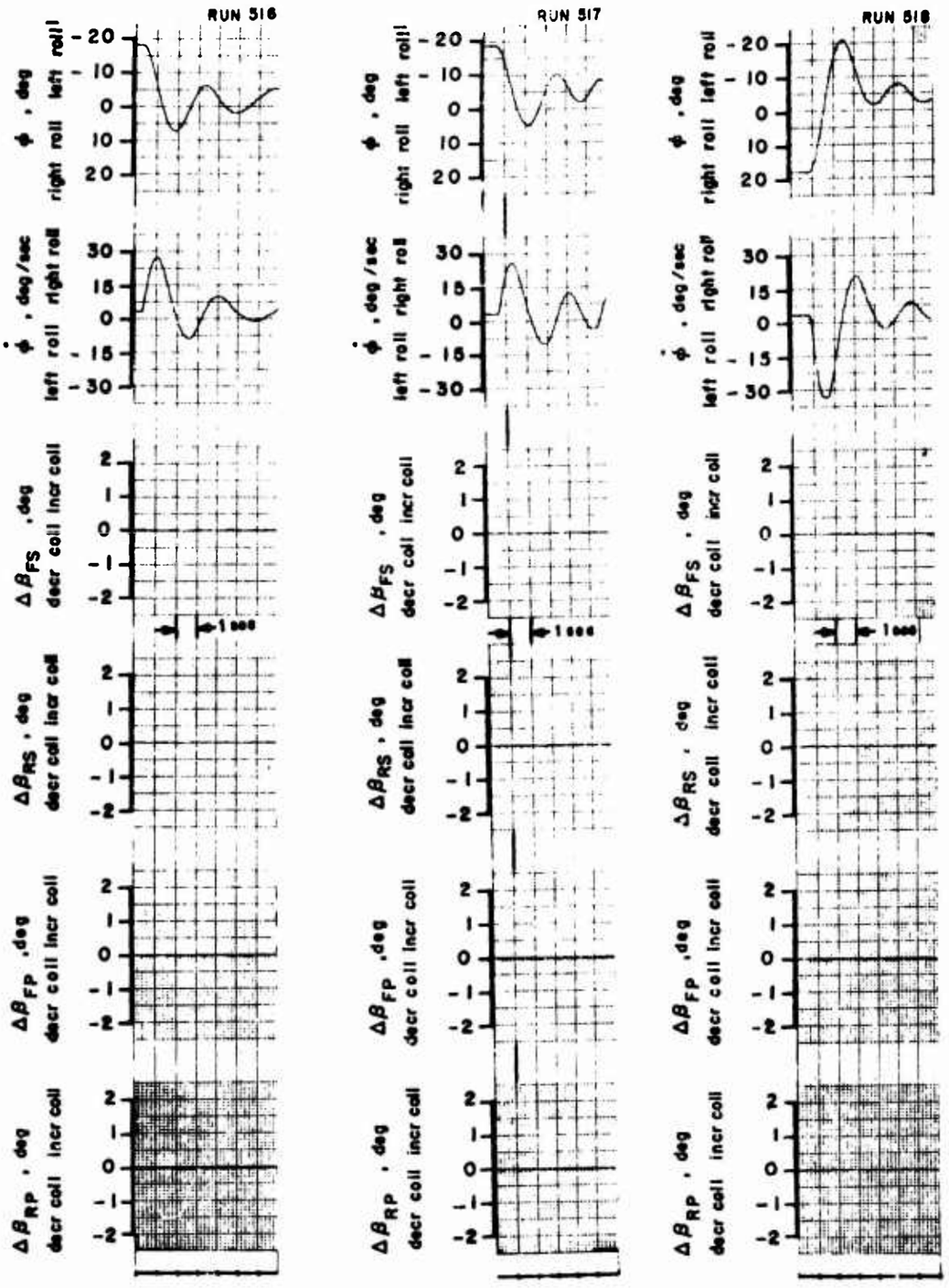

Figure 47. Lateral Transient Response. One Degree of Freedom, ϕ. No Stability Augmentation.

$\beta_{.75R}$ = 25.8°, rpm = 6400.

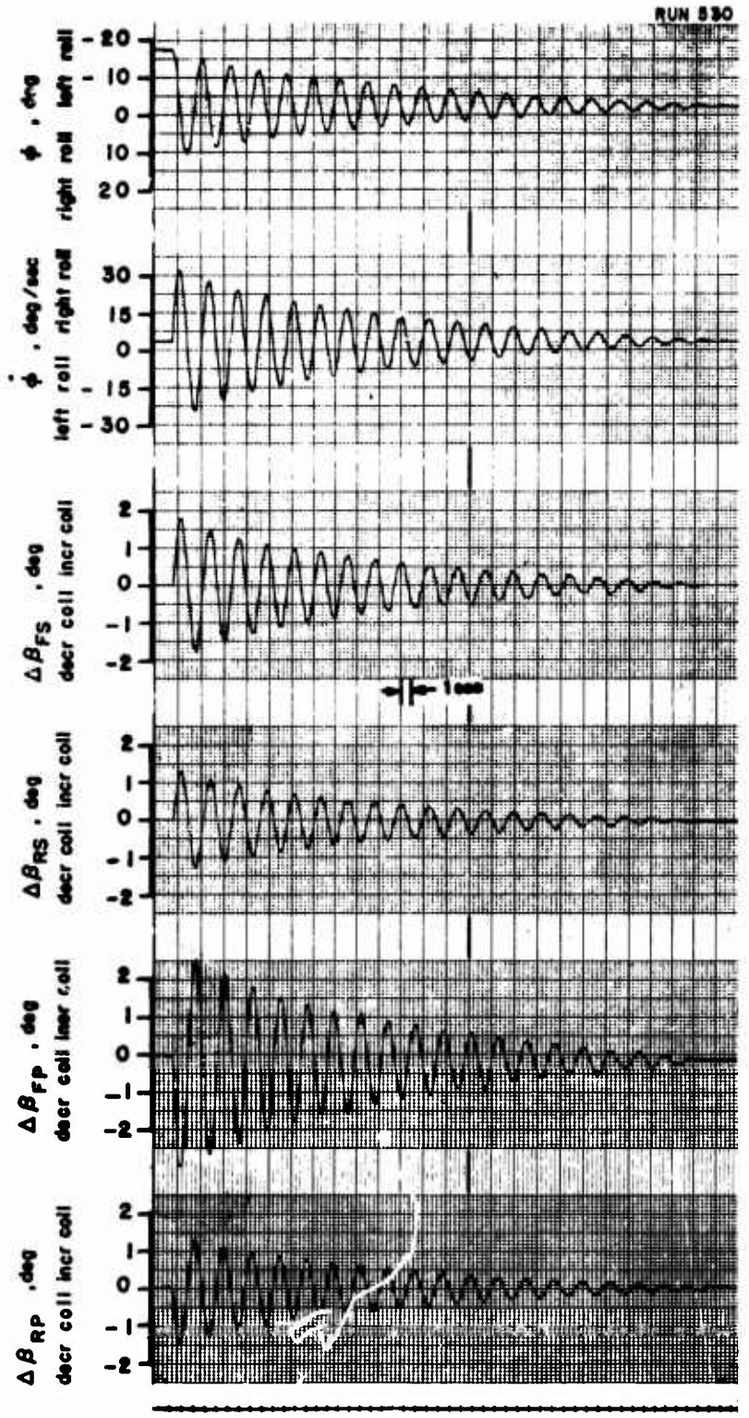

Figure 48. Lateral Transient Response. One Degree of Freedom, ϕ.
$K_{\dot{\phi}}$ = 0.055 sec .

$\beta_{.75R}$ = 25.8°, rpm = zero.

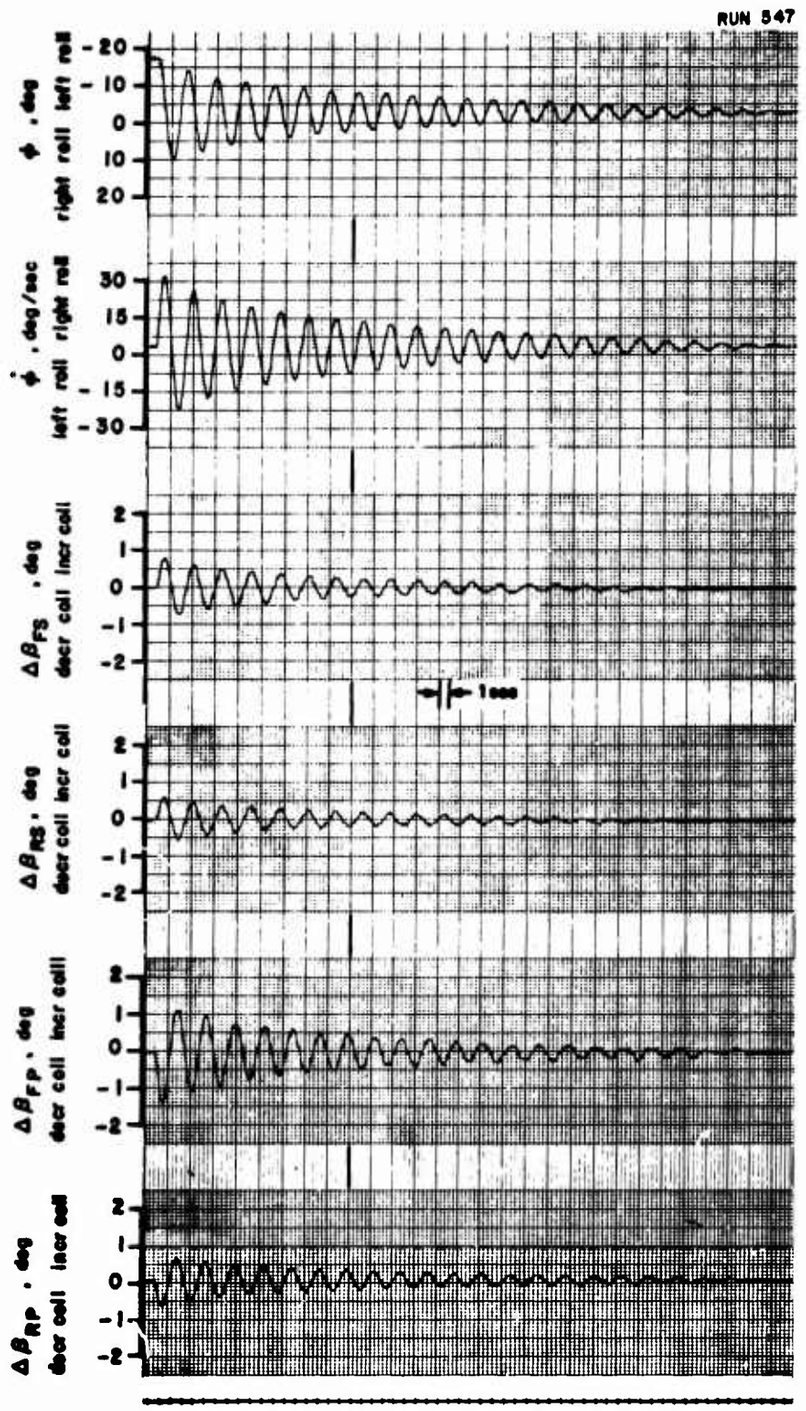

Figure 49. Lateral Transient Response. One Degree of Freedom, ϕ. $K_{\dot{\phi}} = 0.029$ sec .

$\beta_{.75R} = 25.8°$, rpm = zero.

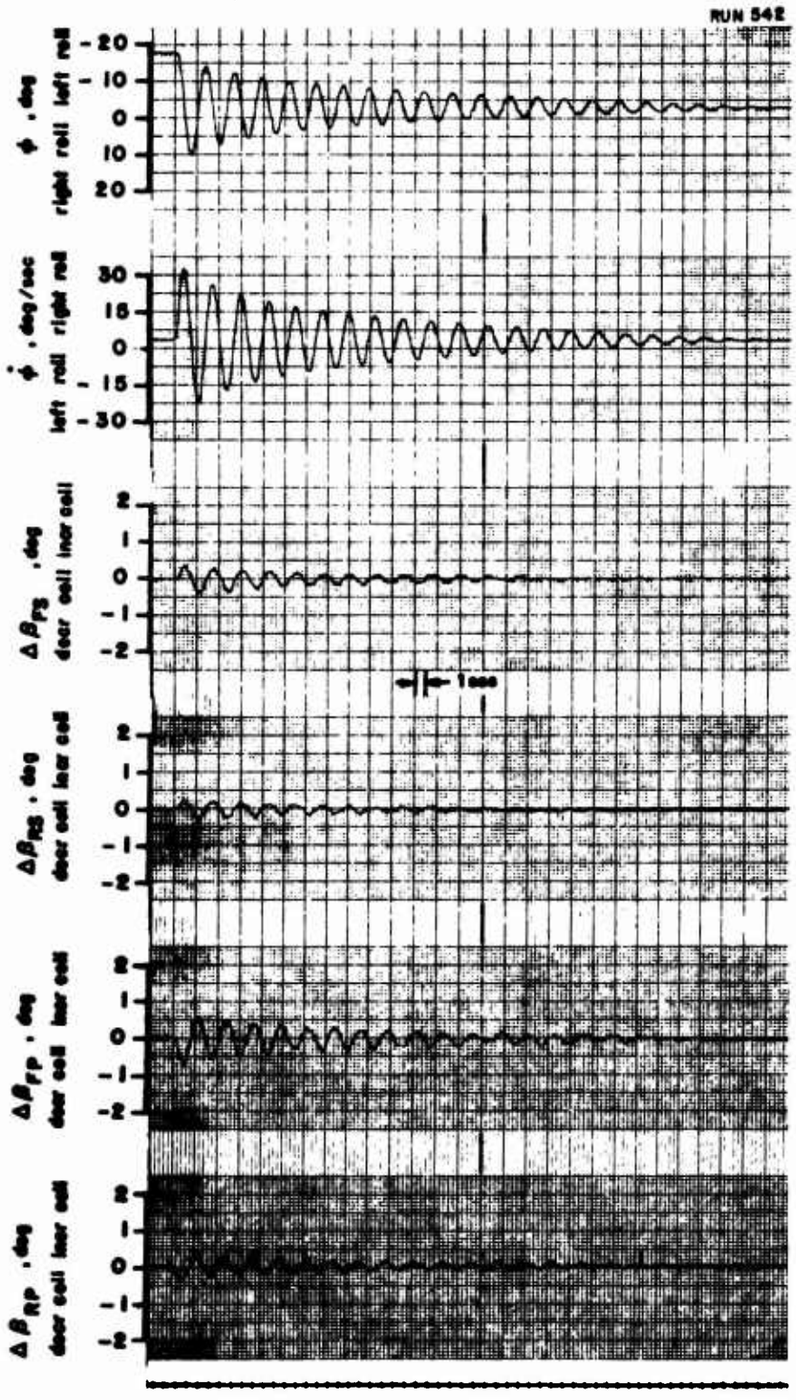

Figure 50. Lateral Transient Response. One Degree of Freedom, ϕ.
$K_{\dot{\phi}}$ = 0.016 sec .
$\beta_{.75R}$ = 25.8°, rpm = zero.

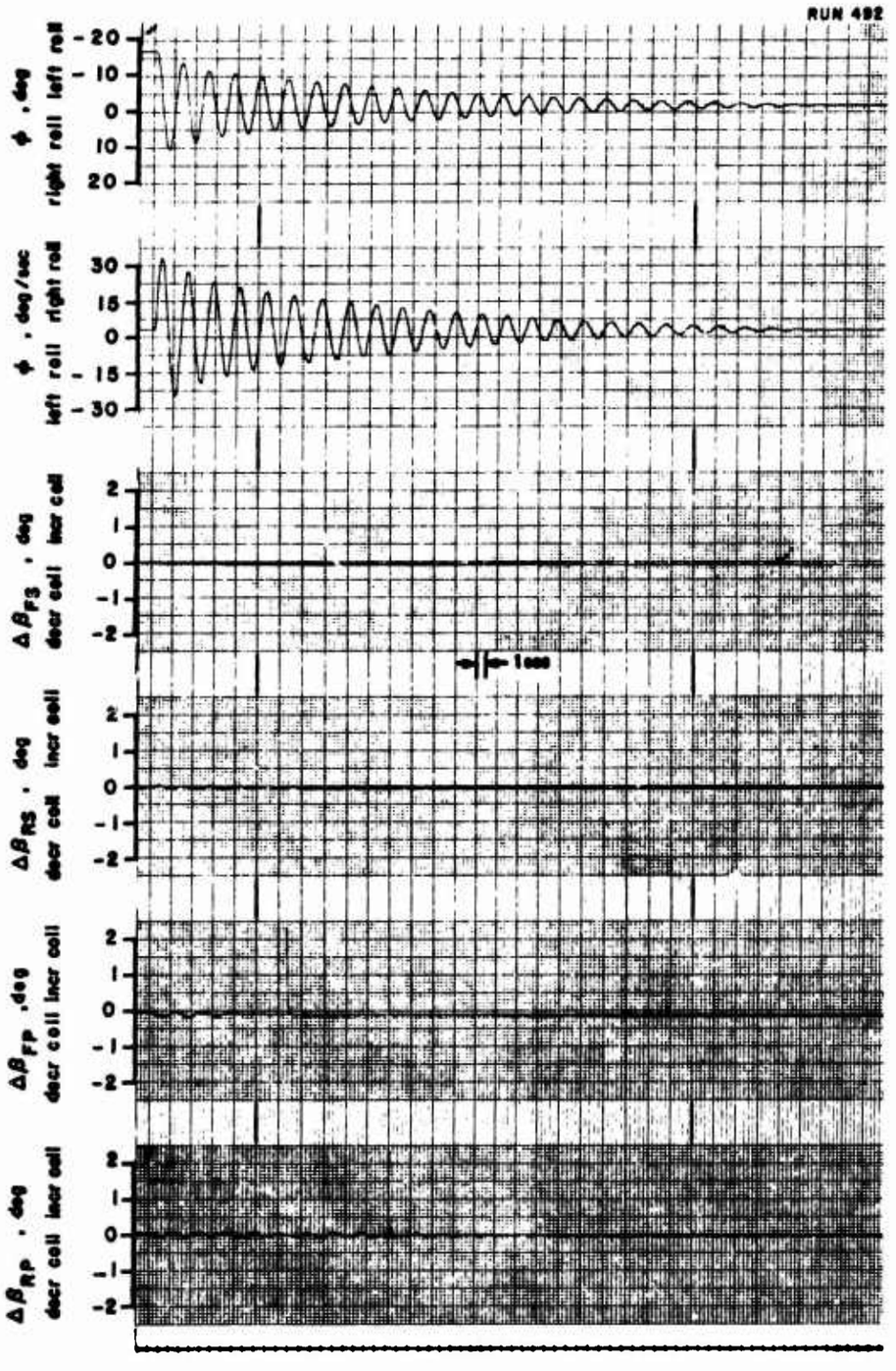

Figure 51. Lateral Transient Response. One Degree of Freedom, ϕ. No Stability Augmentation.
$\beta_{.75R}$ = 25.8°, rpm = zero.

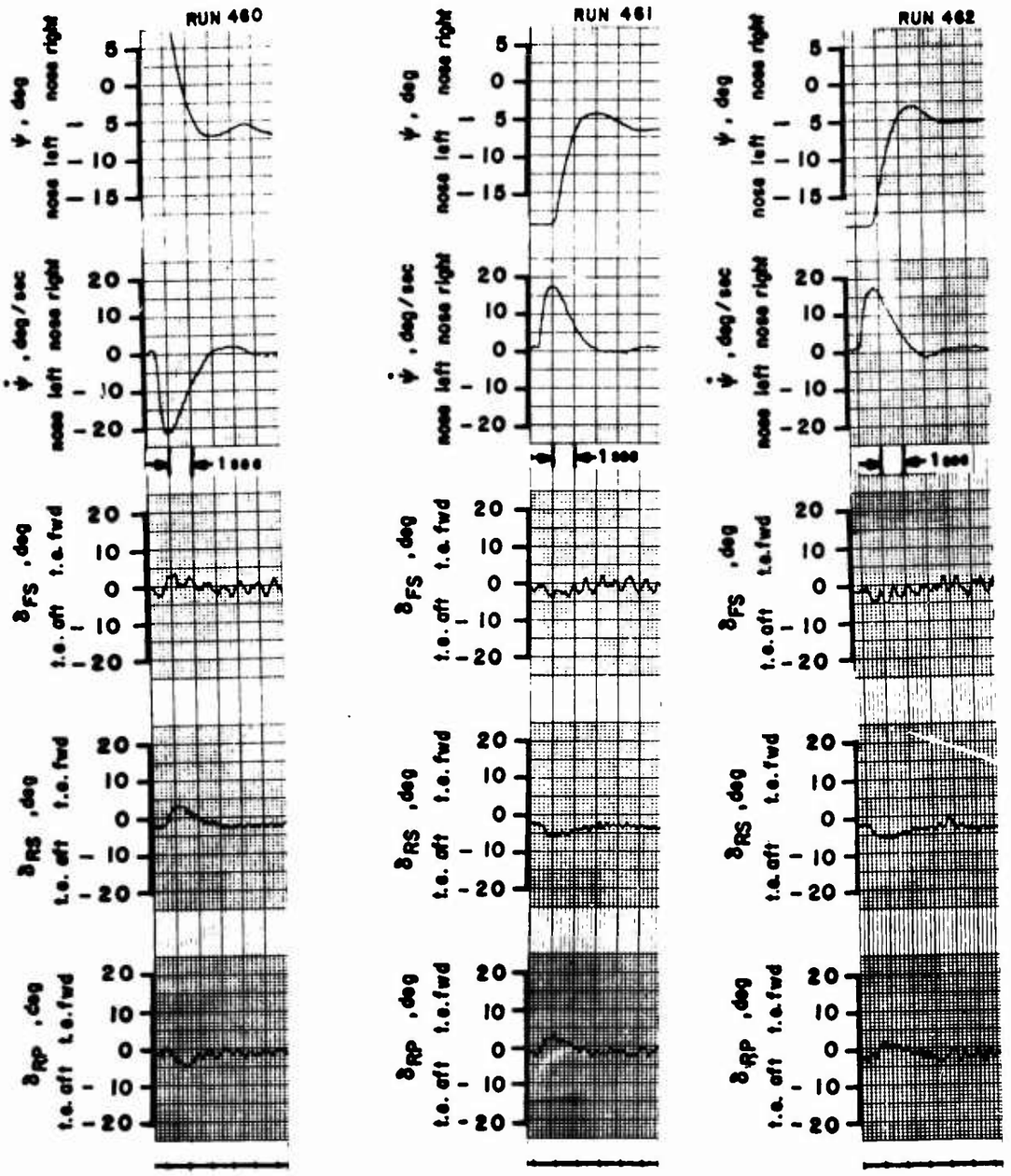

Figure 52. Directional Transient Response. One Degree of Freedom, ψ.
$K_{\dot{\psi}} = 0.083$ sec .
$\beta_{.75R} = 25.8°$, rpm = 7000.

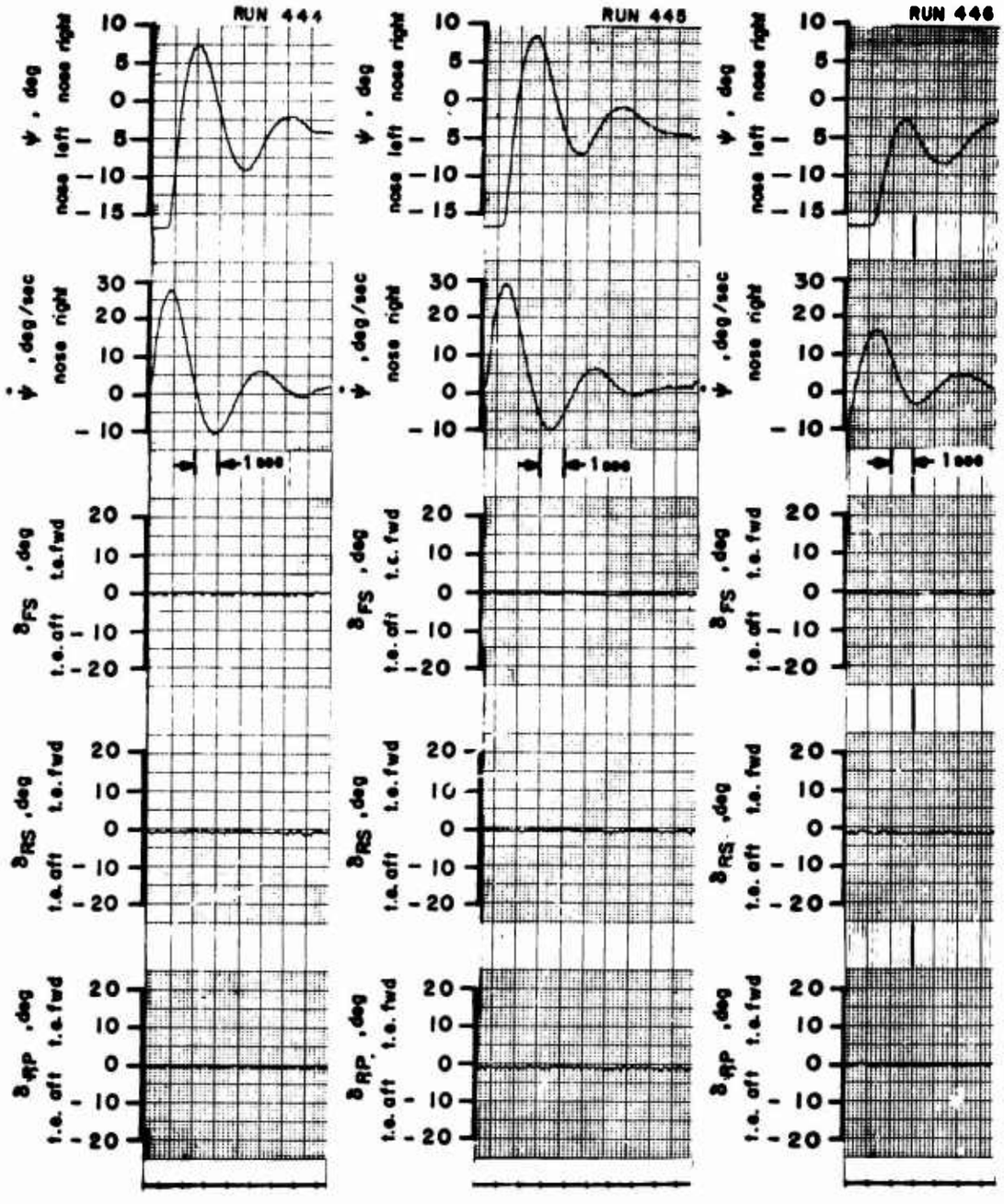

Figure 53. Directional Transient Response. One Degree of Freedom, ψ. No Stability Augmentation.
$\beta_{.75R}$ = 25.8°, rpm = 7000.

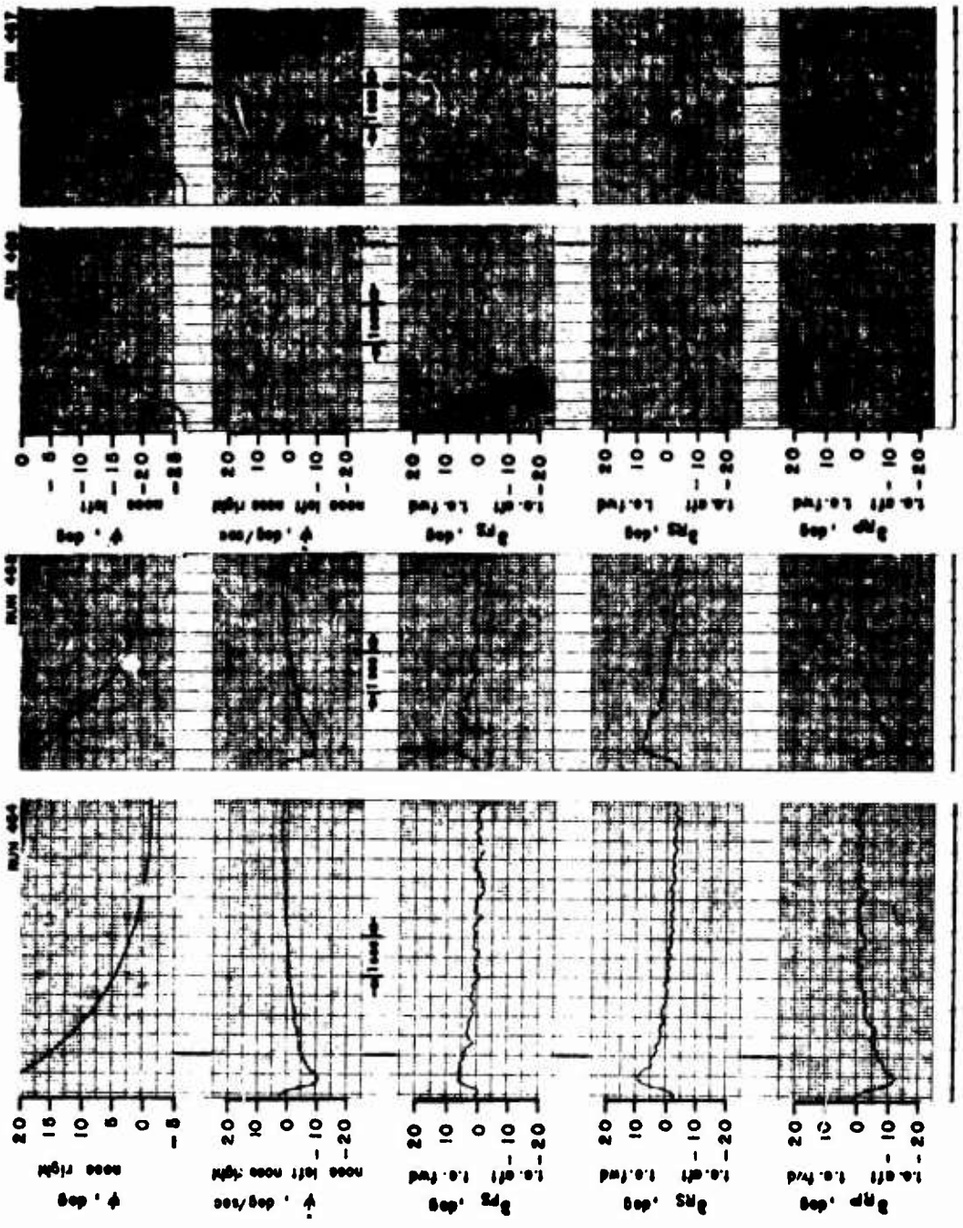

Figure 54. Directional Transient Response. One Degree of Freedom, ψ.
$K_{\dot{\psi}}^{\bullet} = 0.389$ sec .
$\beta_{.75R} = 25.8°$, rpm = 6400.

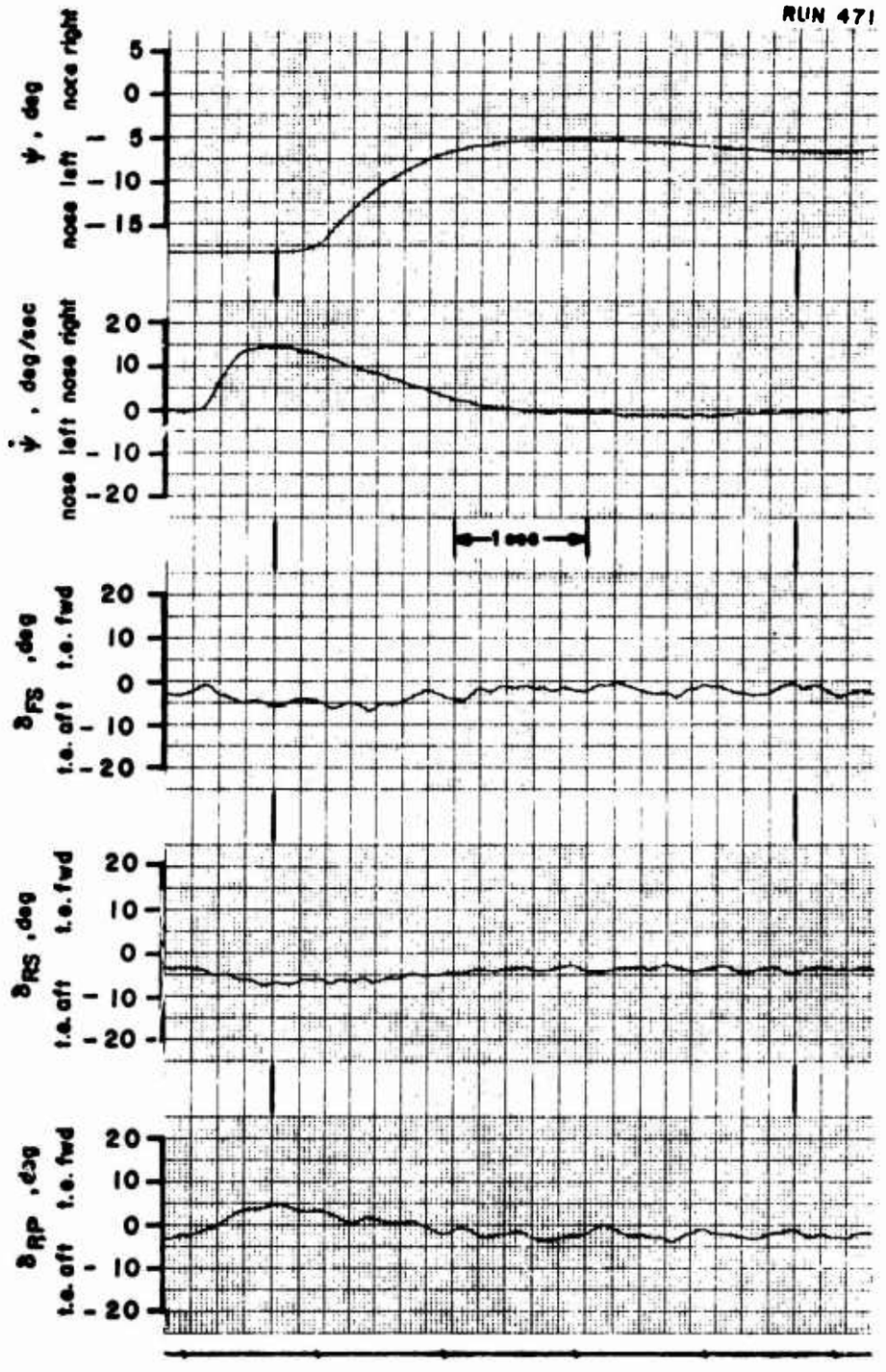

Figure 55. Directional Transient Response. One Degree of Freedom, ψ.
$K_{\dot{\psi}} = 0.209$ sec .
$\beta_{.75R} = 25.8°$, rpm = 6400.

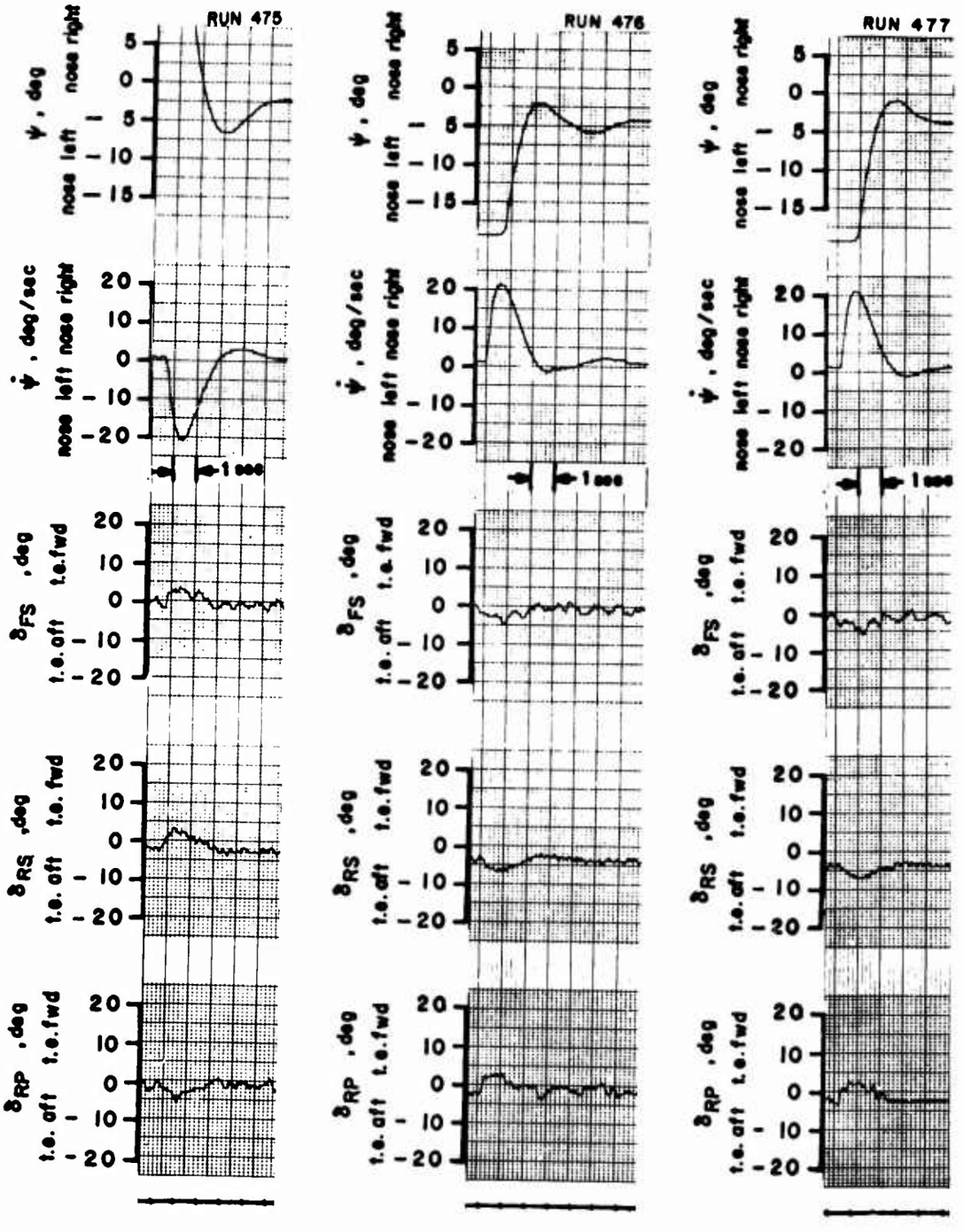

Figure 56. Directional Transient Response. One Degree of Freedom, ψ.
$K_{\dot{\psi}}$ = 0.083 sec .
$\beta_{.75R}$ = 25.8°, rpm = 6400.

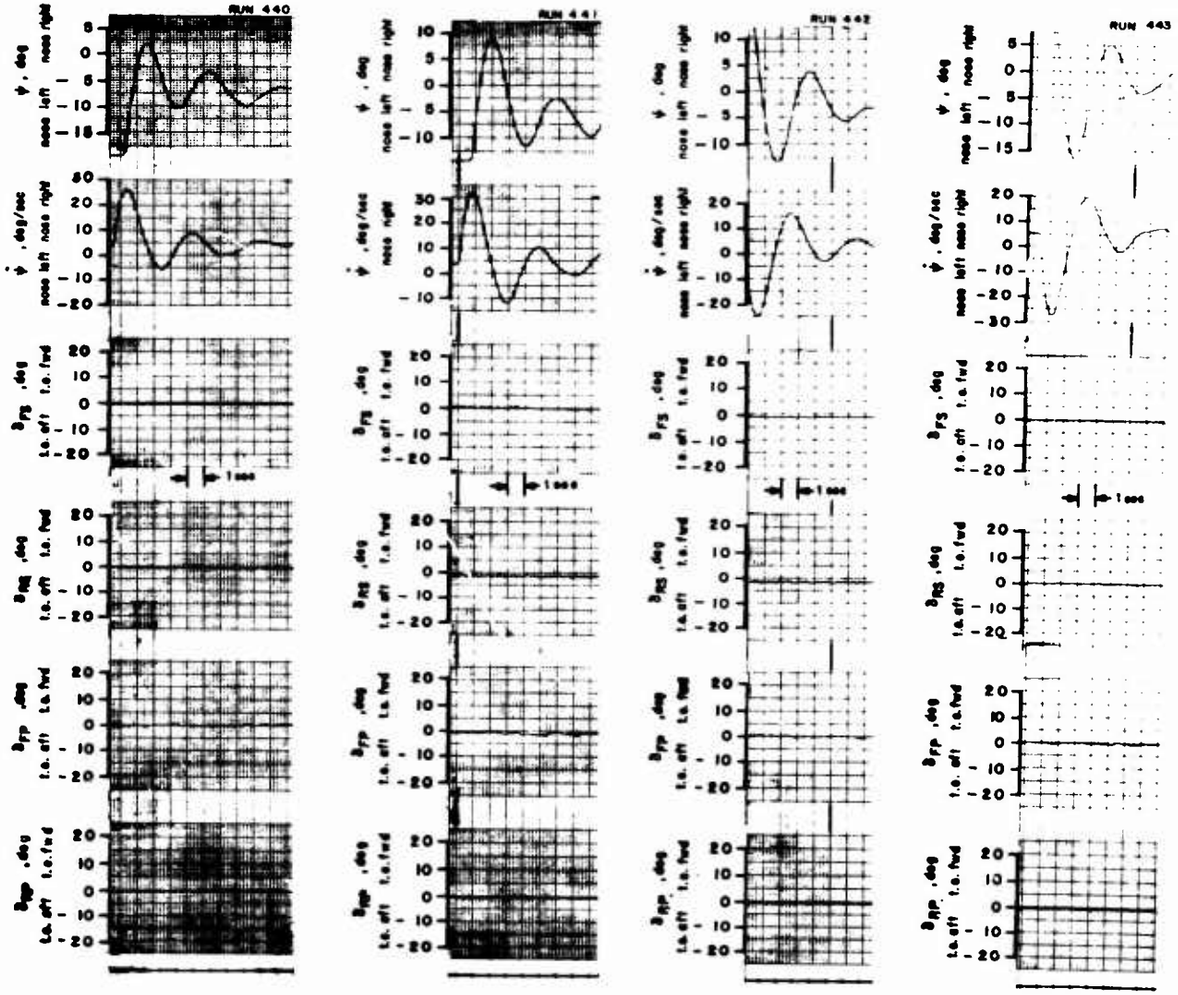

Figure 57. Directional Transient Response. One Degree of Freedom, ψ. No Stability Augmentation.
$\beta_{.75R}$ = 25.8°, rpm = 6400.

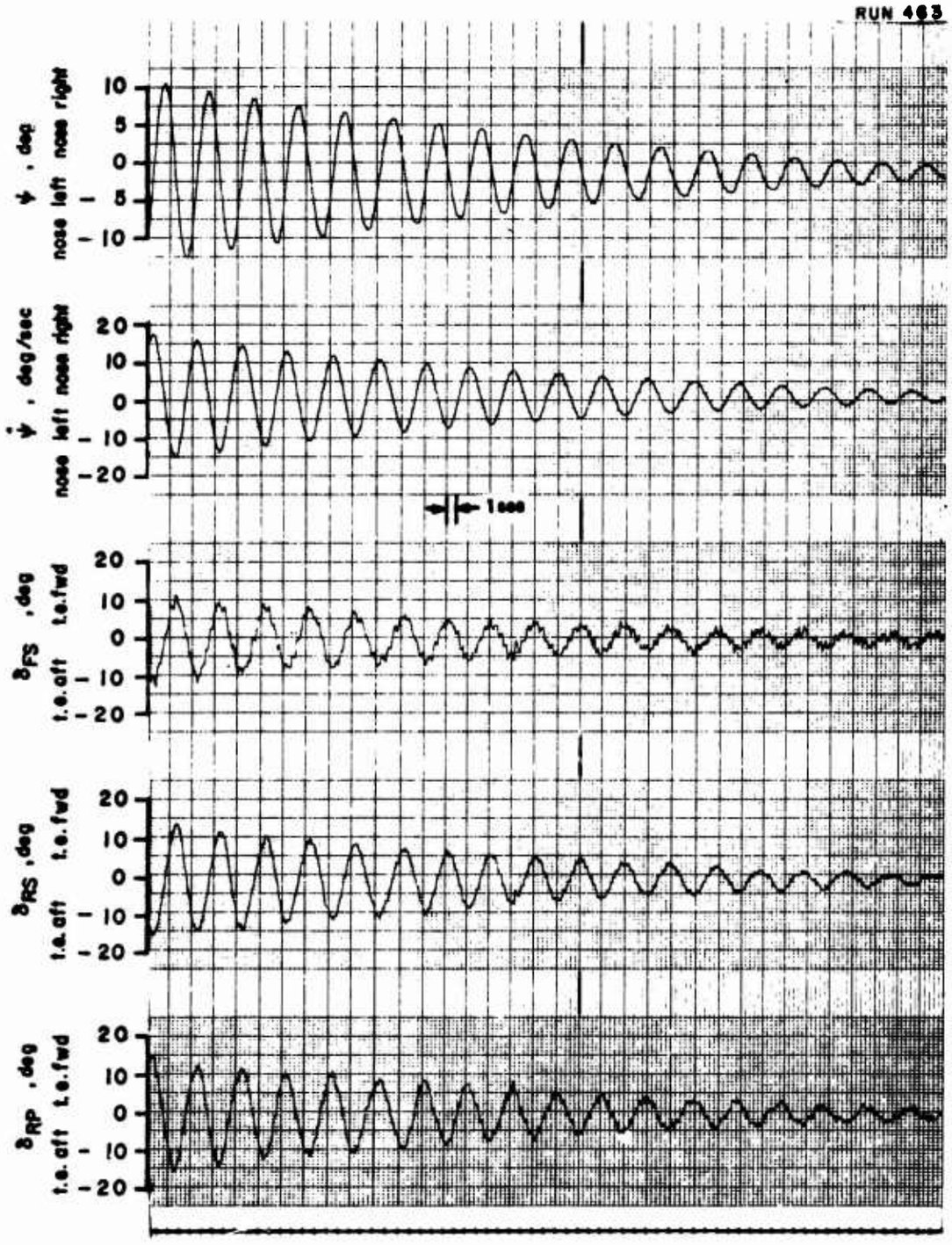

Figure 58. Directional Transient Response. One Degree of Freedom, ψ.
$K_{\dot{\psi}}$ = 0.389 sec .
$\beta_{.75R}$ = 25.8°, rpm = zero.

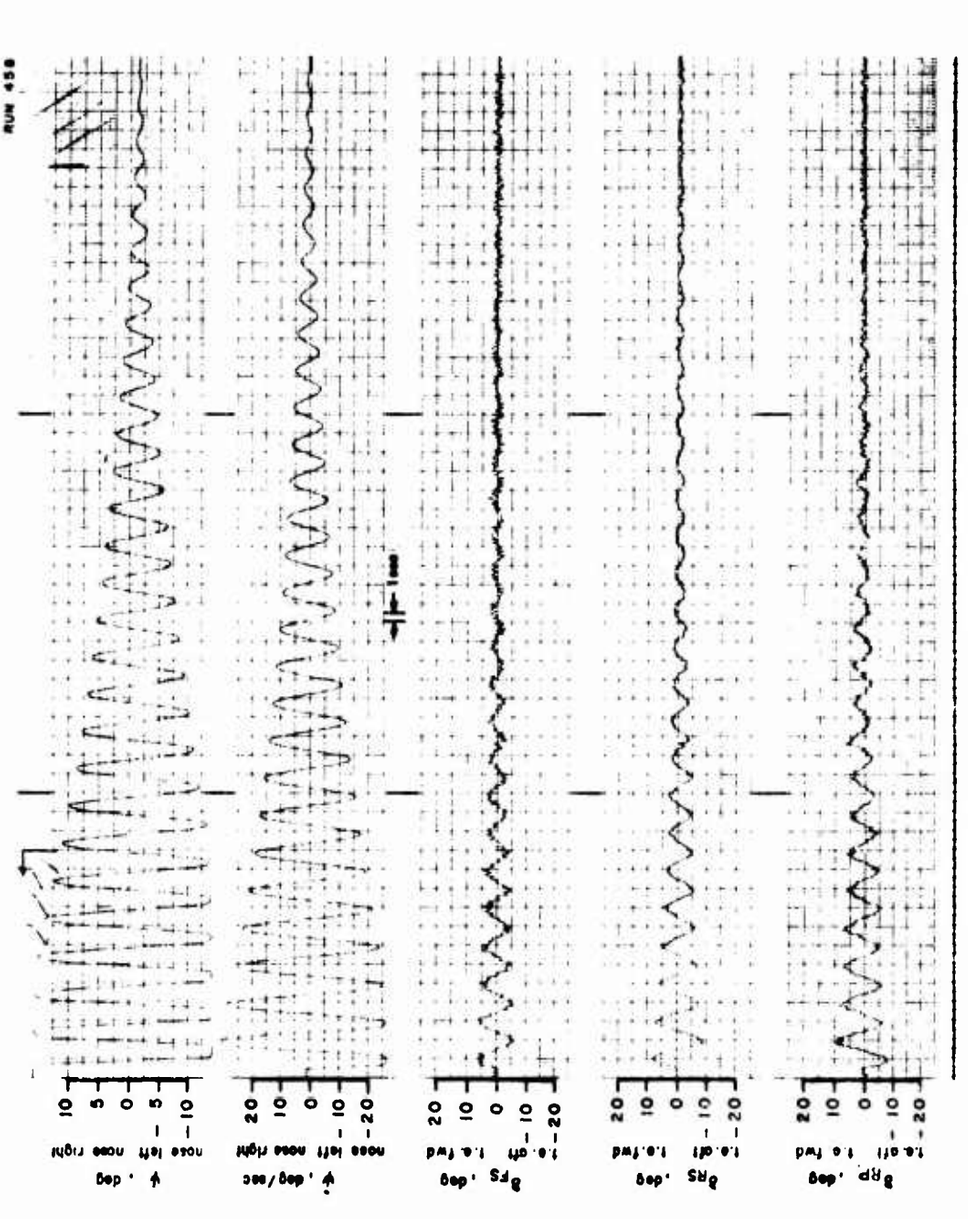

Figure 59. Directional Transient Response. One Degree of Freedom, ψ.
$K_{\psi}^{\bullet} = 0.083$ sec .
$\beta_{.75R} = 25.8°$, rpm = zero.

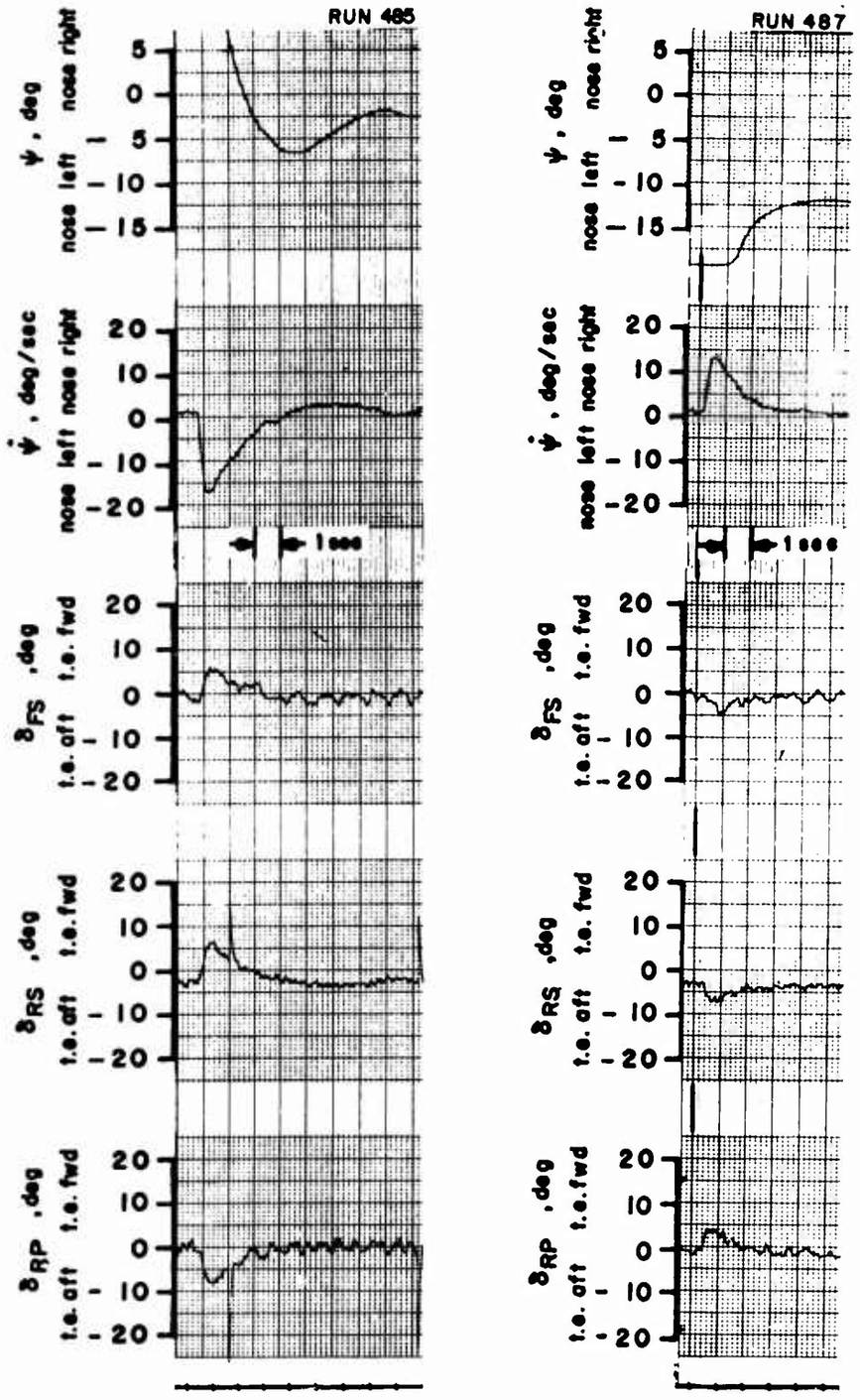

Figure 60. Directional Transient Response. One Degree of Freedom, ψ.
$K_{\dot{\psi}} = 0.209$ sec .
$\beta_{.75R} = 29.2°$, rpm = 6400.

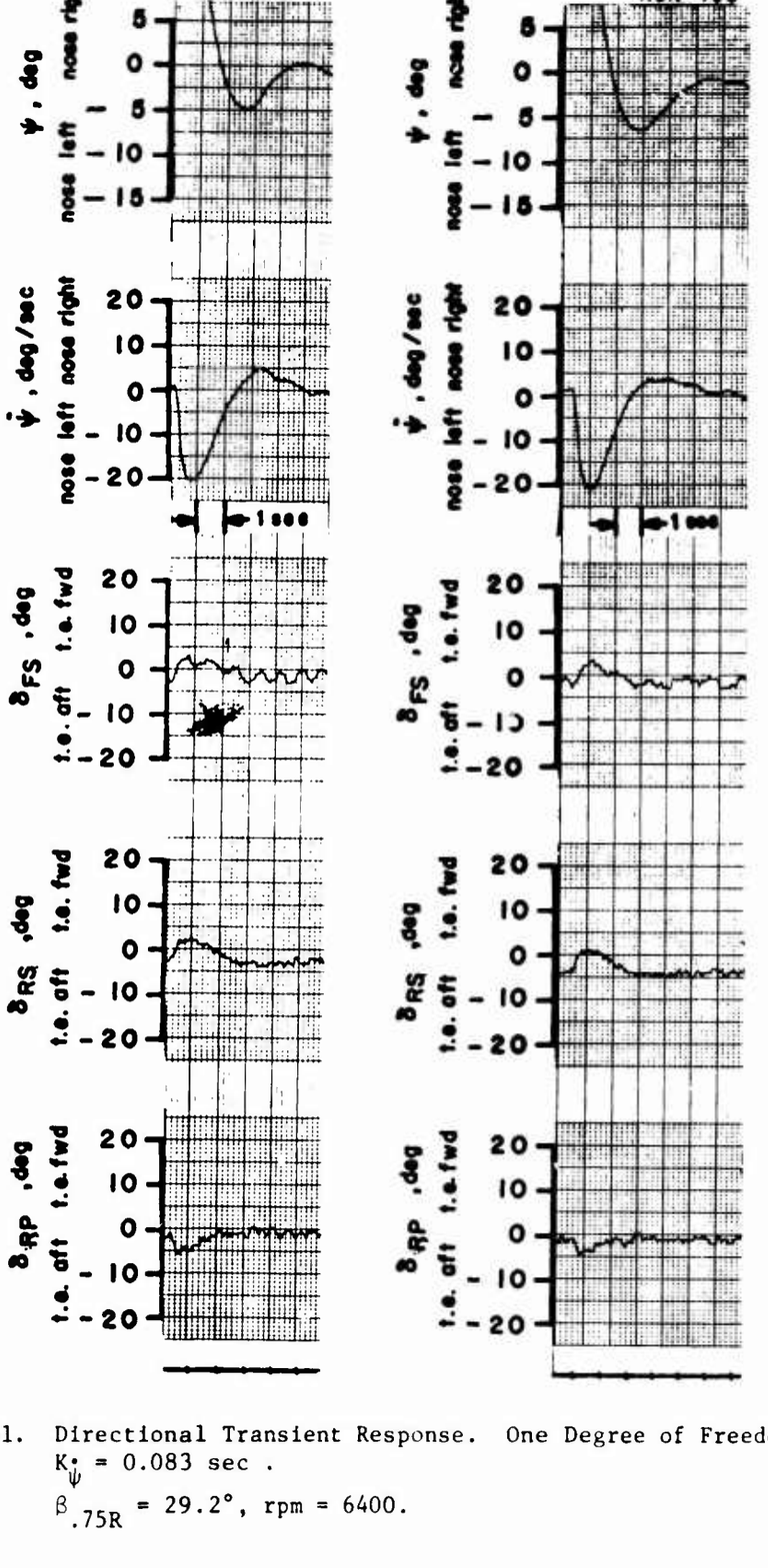

Figure 61. Directional Transient Response. One Degree of Freedom, ψ.
$K_{\dot{\psi}}$ = 0.083 sec .
$\beta_{.75R}$ = 29.2°, rpm = 6400.

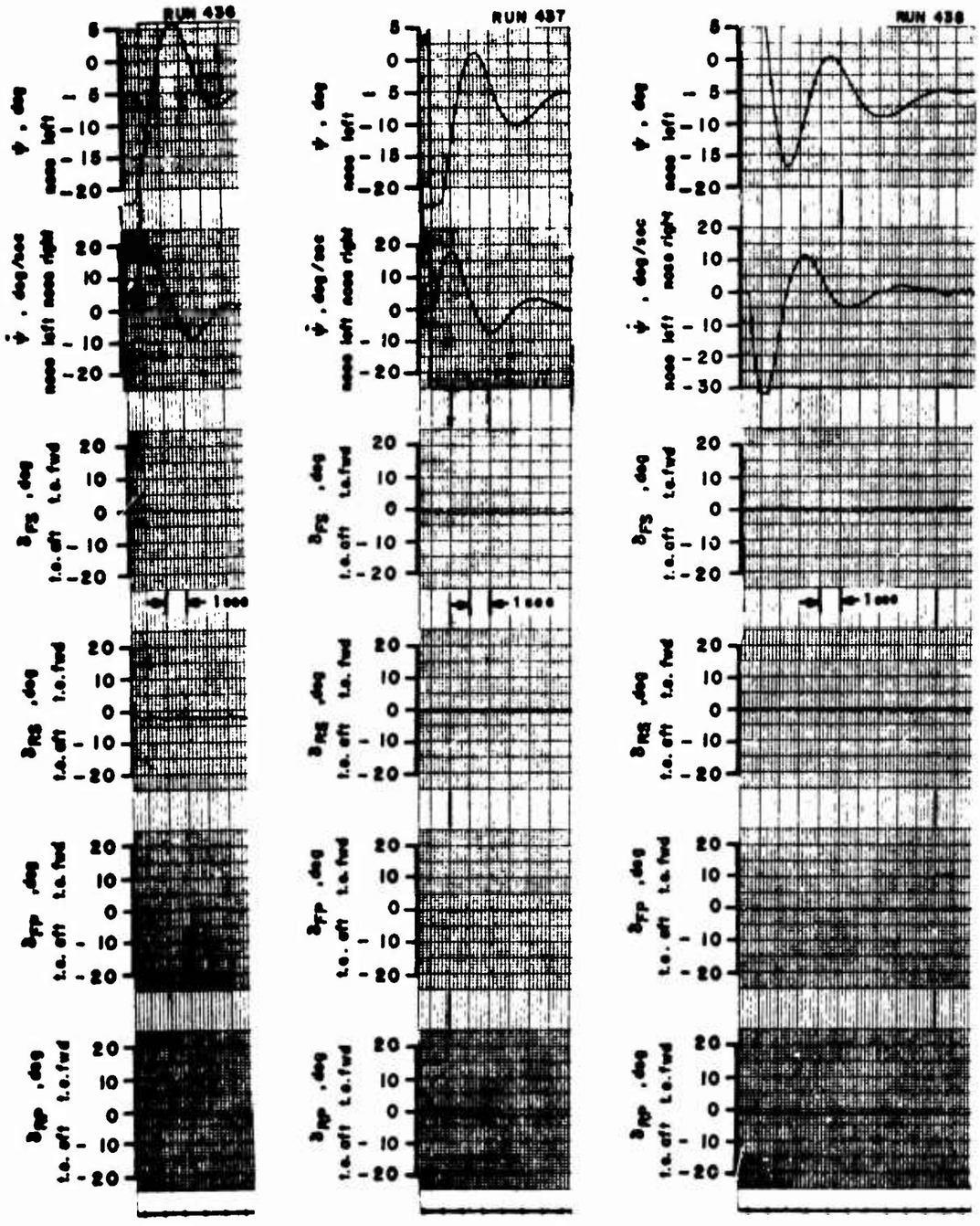

Figure 62. Directional Transient Response. One Degree of Freedom, ψ. No Stability Augmentation.
$\beta_{.75R}$ = 29.2°, rpm = 6400.

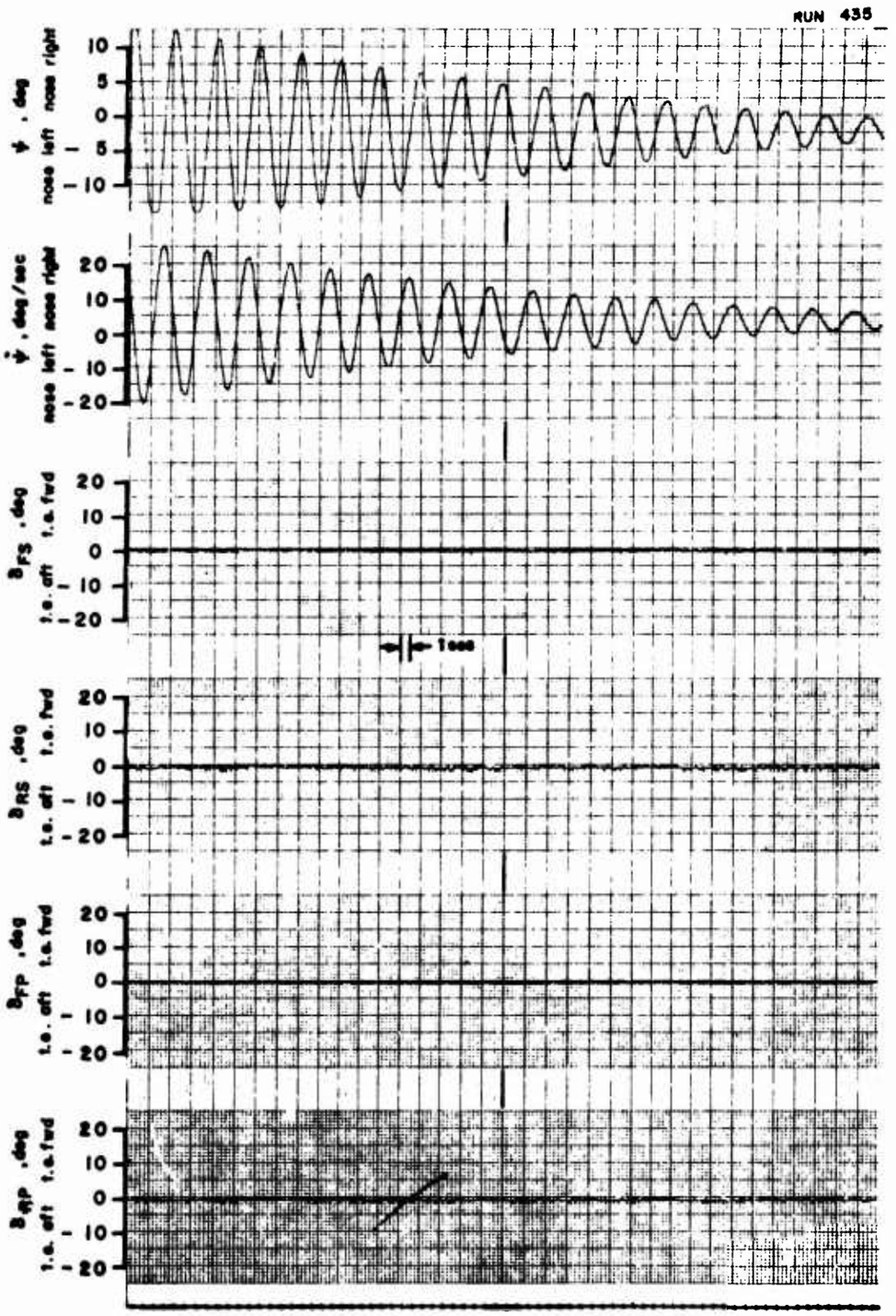

Figure 63. Directional Transient Response. One Degree of Freedom, ψ. No Stability Augmentation. $\beta_{.75R}$ = 29.2°, rpm = zero.

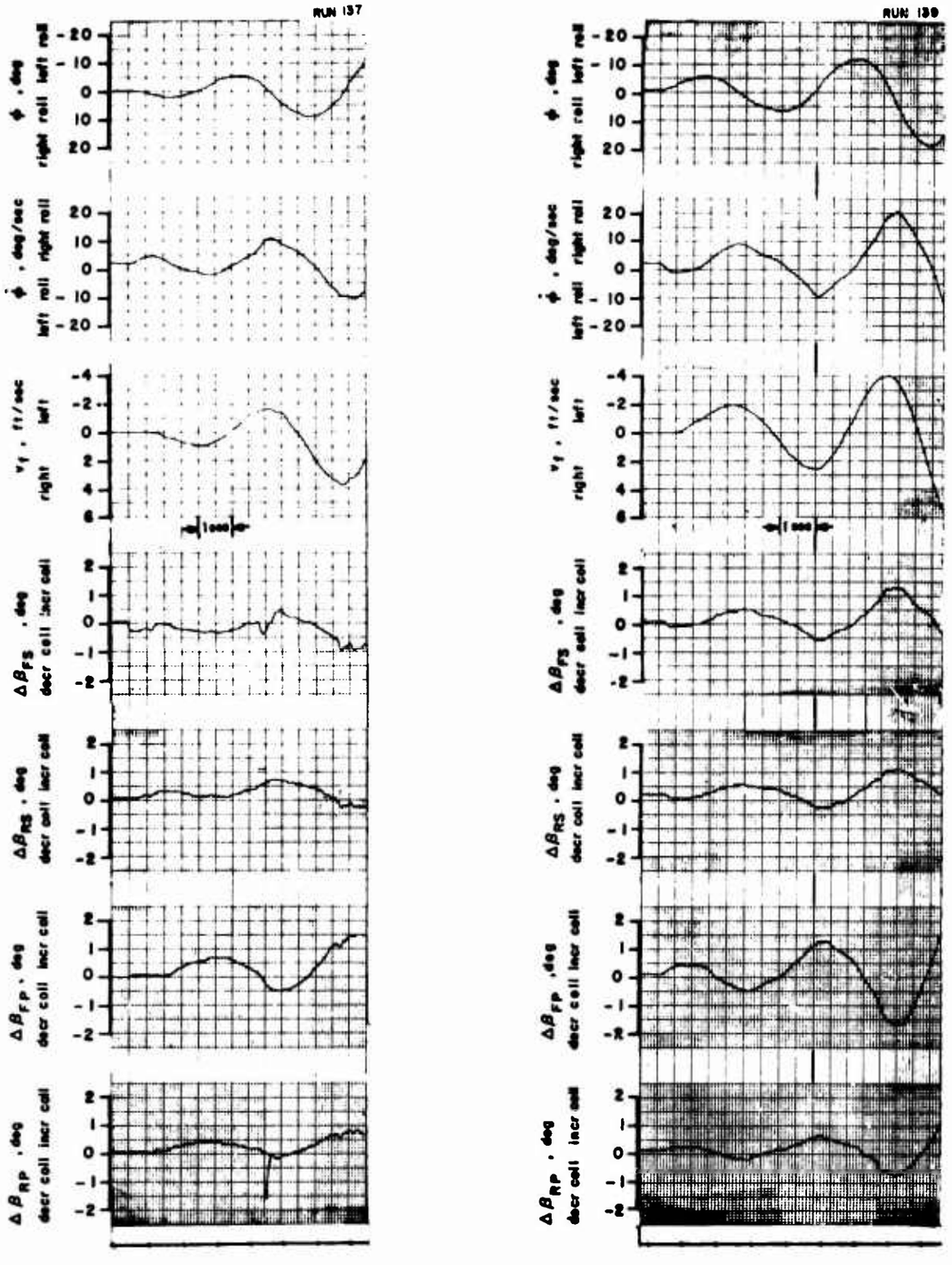

Figure 64. Lateral/Directional Transient Response. Two Degrees of Freedom, ϕ-v_f. $K_{\dot{\phi}}$ = 0.055 sec .

$\beta_{.75R}$ = 25.8°, rpm = 6400.

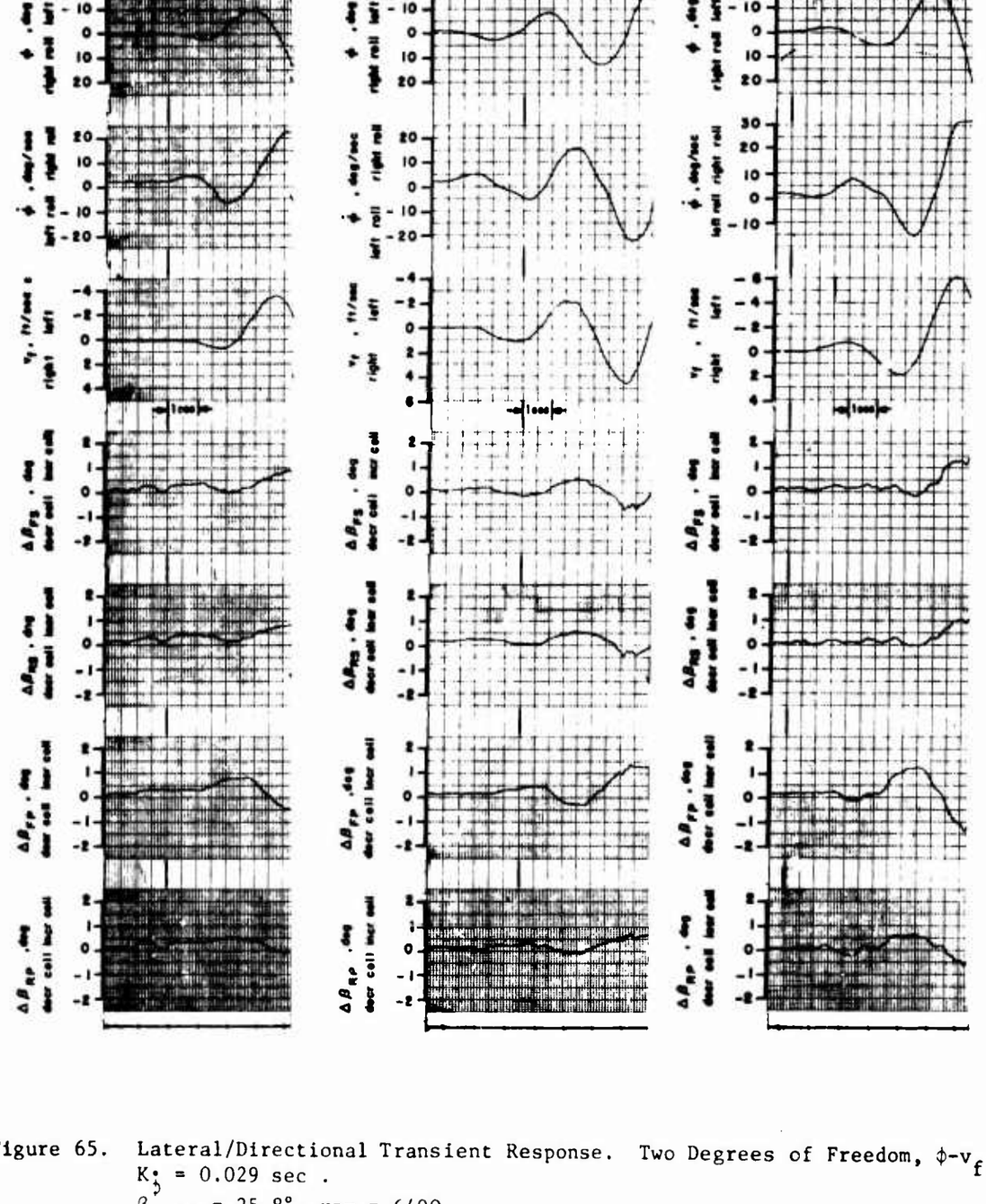

Figure 65. Lateral/Directional Transient Response. Two Degrees of Freedom, ϕ-v_f.
$K_{\dot{\beta}} = 0.029$ sec .
$\beta_{.75R} = 25.8°$, rpm = 6400.

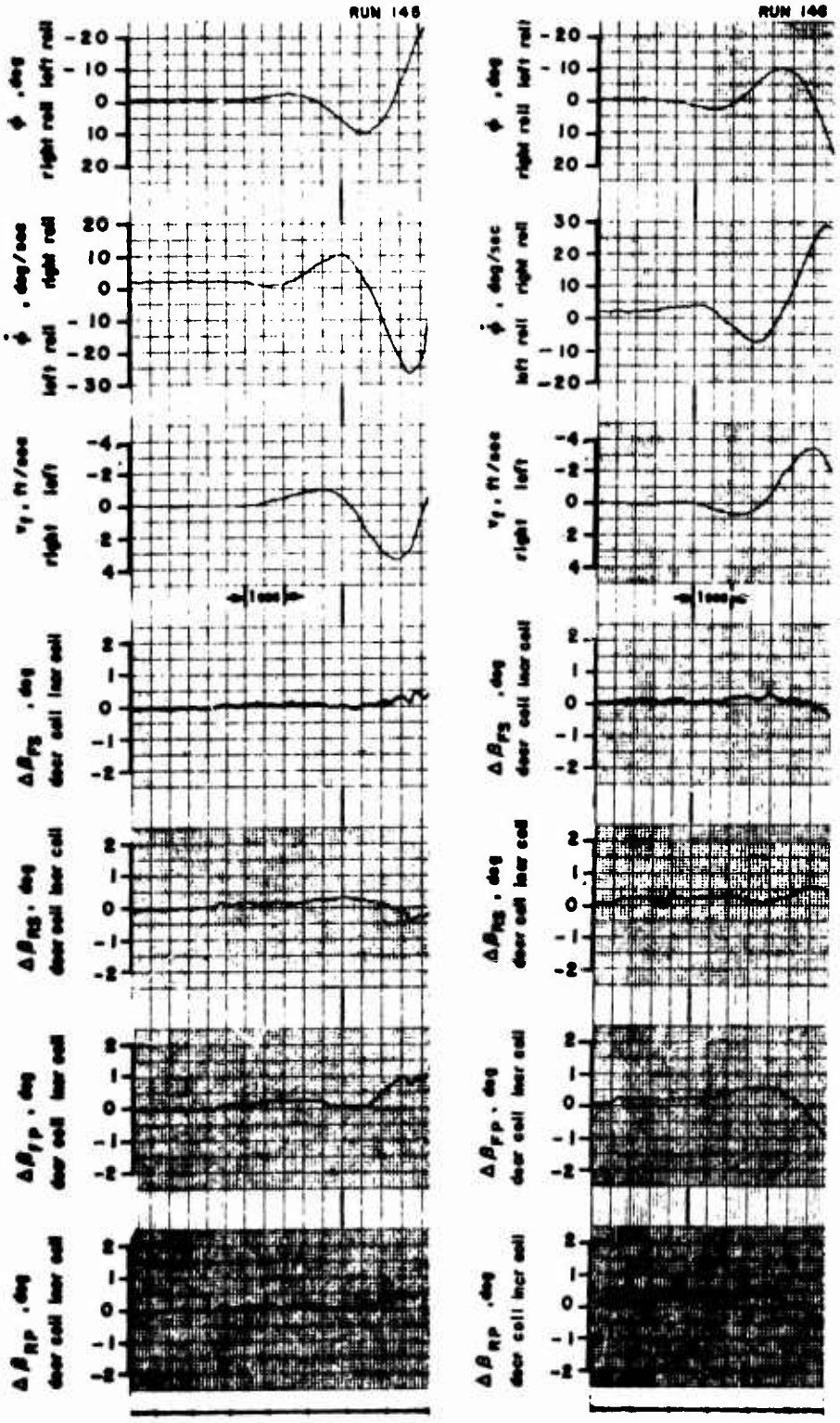

Figure 66. Lateral/Directional Transient Response. Two Degrees of Freedom, ϕ-v_f. $K_{\dot{\phi}}$ = 0.016 sec .
$\beta_{.75R}$ = 25.8°, rpm = 6400.

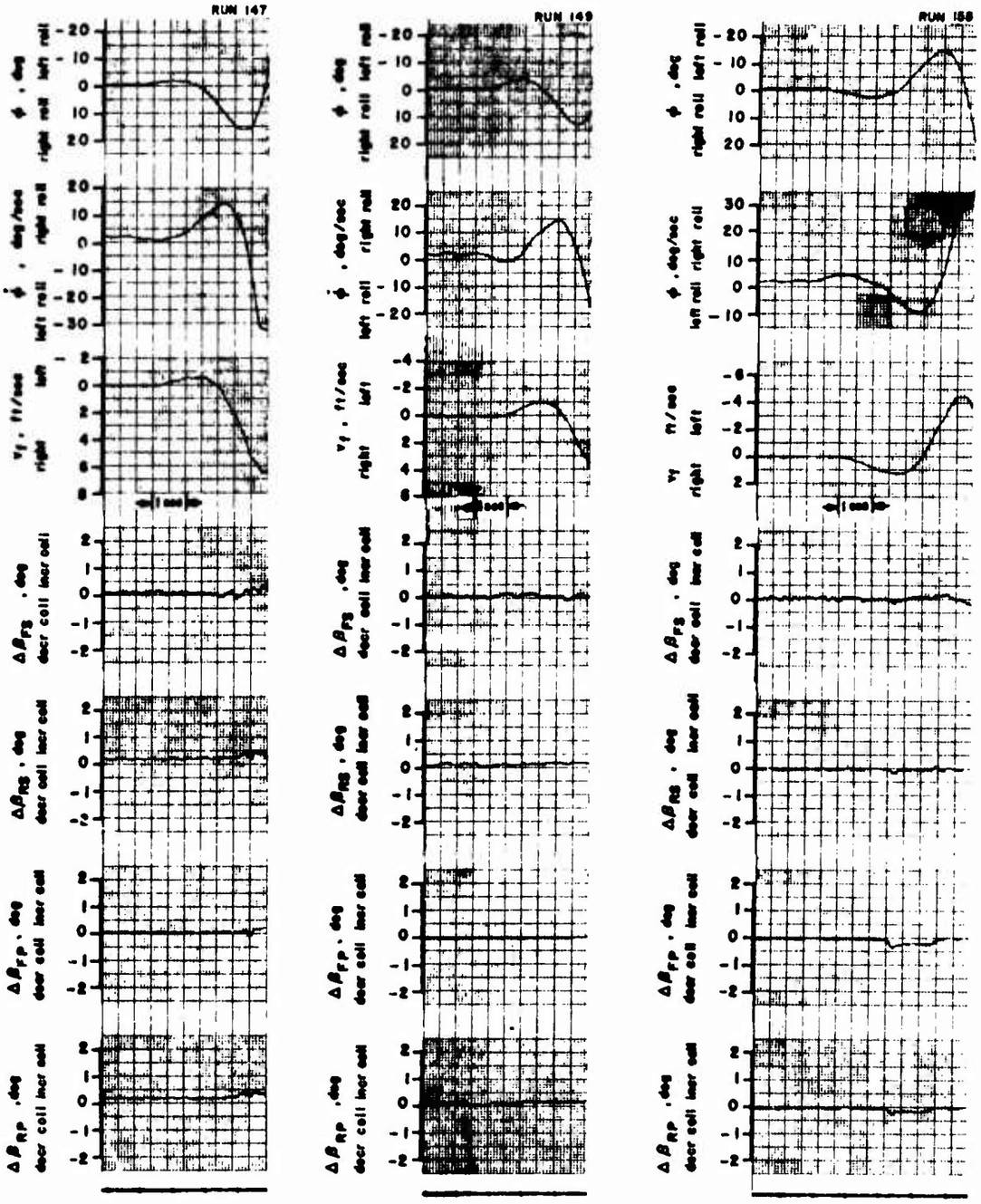

Figure 67. Lateral/Directional Transient Response. Two Degrees of Freedom, ϕ-v_f. No Stability Augmentation.
$\beta_{.75R}$ = 25.8°, rpm = 6400.

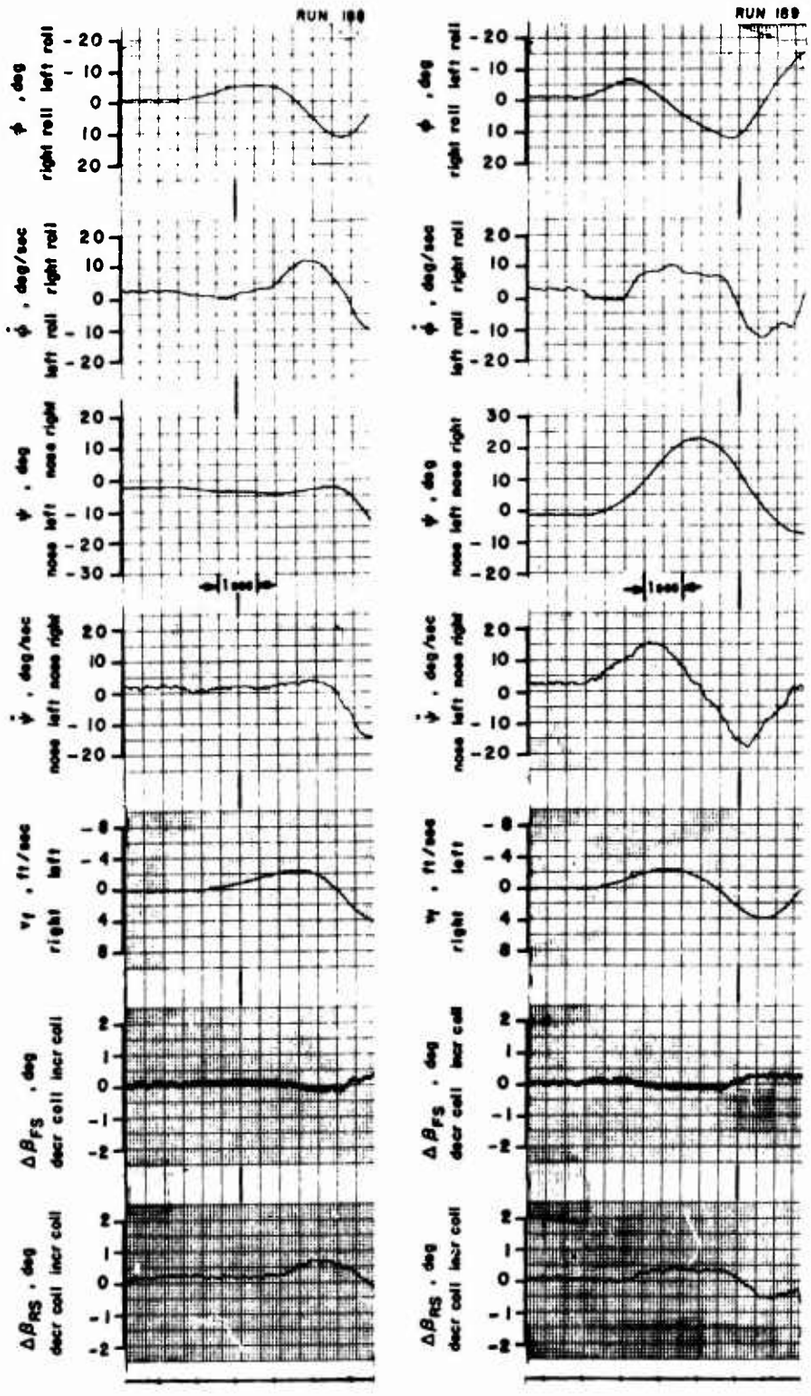

Figure 68. Lateral/Directional Transient Response. Three Degrees of Freedom, ϕ-ψ-v_f. $K_{\dot{\phi}}$ = 0.055 sec .

$\beta_{.75R}$ = 25.8°, rpm = 6400.

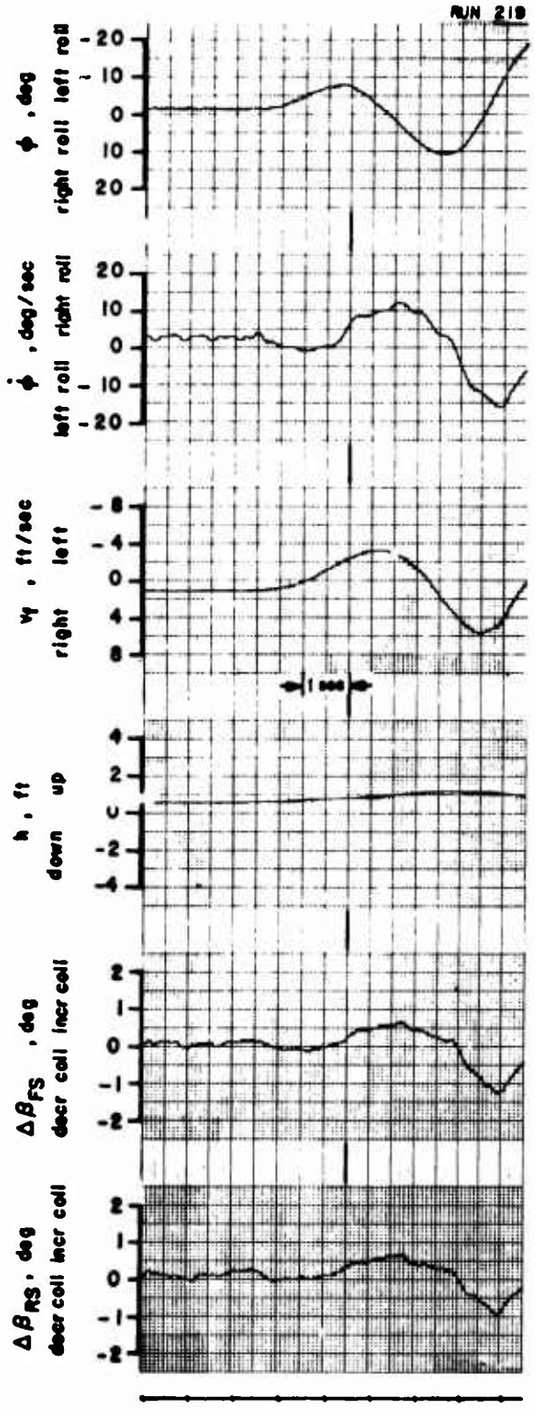

Figure 69. Lateral Transient Response. Three Degrees of Freedom, ϕ-v_f-w_f. $K_{\dot{\phi}}^{*}$ = 0.055 sec . $\beta_{.75R}$ = 25.8°, rpm = 7000.

REFERENCES

1. Michaels, J. L., and Hesby, A. T., AERODYNAMIC STABILITY AND CONTROL AND FLYING QUALITIES, X-22A, Bell Aerosystems Company Report No. 2127-917003, Division of Bell Aerospace Corporation, Buffalo, New York, December 1962.

2. Curtiss, H. C., Jr., Putman, W. F., and Traybar, J. J., GENERAL DESCRIPTION OF THE PRINCETON DYNAMIC MODEL TRACK, Princeton University; USAAVLABS Technical Report 66-73, U. S. Army Aviation Materiel Laboratories, Fort Eustis, Virginia, November 1966, AD 645 883.

3. Putman, W. F., SPECIFICATIONS FOR DESIGN OF A VARIABLE CONFIGURATION QUAD MODEL, Princeton University; Department of Aerospace and Mechanical Sciences Report 839, Princeton, New Jersey, October 1965.

4. Hesby, A. T., WIND TUNNEL TEST DATA REPORT FOR THE FULL SCALE POWERED DUCT MODEL, Bell Aerosystems Company Report No. 2127-921007, Division of Bell Aerospace Corporation, Buffalo, New York, August 1965, pp. 123-125, 138-140.

5. Seckel, Edward, STABILITY AND CONTROL OF AIRPLANES AND HELICOPTERS, New York, Academic Press, 1964.

6. Boyden, Richmond P., and Curtiss, Howard C. Jr., INVESTIGATION OF THE LATERAL/DIRECTIONAL STABILITY CHARACTERISTICS OF A FOUR-PROPELLER TILT-WING VTOL MODEL, Princeton University; USAAVLABS Technical Report 68-19, U. S. Army Aviation Materiel Laboratories, Fort Eustis, Virginia, April 1968.

APPENDIX
EQUATIONS OF MOTION

Linearized equations of motion, applicable to the analysis of various experimentally measured responses, are presented in this appendix.

The longitudinal equations of motion that describe the small perturbation motion of an aircraft from initially level flight, using a stability axis system (Reference 5) are:

$$\begin{aligned} \dot{u} - X_u u - X_w w + g\theta &= 0 \\ \dot{w} - Z_w w - Z_u u - U_o \dot{\theta} &= 0 \\ M_w w + M_{\dot{w}} \dot{w} + M_u u + M_{\dot{\theta}} \dot{\theta} - \ddot{\theta} &= 0 \end{aligned} \tag{1}$$

Two derivatives $X_{\dot{\theta}}$ and $Z_{\dot{\theta}}$ that are usually small are neglected.

Since all of the transient responses were measured and are presented in terms of space-fixed variables, it is convenient to transform equations (1) to a space-fixed system, (Figure 70) with the X_f axis parallel to the horizon, by the following transformations:

$$\begin{aligned} u &= u_f - W_{o_f} \theta \\ w &= w_f + U_{o_f} \theta \end{aligned} \tag{2}$$

where W_{o_f} is equal to zero from the condition of initially level flight.

Substituting relationships (2) into equations (1), the following equations result:

$$\begin{aligned} \dot{u}_f - X_u u_f - X_w w_f + (g - X_w U_{o_f}) \theta &= 0 \\ \dot{w}_f - Z_w w_f - Z_u u_f - Z_w U_{o_f} \theta &= 0 \\ \ddot{\theta} - (M_{\dot{\theta}} + M_{\dot{w}} U_{o_f}) \dot{\theta} - M_w U_{o_f} \theta - M_u u_f - M_{\dot{w}} \dot{w}_f - M_w w_f &= 0 \end{aligned} \tag{3}$$

Because of certain features of the model and the apparatus, two modifications to these equations are necessary such that they will apply to all test conditions.

1. There are two linkages required to attach the model to the servo transducers and mounting system used for this type of testing. These supports provide the horizontal and vertical translational degrees of freedom and contribute additional masses m_h and m_v that "fly" along with the model and, therefore, must also be accelerated by the model. The two linkages are relatively small in weight compared to the "flying" weight of the model but nevertheless should be accounted for by additional mass terms in the equations of motion. Generally, the arrangement and weights of these two supports are such that the mass accelerated by the model in the horizontal direction is larger than that accelerated in the vertical direction. If m_p is the total mass of the model resting on the pivot axis (Figure 71), then the total lifted mass of the model m when "flying" is equal to m_p plus the mass of the vertical link m_v or $m = m_p + m_v$. Similarly, the total accelerated mass in the horizontal direction (m_t) is equal to $m_p + m_v + m_h$ or $m + m_h$. This dynamic model-mount characteristic requires the modification of all terms in the horizontal force equation, except the acceleration term, by a mass ratio defined as m/m_t and equal to 0.936 in value.

2. In certain of the tests (single-degree-of-freedom only) a mechanical spring was added about the model pitch axis to provide a restoring moment which produces an oscillatory motion of the model. In these experiments, the following term should be added:

$$\Delta M_{\theta_m} = - \frac{k_{\theta_m}}{I_y} \tag{4}$$

In the experiments where a spring was employed, the value of the spring constant, k_{θ_m}, is given in Table III.

Adding the necessary terms to account for these three effects, the complete equations of motion that apply to the measured transients obtained in this facility are:

$$\dot{u}_f - \frac{m}{m_t} X_u u_f - \frac{m}{m_t} X_w w_f + \frac{m}{m_t} (g - X_w U_{o_f})\,\theta = 0$$

$$\dot{w}_f - Z_w w_f - Z_u u_f - Z_w U_{o_f}\,\theta = 0$$

$$\ddot{\theta} - (M_{\dot{\theta}} + M_{\dot{w}} U_{o_f})\,\dot{\theta} + \left(\frac{k_{\theta_m}}{I_y} - M_w U_{o_f}\right)\theta - M_u u_f - M_{\dot{w}} \dot{w}_f - M_w w_f = 0 \tag{5}$$

For the restricted degree of freedom tests, then the following reduced sets of equations apply.

1. In two degrees of freedom, with $k_{\theta_m} = 0$:

   a. θ, u_f ($w_f = 0$)

$$\dot{u}_f - \frac{m}{m_t} X_u u_f + \frac{m}{m_t} (g - X_w U_{o_f}) \theta = 0$$

$$\ddot{\theta} - (M_{\dot{\theta}} + M_{\dot{w}} U_{o_f}) \dot{\theta} - M_w U_{o_f} \theta - M_u u_f = 0 \qquad (6)$$

   b. θ, w_f ($u_f = 0$)

$$\dot{w}_f - Z_w w_f - Z_w U_{o_f} \theta = 0$$

$$\ddot{\theta} - (M_{\dot{\theta}} + M_{\dot{w}} U_{o_f}) \dot{\theta} - M_w U_{o_f} \theta - M_{\dot{w}} \dot{w}_f - M_w w_f = 0 \qquad (7)$$

2. In the single-degree-of-freedom experiments, with the mechanical spring and $u_f = 0$, $w_f = 0$, the equation that applies is:

$$\ddot{\theta} - (M_{\dot{\theta}} + M_{\dot{w}} U_{o_f}) \dot{\theta} + \left(\frac{k_{\theta_m}}{I_y} - M_w U_{o_f} \right) \theta = 0 \qquad (8)$$

3. In the experiments where feedback is used, a term $M_{\Delta\beta_{PITCH}} \Delta\beta_{PITCH}$ should be added to the right hand side of the pitching moment equation, and then the equation governing $\Delta\beta$ is:

$$\Delta\beta_{PITCH} = K_{\dot{\theta}} \dot{\theta} \qquad (9)$$

   By substitution of these expressions into the pitching moment equation, an effective pitch damping is obtained:

$$\bar{M}_{\dot{\theta}} = M_{\dot{\theta}} + K_{\dot{\theta}} M_{\Delta\beta_{PITCH}} \qquad (10)$$

The lateral/directional equations of motion that describe the small perturbation motion of an aircraft from initially level flight are (Reference 5):

$$\dot{v} - Y_v v + U_o \cos \eta\, r - g \phi + U_o \sin \eta\, p = 0$$

$$- L_v v - L_r r + \dot{p} - L_p p = 0$$

$$- N_v v - \dot{r} - N_r r - N_p p = 0 \qquad (11)$$

These equations are written with respect to principal axes, inclined nose down from the horizon by an angle η (Figure 9).

The gimbal mount supporting the model provides roll freedom about the principal body axis (X''), and yaw freedom about a space-fixed axis ($\bar{Z}_f$) as shown in Figure 11. It is not possible to provide body-axis freedom about the X'' and Z'' axes with a simple geometric linkage. For small disturbances from initially level flight, the difference between the equations of motion in principal axes (X'', Z'') and gimbal axes ($X'', \bar{Z}_f$) is of second order. Reference 6 may be consulted for further detail. The relationships between the principal axis angular rates (p,r) and the gimbal axis rates ($\dot{\phi}, \dot{\Psi}$) are:

$$p = \dot{\phi}$$

$$r = \dot{\Psi} \cos \phi \approx \dot{\Psi} \qquad (12)$$

As in the longitudinal case, it is convenient to transform the lateral velocity to a space-fixed system to correspond to the manner in which the data is presented. The transformation equation is:

$$v = v_f - U_{o_f} \cos \eta\, \Psi - U_{o_f} \sin \eta\, \phi \qquad (13)$$

Substituting the relationships (12) and (13) into (11),

$$\dot{v}_f - Y_v v_f + Y_v U_{o_f} \cos \eta\, \Psi - (g - Y_v U_{o_f} \sin \eta)\, \phi = 0$$

$$- L_v v_f - L_r \dot{\Psi} + L_v U_{o_f} \cos \eta\, \Psi + \ddot{\phi} - L_p \dot{\phi} + L_v U_{o_f} \sin \eta\, \phi = 0$$

$$- N_v v_f - \ddot{\Psi} - N_r \dot{\Psi} + N_v U_{o_f} \cos \eta\, \Psi - N_p \dot{\phi} + N_v U_{o_f} \sin \eta\, \phi = 0 \qquad (14)$$

As in the case of the longitudinal equations, two modifications to these equations are necessary such that they will apply to all test conditions.

1. The linkage arrangement associated with the model mounting system described previously is accounted for by a factor m/m_t in the sideforce equation as in the horizontal force equation in the longitudinal case (Figure 7).

2. Mechanical springs were added about the model roll axis and the model yaw axis to produce oscillatory motions in the single-degree-of-freedom tests. The following terms should be added for these tests.

$$\Delta L_{\phi_m} = - \frac{k_{\phi_m}}{I_x}$$

$$\Delta N_{\psi_m} = - \frac{k_{\psi_m}}{I_z} \qquad (15)$$

The values of the spring constants are given in Table III.

With these modifications, the equations of motion that apply to the experiments are

$$\dot{v}_f - \frac{m}{m_t} Y_v v_f - \frac{m}{m_t} Y_v U_{o_f} \cos \eta \, \psi - \frac{m}{m_t} (g - Y_v U_{o_f} \sin \eta) \phi = 0$$

$$- L_v v_f - L_r \dot{\psi} + L_v U_{o_f} \cos \eta \, \psi + \ddot{\phi} - L_p \dot{\phi} + \left(\frac{k_{\phi_m}}{I_x} + L_v U_{o_f} \sin \eta \right) \phi = 0$$

$$- N_v v_f - \ddot{\psi} - N_r \dot{\psi} + \left(N_v U_{o_f} \cos \eta - \frac{k_{\psi_m}}{I_z} \right) \psi - N_p \dot{\phi} + N_v U_{o_f} \sin \eta \, \phi = 0 \qquad (16)$$

For the restricted degree of freedom tests, the following reduced set of equations apply.

1. In two degrees of freedom, with $k_{\psi_m} = k_{\phi_m} = 0$:

   a. v_f, ϕ ($\psi = 0$)

$$\dot{v}_f - \frac{m}{m_t} Y_v v_f - \frac{m}{m_t} (g - Y_v U_{o_f} \sin \eta)\, \phi = 0$$

$$- L_v v_f + \ddot{\phi} - L_p \dot{\phi} + L_v U_{o_f} \sin \eta\, \phi = 0 \qquad (17)$$

   b. ϕ, ψ ($v_f = 0$)

$$- L_r \dot{\psi} + L_v U_{o_f} \cos \eta\, \psi + \ddot{\phi} - L_p \dot{\phi} + L_v U_{o_f} \sin \eta\, \phi = 0$$

$$- \ddot{\psi} - N_r \dot{\psi} + N_v U_{o_f} \cos \eta\, \psi - N_p \dot{\phi} + N_v U_{o_f} \sin \eta\, \phi = 0 \qquad (18)$$

   c. v_f, ψ ($\phi = 0$)

$$\dot{v}_f - \frac{m}{m_t} Y_v v_f + Y_v U_{o_f} \cos \eta\, \psi = 0$$

$$- N_v v_f - \ddot{\psi} - N_r \dot{\psi} + N_v U_{o_f} \cos \eta\, \psi = 0 \qquad (19)$$

2. In the single-degree-of-freedom experiments with mechanical springs, the equations of motion are

   a. ϕ ($\psi = 0$, $v_f = 0$)

$$\ddot{\phi} - L_p \dot{\phi} + \left(\frac{k_{\phi_m}}{I_x} + L_v U_{o_f} \sin \eta \right) \phi = 0 \qquad (20)$$

   b. ψ ($\phi = 0$, $v_f = 0$)

$$- \ddot{\psi} - N_r \dot{\psi} + \left(N_v U_{o_f} \cos \eta - \frac{k_{\psi_m}}{I_z} \right) \psi = 0 \qquad (21)$$

3. In the lateral/directional experiments with feedback, a term $L_{\Delta\beta_{ROLL}}\ \Delta\beta_{ROLL}$ should be added to the right hand side of the rolling moment equation, and a term $N_{\Delta\delta}\ \Delta\delta$ should be added to the right hand side of the yawing moment equation. The equations governing $\Delta\beta_{ROLL}$ and $\Delta\delta$ are

$$\Delta\beta_{ROLL} = K_{\dot{\phi}}^{\cdot}\ \dot{\phi}$$

$$\Delta\delta = K_{\dot{\psi}}^{\cdot}\ \dot{\psi} \qquad (22)$$

As in the longitudinal case, the effect of these feedbacks may be considered as increments to the damping derivatives

$$\bar{L}_p = L_p + K_{\dot{\phi}}^{\cdot}\ L_{\Delta\beta_{ROLL}}$$

$$\bar{N}_r = N_r + K_{\dot{\psi}}^{\cdot}\ N_{\Delta\delta} \qquad (23)$$

The above equations apply to the hovering case as well as forward flight. In hover, U_{O_f} is equal to zero. Also, in hovering flight and from symmetry considerations, it would be expected that X_w and Z_u are equal to zero.

SPACE-FIXED AXIS

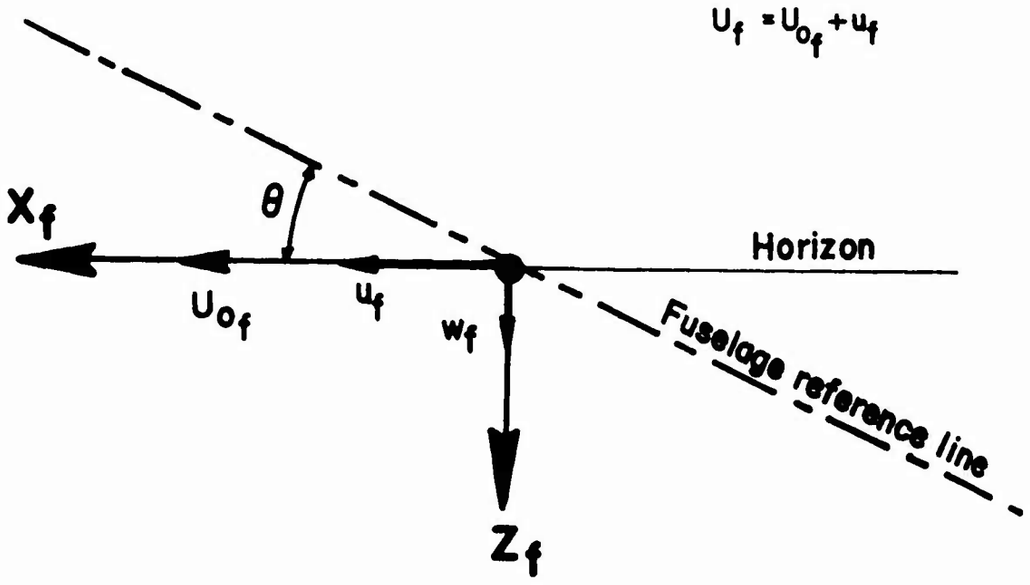

STABILITY AXIS

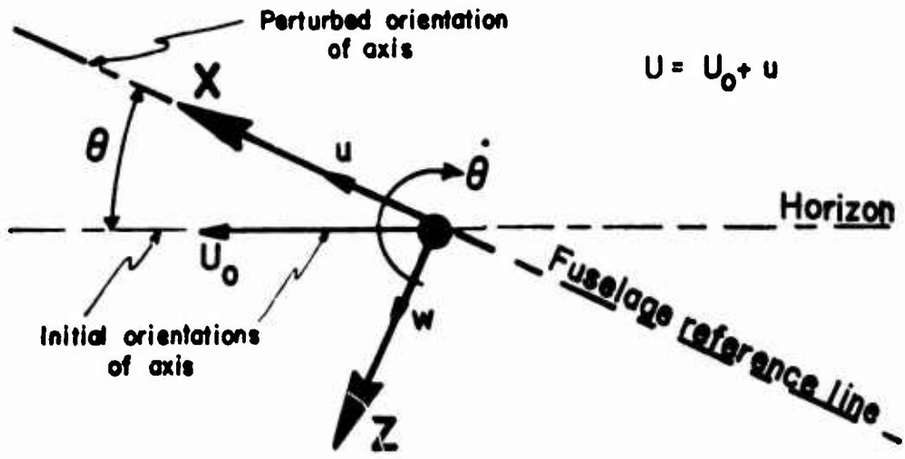

(body fixed; initially aligned with freestream velocity at forward speeds or with horizon in hover)

Figure 70. Definitions of Space-Fixed and Stability Axis Systems.
Variables are Shown in Their Positive Sense.

MODEL AND LINKAGE MASS ARRANGEMENTS

Note

Lifted mass $m = m_p + m_v$

Total horizontal mass $m_t = m_p + m_v + m_h = m + m_h$

Mass ratio: $\frac{m}{m_t} = \frac{m_p + m_v}{m + m_h}$

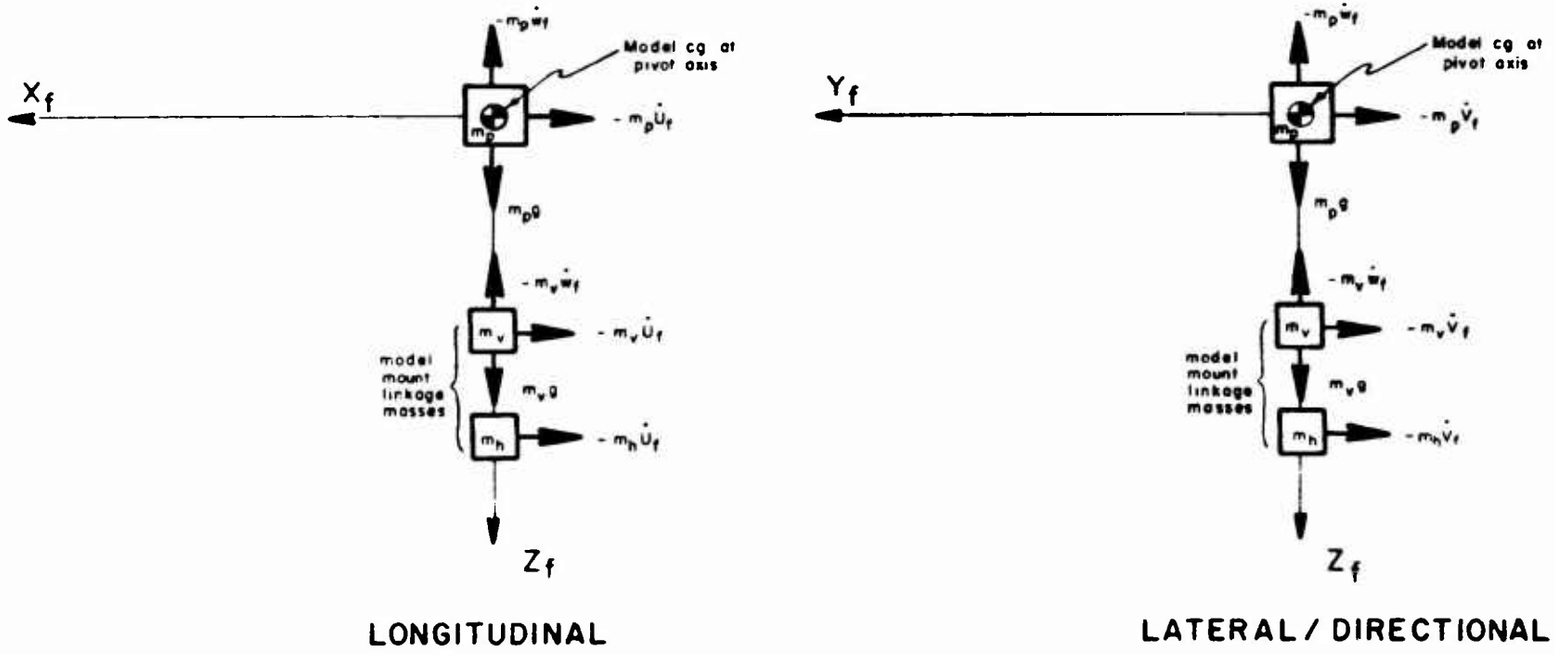

Figure 71. Model and Link Mass Arrangements and Reference Systems for Model cg (Pivot Axes).

Unclassified

Security Classification

DOCUMENT CONTROL DATA - R & D

(Security classification of title, body of abstract and indexing annotation must be entered when the overall report is classified)

1. ORIGINATING ACTIVITY (Corporate author) Department of Aerospace and Mechanical Sciences Princeton University Princeton, New Jersey	2a. REPORT SECURITY CLASSIFICATION Unclassified 2b. GROUP

3. REPORT TITLE

An Investigation of the Dynamic Stability Characteristics of a Quad Configuration, Ducted-Propeller V/STOL Model, Phase I - Hovering

4. DESCRIPTIVE NOTES (Type of report and inclusive dates)

Final Data Report

5. AUTHOR(S) (First name, middle initial, last name)

William F. Putman Howard C. Curtiss, Jr.
Joseph J. Traybar John P. Kukon

6. REPORT DATE	7a. TOTAL NO. OF PAGES	7b. NO. OF REFS
September 1968	116	6

8a. CONTRACT OR GRANT NO.	9a. ORIGINATOR'S REPORT NUMBER(S)
DAAJ02-67-C-0025 b. PROJECT NO. Task 1F125901A14233 c. d.	USAAVLABS Technical Report 68-49A 9b. OTHER REPORT NO(S) (Any other numbers that may be assigned this report) Aerospace Sciences Report 835

10. DISTRIBUTION STATEMENT

This document has been approved for public release and sale; its distribution is unlimited.

11. SUPPLEMENTARY NOTES	12. SPONSORING MILITARY ACTIVITY
Volume I of a 4-volume report	U. S. Army Aviation Materiel Laboratories Fort Eustis, Virginia

13. ABSTRACT

Results are presented of experiments conducted to measure the dynamic stability characteristics of a quad configuration, ducted-propeller, dynamically similar model, V/STOL aircraft near hover. The data presented include longitudinal and lateral transient response characteristics of the dynamic model. Also included is a comparison with full-scale duct characteristics of the lift, drag, and pitching moment characteristics of an isolated duct from the model.

The model employed in the experiments is a generalized research model which was arranged to represent closely the Bell X-22A V/STOL aircraft.

The data presented in this report represent the first phase of a three-phase investigation of the dynamic stability of this type of V/STOL aircraft. The other two phases pertain to the longitudinal and lateral/directional characteristics at four low-speed and high-duct-incidence trim conditions.

DD FORM 1 NOV 68 1473 REPLACES DD FORM 1473, 1 JAN 64, WHICH IS OBSOLETE FOR ARMY USE.

Unclassified

Security Classification

14 KEY WORDS	LINK A		LINK B		LINK C	
	ROLE	WT	ROLE	WT	ROLE	WT
V/STOL						
Dynamics Stability						
Longitudinal Stability						
Lateral Stability						
Transient Response						
Bell X-22A						
Hovering Characteristics						